Mountain Bicycle Rear Suspension Dynamics and Their Effect on Cyclists

John Karl Titlestad

UNIVERSITY
of
GLASGOW

A thesis submitted for the degree of Master of Science

Department of Mechanical Engineering

University of Glasgow

ProQuest Number: 10647743

ProQuest 10647743

Abstract

The research documented in this report was conducted to understand better the anomaly between the predicted benefits of rear suspension systems for mountain bicycles and the preferred choice of rigid framed mountain bicycles by professional cyclists in the Union Cycliste Internationale (U.C.I.) world cup and world championship events.

To investigate the effects of rear suspension systems, a rig was designed on which two mountain bicycles were tested, one with (SU)and one without (HT) a rear suspension system. The purpose of this rig was to isolate the effects of rear wheel impact in order to conduct comparative performance tests of the bicycles with a number of cyclists. The rig held the front forks of the bicycle under test vertical and stationary while the rear wheel travelled on a large diameter roller. 'No bump' tests were conducted with the roller covered by carpet and with a drag load provided by a friction belt, while for the 'bump' tests wooden strips were attached across the surface of the roller and the friction belt was removed. Subjects, aged 22.3 ± 2.54 years, performed bump and no bump tests with both bicycles under sub-maximal conditions.

The physiological and psychological effects on cyclists riding the two types of bicycle on the simulated track of the rig were measured by the cyclists' oxygen consumption ($\dot{V}O_2$), heart rate, RPE (Borg 6-20 scale), and comfort (scale 1-5) rating. The dynamic behaviour of the bicycles was also observed by measuring the vertical acceleration of the saddle and handlebars, the chain tension, tangential crank velocity at the pedals, the force applied to

i

the front mounting bracket and the tangential surface velocity of the roller. A DADS model of the bicycle/rider dynamics was developed and the results from this model were compared with the measured dynamic behaviour of the two bicycles.

Results from the bump tests show a significant advantage for the SU bicycle over the HT bicycle in oxygen consumption (9.14 ml $\cdot$ kg^{-1} $\cdot$ min^{-1}, P < 0.001), heart rate (34.43 beats $\cdot$ min^{-1}, P < 0.001), energy expenditure (14.43 KJ $\cdot$ min^{-1}), RPE (1.83, P < 0.05), comfort (1.87, P < 0.001), maximum saddle and handle bar acceleration (1.45 and 0.54 g's respectively) and displacement (11.8 and 7.5 mm respectively), maximum and mean pedal force (122 and 59 N respectively) and mean pedal power output (64 Watts), and the horizontal force of bump impact measured at the front mounting bracket (197 N).

During the no bump test there was a small (2.18 ml $\cdot$ kg^{-1} $\cdot$ min^{-1} and 2.97 KJ $\cdot$ min^{-1} respectively) but significant (P < 0.005 and P < 0.025 respectively) increase in oxygen consumption and energy expenditure of the subject on the SU bicycle but no significant difference between the bicycles in the heart rate, RPE or comfort of the subject. There was a significant (P < 0.025 and P < 0.05 respectively) but small increase in the maximum and mean pedal force (34 and 16 N respectively) and mean pedal power output (14 Watts, P < 0.025) for the HT bicycle. There was no significant difference between the other mechanical values.

The physiological, psychological, mechanical and simulation results correlated well for the bump test. The results from the rig simulation confirmed that energy was lost from each bump impact and proved a useful tool in the analysis of the mechanical results, with which they correlated well. The physiological and mechanical results show that the SU bicycle offers significant advantages over the HT bicycle during the bump test. The results for the no bump test do not correlate for some variables, but the differences are very small between the two bicycles.

Acknowledgements

to my Mum, Dad and Sister

Contents

List of Figures

List of Tables

Nomenclature

This list of symbols are used within the text, figures and tables of this document:

A .... area

C .... circumference

Cd .... coefficient of drag

E .... energy

Ek .... kinetic energy

Ep .... potential energy

F .... force

I .... inertia

M .... mass

P .... power

V .... voltage

X .... variable used for different purposes

a .... acceleration

d .... diameter

f .... frequency

g .... gravity (9.806 $m \cdot s^{-2}$)

r .... radius

t .... time

ν .... velocity

w .... width

ω .... rotational velocity

Abbreviations

This list of abbreviations are used within the text, figures and tables of this document:

DADS .... Dynamic Analysis and Design System

DTM .... DADS Tyre Model

HT .... rigid frame, front suspended mountain bicycle

P .... statistical confidence level

PSD .... Power Spectral Density

RPE .... rate of perceived exertion

RQ .... respiratory quotient

STM .... Sprung Tyre Model

SU .... full suspension mountain bicycle

U.C.I. .... Union Cycliste Internationale

$\dot{V}O_2$ .... rate of volume of oxygen used

accel .... acceleration

amp .... amplifier

bkt .... bracket

brg .... bearing

cg .... centre of gravity

cyc .... cycle

disp .... displacement

frc .... friction

frt .... front

grnd .... ground

max .... maximum

min .... minimum

mtb .... mountain terrain bicycle

oth .... other

pdl .... pedal

pos .... position

rd .... road

s .... standard deviation

srf .... surface

tot .... total

vel .... velocity

vol .... voltage

Chapter 1

Introduction

Off-road cycling, or mountain biking, has developed as an important element of the sport of cycling in the last 20 years. It gained international recognition from the Union Cycliste Internationale (U.C.I.) in 1991 and became an Olympic sport in 1996 (U.C.I. Web Page 2001). The most significant distinction between competitive bicycles is whether or not they have a full suspension system, but at the present time there is a lack of evidence about which type of bicycle offers an advantage under which conditions. On the whole, professional cross-country cyclists do not ride full suspension bicycles. The reason suspension systems were introduced to off-road cycling was to increase control and comfort when cycling over rough terrain, allowing the cyclist to go faster. Unlike road cycling, aerodynamics is not as critical an element in the sport of mountain bicycling. The percentage power used by a mountain cyclist to overcome aerodynamic resistance is far lower than that of a road cyclist, largely due to the lower speeds and higher rolling resistance when cycling over rough terrain (see Appendix B, Section B.2).

During the 2000 season mens U.C.I. World Cup Series, which consisted of 8 races, and the U.C.I. World Championships, there were only 3 riders with rear suspension

systems placed in the top 3 out of a possible 27 places and there were no full suspension victories in any of these cross-country races (Williams 2000) (anon 2000) (Graves 2000). The 2001 season had similar results, however it did produce the first full suspension victory in a World Cup event. It would appear from the race results that hard tail bicycles are faster than full suspension bicycles for cross country racing. However, research studies indicate that there can be advantages in using a full suspension system.

The development of suspension systems, and the effect of suspension systems on performance, are the topics of much debate (Wang & Hull 1996) (Berry et al. 1993) and have required a number of design problems, that are unusual to engineers, to be addressed. These arise because a very complex engine, the cyclist, powers a bicycle. There is limited amount of power available from the cyclist, which means that the efficiency of the bicycle/cyclist system should be as high as possible to improve endurance. Wang & Hull (1996) point out that studies of off-road motor cycle suspension systems have not addressed the problem of efficiency, and suggest that this is because of the ample power available. However, this is not the case for pedal cycles. Suspension systems have an effect on the cyclist and on the power generated at the rear wheel. There are benefits in some areas of the bicycle/cyclist system and losses in others.

The preview of work in the field shows that some anomalies exists between test evidence, time trials and race results. It was felt that further work could help to clarify the differences and provide a better understanding of rear suspension systems. The objectives of this research were to compare the effect of rear wheel bump impact on the physiology and psychology of riders during sub-maximal cycling on one fully suspended (SU) and on one front suspended (or hard tail, HT) bicycle. To achieve this a rig was designed. The rig held the front of the bicycle while the rear wheel ran on a large roller. It was decided that tests conducted under laboratory conditions would be more

appropriate than field tests since the variables could then be controlled and the tests repeated.

The aim of the testing was to isolate and to determine the effects of impact load on the rear wheel of a mountain bicycle on a number of areas. The first area is that of the physiological variables of oxygen consumption and heart rate. Secondly there are the psychological variables: perceived exertion (RPE) (Borg 6-20 scale) and subject comfort (scale 1-5) rating. Thirdly, there are the mechanical variables: saddle and handlebar acceleration, pedal and roller surface velocity and forces exerted on the pedals and at the front of the bicycle (from which an estimate of the forces applied at the contact point of the roller and the rear wheel of the bicycle could be derived). Finally there is the development of the DADS (Dynamic Analysis and Design Systems) (http://www.lmsintl.com/) model to simulate the rig in order to help with the analysis of the mechanical data from the experiments and with a view to the optimisation of rear suspension systems in the future.

This report documents and discusses:

1. the research to date in the field of bicycle research with an emphasis on mountain bicycle suspension systems;

2. the design of the cycling rig;

3. the development of a reliable procedure for testing the bicycles with a number of cyclists;

4. the physiological and psychological effects on cyclists, during riding of the two types of bicycle on the simulated track of the rig, measured by the cyclists' oxygen consumption ($\dot{V}O_2$), heart rate, energy expenditure, RPE (Borg 6-20 scale), and

comfort (scale 1-5) rating;

5. the dynamic behaviour of the bicycles as evidenced by measured results of the chain tension and tangential crank velocity at the pedals, the force applied to the front mounting bracket and the tangential surface velocity of the roller;

6. the development of a dynamic model of the cycling rig using DADS (Dynamic analysis and Design Software);

7. the comparison of results from the HT and SU bicycles during testing and dynamic simulation, and comparison of the analytical methods;

8. the conclusions drawn, based on analysis of the data and the direction of future work in the field of mountain bicycle rear suspension.

Chapter 2

Literature Review

2.1 Research Papers

Bicycle suspension systems are not new. Whitt & Wilson (1982) have presented pictures of 19th century safety bicycles, with suspension systems to compensate for the lack of pneumatic tyres. These were not machines that could be ridden down rough, steep mountains at high speed, but the idea of suspension systems on bicycles has been around for a long time, and so have the problems.

> "...the difficulty experienced by inventors on the line of anti-vibrators appears to be, that while acquiring the desired elasticity in the proper direction, an elasticity in the other directions has followed, making the machine feel unsteady and capricious, especially in the steering. This undoubtedly valid difficulty in the way is worthy of careful consideration before accepting an anti-vibrator: in fact the very desired end can be easily missed in an imperfect device, as it might, while holding momentum in one direction lose it in another." (Scott 1889)

Whitt & Wilson (1982) recognise that vibration is uncomfortable and that there will be energy losses proportional to the roughness of the track. They state that 'some form of sprung wheel or sprung frame can greatly reduce the kinetic energy or momentum losses.'

Wang & Hull (1996) have categorised off-road cycling energy losses as terrain induced and rider induced. Their study concentrated on rider-induced loads and they determined from a dynamic model simulation that the rear suspension system dissipates 1.3 % (6.9 Watts) of the input power of the cyclist, as heat, due to the compressions of the shock absorber that result from the cyclic loading of the pedals. Wang & Hull (1997) showed that the average power loss could be reduced from 6.9 to 1.2 Watts by optimising the pivot point of a single pivot rear suspension system using a dynamic model. They calculated that this loss of energy would equate to a 46 second loss of time over a 1000 metre climb on a 6 percent slope. A similar optimum pivot point was determined by Good & McPhee (1999) using a genetic algorithm minimising the maximum value of the bicycle's frame rotation (Good & McPhee 2000). However, against these losses must be set the possible benefits of lower levels of human energy expenditure, better traction for both up and down hill cycling, and the ability to control the bicycle at faster down hill speeds (Seifert et al. 1997) (Kukoda 1992) (Needle & Hull 1997). It is difficult to quantify these benefits because they depend on so many variables including the physiology and psychology of the cyclist, the roughness of the track and the design of the suspension system. Seifert et al. (1997) have measured definite trends in the 24-hour change in creatine kinase[1], in volume of oxygen consumed ($\dot{V}O_2$) and in heart rate for subjects riding over a constructed level bumpy course that indicate an advantage for the full suspension bicycle. In time trials over a cross country trail

---

[1]Creatine kinase is a marker of skeletal muscle damage which results from muscle stress and strain and is used to give an indication of the amount of previous exercise.

they found that the front suspension bicycle was significantly ($P < 0.02$) faster than the rigid frame and the full suspension bicycles. However, they found no significant differences between bicycles in ascent and descent time trials.

Berry et al. (1993) have made similar measurements under laboratory conditions. They attached a bump to the belt of a power driven treadmill angled to a 4% slope and tested bicycles with no suspension system, with a front suspension system, with a rear suspension system and with a full suspension system. Their results do not indicate a consistent pattern. The full suspension bicycle riding over bumps gave a significant advantage in $\dot{V}O_2$ compared to the rigid frame, but no significant difference in heart rate, whereas the rear suspension only bicycle gave a significant advantage on heart rate, but not in $\dot{V}O_2$.

A further problem for bicycles with suspension systems is that they are heavier than their hard tail counterparts (Needle & Hull 1997). Berry et al. (2000) state that Howe (1995) estimated that gravity may provide 90% of the resistive force to uphill road cycling. Therefore, a lighter bicycle will have definite advantages in reducing the amount of work required to cycle up a hill. However, Berry et al. (2000) found that there is no significant difference in the $\dot{V}O_2$, heart rate or RPE values of the subject riding suspension mountain bicycles of different masses (11.6 to 13.6 kg) on a bumpy surface with different gradients of up to 5%. They recognised that the variations in masses are small and, if there were differences between the bicycles they were too small to be measured. However, the mass range investigated is larger than the difference between a full suspension bicycle and its hard tail counterpart.

Wilczynski & Hull (1994) claim that the 'design methodology typically used in the bicycle industry is an evolutionary one, which entails a cut-and-try approach.' They go on to say that this methodology is time-consuming, design specific, and does not

necessarily lead to an optimised design. To change this methodology an engineering approach must be implemented (Wilczynski & Hull 1994), however it must include the 'human element'. The cyclist is an integral part of the bicycle/cyclist system. They set out to develop a dynamic system model for estimating surface induced loads during off-road cycling, and concluded that substantial vibrations were transmitted to the body. Based on this finding suspension systems were deemed desirable. However, they do introduce losses into the bicycle/cyclist system.

De Lorenzo & Hull (1999a) designed a hub dynamometer for measuring wheel forces during off-road cycling, and found that the rider distributes the majority of his weight on the rear wheel of the bicycle, and that very little weight was supported by the hands.

Needle & Hull (1997) set out to quantify and optimise off-road bicycle performance by constructing an adjustable dual suspension off-road bicycle. They determined that, for a single swing arm rear suspension system, the optimum pivot point was 8.4 cm above the bottom bracket. This was close to the simulated results from Wang & Hull (1997).

MacRae et al. (2000) conducted uphill time trials on an 'on road' asphalt course and on an 'off road' course to compare performance of a front suspension bicycle and a dual suspension bicycle. There was no significant difference in times or physiological measurements, but the power transmitted through the pedals on the dual suspension bicycle was significantly ($P < 0.001$) higher than on the front suspension bicycle. MacRae et al. (2000) hypothesise that energy is *"translated back into the bicycle/rider"* to explain this, but it is not a convincing explanation, as human energy cannot be acquired from a mechanical system.

Nielens & Lejeune (2001) determined that there is no difference between subject $\dot{V}O_2$ and heart rate when riding a fully suspended, front suspended and a fully rigid mountain bicycle on a smooth surface.

Martin et al. (1998) derived a mathematical model for estimating cycling power. Although the model was derived for road cycling, it has been adapted for describing off-road cycling (see Appendix B.2).

From this review it is evident that there are many effects influencing existing data. No research has been done to isolate rear wheel impact effects, on both full suspension and hard tail bicycles, to gain improved understanding.

2.2 Patents

One of the areas where mountain bicycle rear suspension systems were investigated was from patents. This was done to gain insight from the research conducted for the patent and the claims made in the patents. The primary concern of the patents was with the configuration of the suspension system and the mode of operation.

Leitner (1996) states that pivoting spring suspension systems for at least the rear wheel do provide higher performance in off road bicycles . Further, Leitner (1996) recognises the problem of surge in chain tension and its effect on the operation of single swing arm suspension systems, which he has termed 'jacking', which can compromise rider control. This problem is described as 'intolerable to a bicyclist seeking peak performance' (Leitner 1996), and a parallel is made with motorcycles for which the loss of power from jacking is considered inconsequential. Harris (1995) states that the problems associated with the suspension system, resulting from increased travel

and the use of softer springs for bump compliance, are amplified under race conditions. However, the problems are neither fully nor clearly discussed. Harris (1995) expresses a need for a bicycle rear wheel suspension system which will meet the needs of competitive mountain bicycle racing. However, neither Leitner (1996) nor Harris (1995) discuss any physiological advantages of rear suspension systems nor do they discuss why the rigid framed mountain bicycles are the preferred choice for world cup race events.

As these are patent documents, they are concerned only with the mechanical functioning of the suspension system that they wish to patent. They record no experiments to prove that bicycles with rear suspension systems are superior to HT bicycles.

Chapter 3

Experiments

3.1 Objectives

The objectives of the experiments were to investigate a number of issues by testing a number of subjects on an HT and an SU bicycle . The first issue was to determine if there was a difference in physiological variables, $\dot{V}O_2$, heart rate and energy expended, of the subject between the HT and SU bicycles when riding on a bumpy surface, and the difference when riding on a smooth surface. The second, was to determine if there was a difference in psychological variables, RPE and comfort rating, of the subject between the HT and SU bicycles when riding on a bumpy surface, and the difference when riding on a smooth surface. The third, was to determine the difference between the mechanical variables of the HT and SU bicycles, the saddle and handlebar acceleration, the pedal and roller surface velocity, the force exerted on the pedals and the wheel roller contact force[1], when the bicycles are ridden on a bumpy and on a smooth surface. The

---

[1]the wheel roller contact force was not directly measured . The horizontal force applied to the front wheel axle was measured as an estimate of the wheel roller contact force (see Section 3.6.4 p. 39).

tests used to determine these differences were to be conducted in a laboratory with a controlled environment so that the results are repeatable for all the tests and can therefore be accurately compared.

It was an objective to isolate the effect of the rear wheel impact from a bump. The impact force of the bumps was applied only to the rear of the bicycle so as to isolate the effect of the bump impact on the rear wheel. The energy used by the cyclist to maintain balance and control and to determine the line of attack on a bump, and the stress and excitement involved in riding on a trail was removed so that the proportion of the total energy used to overcome rear wheel impact was increased. In other words, everything that might require energy to be expended by the cyclist other than powering the bicycle and overcoming rear wheel impact was removed.

Once a difference had been measured, the objective was to determine where the energy had been dissipated in the cyclist/bicycle system and determine the advantages and disadvantages of rear wheel suspension systems.

3.2 Requirements

3.2.1 Rig Requirements

Treadmill tests as used by Berry et al. (1993) impose a significant and stressful task on the rider to simply stay on the treadmill, and this has an unknown influence on the results. The treadmill also places limits on the spacing of the bumps and on maximum speed, and the inertial effects of impact with the bumps are not accurately simulated because they are affected by the characteristics of the treadmill drive motor. It was decided that tests conducted with the front fork held rigid while the rear wheel was

driven against a heavy roller would offer the advantage of a better simulation of the rear wheel dynamics. This procedure would result in a reduced number of variables and the ability to conduct tests over a range of speeds and levels of exertion.

The purpose of the rig was to simulate the impact load on the rear wheel of a mountain bicycle encountering a bump on a trail and to carry out controlled, repeatable experiments to compare rider performance on the two bicycles.

In order to determine the effects of rear wheel impact, a rig was designed to hold the bicycle stationary and vertical thus removing any operations that require energy expenditure such as control, balance, and stress from trail riding.

Rear wheel impact was simulated by placing two bumps on a single roller on which the rear wheel ran. During no bump tests, a braking system (a strap brake around the roller) was used to increase the resistance so as to match the work rate of the subject during the no bump test to that during the bump test (see Section 3.5.3).

The structure had to be safe and be capable of supporting the mass of a cyclist and bicycle for the duration of the testing period. It also had to be modular so that the rig could be broken down for installation in laboratories .

3.3 The Cycling Test Rig

The cycling rig (see Figure 3.1) consists of a bracket to hold the front forks of the bicycle and a 610 mm diameter steel roller against which the rear wheel rotates. The inertia of the roller was set to simulate a subject of 74 kg mass (mean mass of subjects was 73.03 ±6.09 kg) and a mountain bicycle of 12 kg mass to ensure that deceleration caused by bump impact on the rig was equivalent to that caused by bump impact while cycling
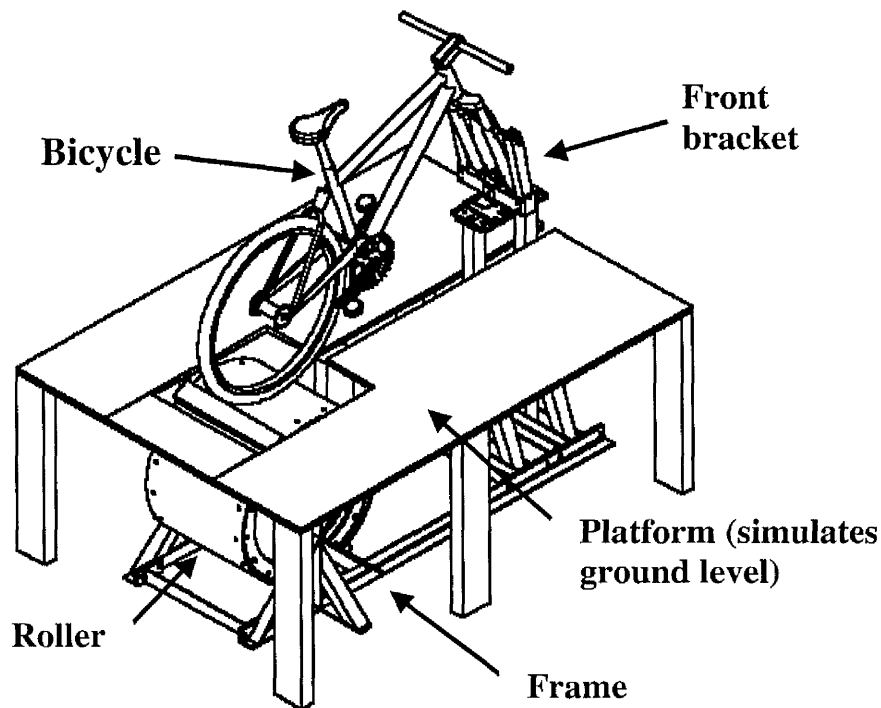
Figure 3.1: Isometric view of cycling rig

on the road (see appendix B.1.2 for calculations). A strip of carpet was attached to the roller to simulate riding on a soft surface and to increase traction between the roller surface and the rear wheel tyre. Two bumps were formed by evenly spaced rectangular wooden blocks (70 mm by 30 mm) bolted across the roller. Different bumps sizes were used in the preliminary testing and the size was chosen which provided as large a bump impact as could be applied while still allowing the cyclist to cycle at a sub-maximal level (see Section 3.5.3). The bicycle was held in the vertical plane by a fixed axle so that the subjects did not expend energy to balance the bicycle or use their upper body to respond to front wheel impact. The bicycle was free to rotate about the front axle and to move on its front shock absorbers, which compress when the rear wheel is impacted because the centre of gravity of the subject is between the two wheels.
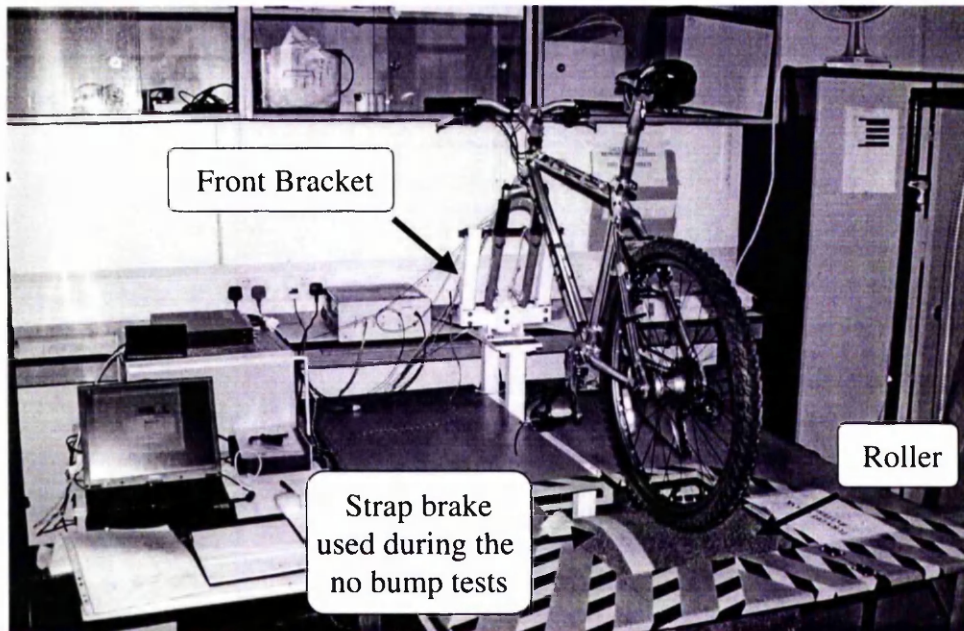
Figure 3.2: Photo of cycling rig during a no bump test. Note the strap brake indicated on the photograph.

The braking force was applied during the no bump tests by a web strap passed over the roller and loaded by weights (see Figure 3.2). This braking system remained cool and provided a consistent braking force, matching the resistance applied by the bumps during the bump test, throughout each test. See appendix E for drawings of the rig assembly and the subassemblies.

3.3.1 The Frame

The frame was modular for transportation purposes. The modules consisted of welded constructions. It was designed to hold the roller on which the rear wheel of the bicycle ran and the front bracket which held the bicycle at the front hub vertical and stationary

Mounting points for the
front bracket (the
mounting point is
variable to allow for
different wheel bases)

Mounting points for the
hub axles of the roller

Z

X

Y
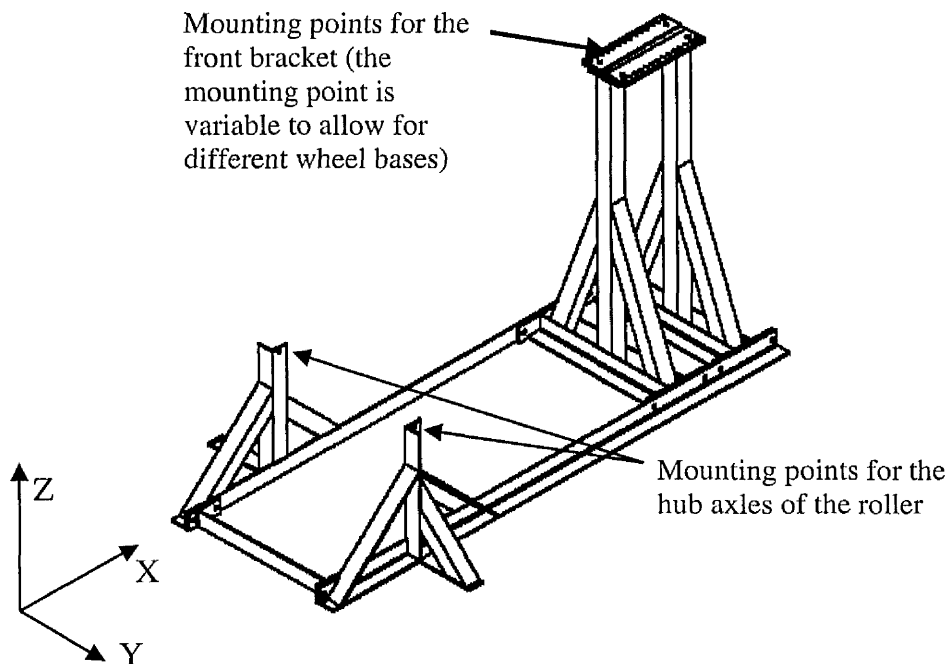
Figure 3.3: Isometric view of frame

in the X direction (see Figure 3.3). The mounting point for the front bracket allowed for adjustment for bicycles of different wheel bases to be used. This ensured that the rear axle of the bicycle remained vertically over the axle of the roller. The platform, shown in Figure 3.1 was fixed to the vertical supports that hold the mounting point for the front bracket.

3.3.2 The Front Bracket

The front bracket was a welded and post machined structure constructed from mild steel plate and square tube. It was designed with two objectives. Firstly, to hold the front suspension forks of the bicycle vertical and the front wheel axle stationary while allowing the bicycle to rotate around axle AA (see Figure 3.4) The stanchions of the

Fork support arms
(supports the top of
the shock absorber
stanchions and
rotates about AA)

Brake stanchion bracket
(fixes the brake stanchions
to the Fork Support Arms)

A

Front wheel
Axle (supports the base
of the shock absorber
stanchions and rotates
about AA)

Cantilever beam

A
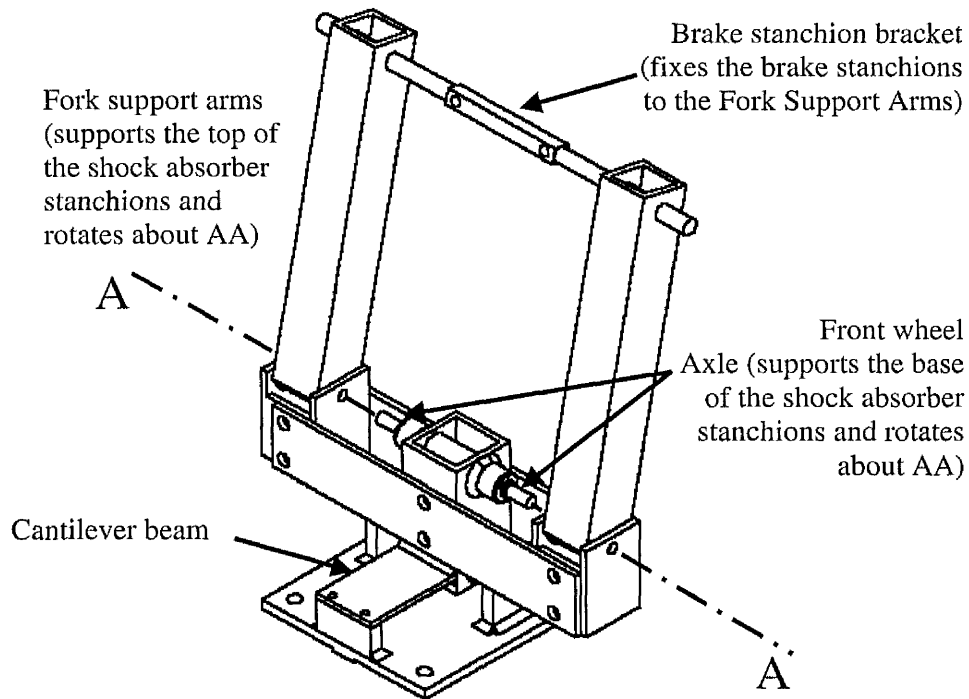
Figure 3.4: Isometric view of front bracket with stanchion supports.

suspension forks were fixed to the front wheel axle and the brake stanchions. This allowed the suspension system at the front of the bicycle to operate properly. The fixed front axle prevented the bicycle from moving in the X and Z directions. The brake stanchion support held the stanchions and the bicycle vertical, in the XZ plane, but free to rotate about the front wheel axle. Secondly, to measure only the horizontal force applied to the front wheel axle. This force was measured using strain gauges (see Section 3.4.2). The vertical force applied at the front wheel axle was supported by the main pivot axle. (The main pivot axle is visible in figure 3.6 and is clearly labelled in Figure E.4, p. 170, item number 2.) Rotation about this axle was prevented by the cantilever beam.

3.3.3 The Roller

Bump (wooden block
70mm by 30 mm)

Clamping rods

Clamping rings

24-inch bicycle
wheel rim

Roller Pipe (provides the
surface to which the carpet
and bumps are attached and
is the major component of
the roller's mass)
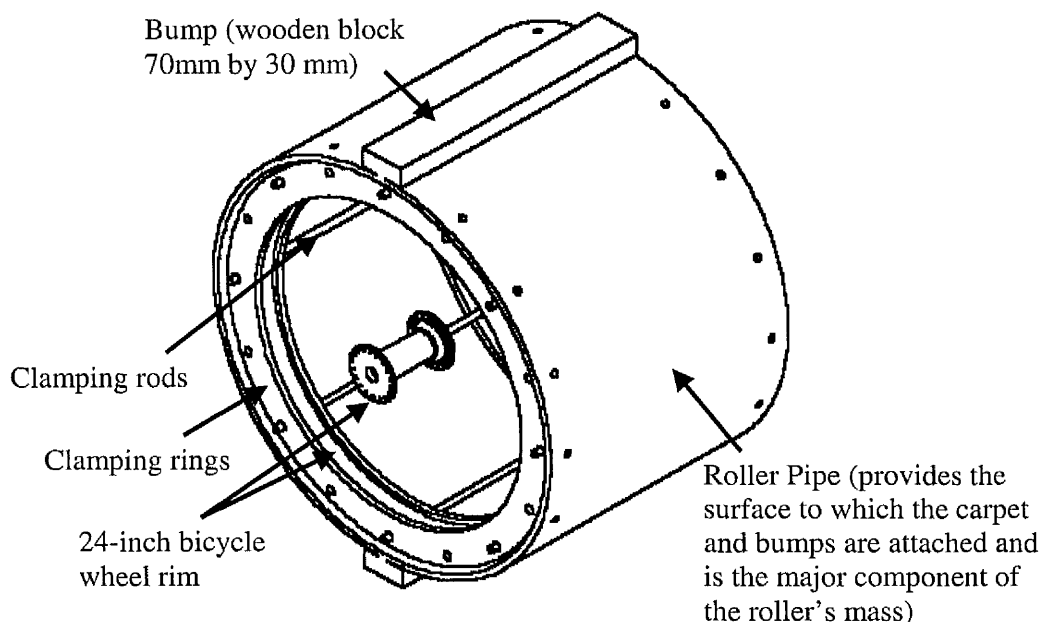
Figure 3.5: Isometric view of roller

The roller was constructed out of 0.61 metres diameter, 9 mm thick rolled mild steel welded piping. The welded piping provided most of the mass required to achieve the correct inertia, that was equivalent to the mass of the cyclist and the bicycle. The radius of circular profile of the pipe varied by a maximum of 3 mm. A 24 inch[2] bicycle wheel was clamped between a metal ring welded to the inside of the pipe and a second free metal ring with 8 bolts, at each end of the pipe (see Figure 3.5). The two wheels provided the axle around which the roller rotated.

Bumps (70 mm by 30 mm wooden blocks) and carpet were bolted to the surface of the roller, providing the riding surface.

---

[2]Imperial units are the standard units used in the bicycle industry to describe wheel size (24"=0.610 m).

3.4 Instrumentation

3.4.1 Acceleration Measurement

The vertical saddle and handlebar acceleration were measured using accelerometers. The saddle accelerometer was fitted to the seat post just under the saddle of the bicycle so that it measured the acceleration of the frame at the saddle, and not the acceleration of the saddle surface, thus avoiding the effects of the padding in the saddle. The handlebar accelerometer was mounted on the top of the steerer tube of the front shock absorber.

3.4.2 Force Measurement

Force was determined by measuring strain and then calibrating the strain to a given force (see Section 3.4.4 for force calibration). Strain was measured using strain gauges arranged in full Wheatstone bridge configurations and placed on a cantilever beams where the expected maximum strain was to be 1000 μ strain. Full Wheatstone bridges were used to compensate for any change in temperature.

Front Bracket Force Measurement

The front bracket force is the measure of the horizontal force applied to the front wheel axle. It was measured using a wheatstone bridge, as discussed above, attached to cantilever beam. The location of the bridge can be seen in Figure 3.6. The vertical load at the front bracket was supported by the main pivot (as described in Section 3.3.2), and the moment produced by the horizontal force about this pivot is countered by the

Front wheel axle ⟶

Strain gauge position
(output voltage
proportional to the
horizontal force at
Front Wheel Axle)

Main axle about
which the front wheel
axle rotates
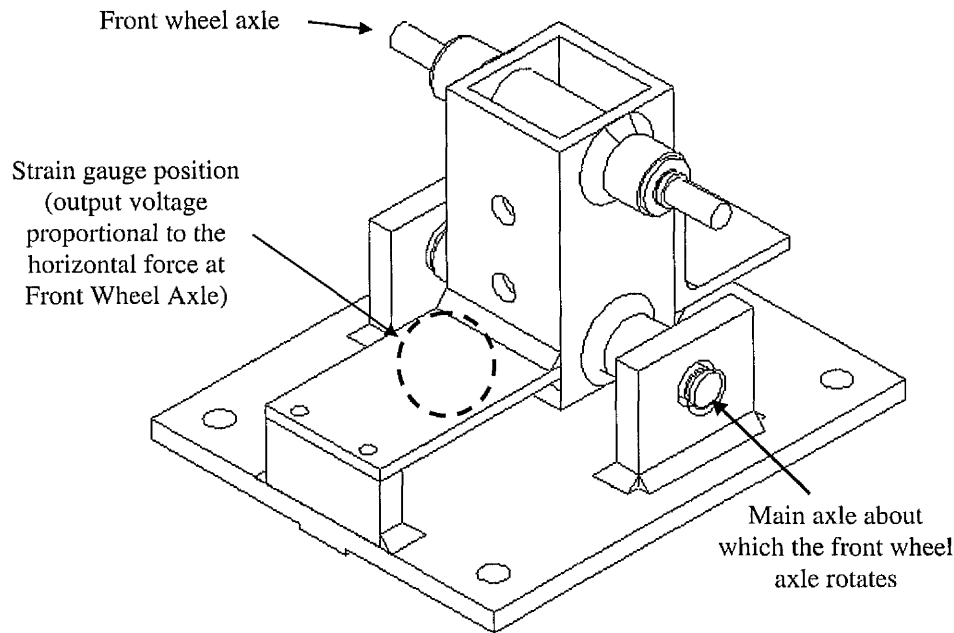
Figure 3.6: Isometric view of front bracket without stanchion supports.

cantilever beam. The measure of this force gave an estimate[3] of the amplitude of the force between the roller surface and the rear tyre.

Pedal Force Measurement

The torque transmitted through the chain rings was measured. From this the resultant perpendicular pedal force applied to the crank arms was calculated. This allowed for the comparison of the effect of bump impact and no bump impact on the pedal force and transmitted power between the HT and SU bicycles during both the bump and no bump tests.

---

[3]The estimate of the force between the rear tyre and the roller surface, after critical analysis of the data, was found to have inertial loads from the movement of the cyclist. This point is discussed further in Sections 3.6.4 p. 39, and Section 6.2.3 p. 93.
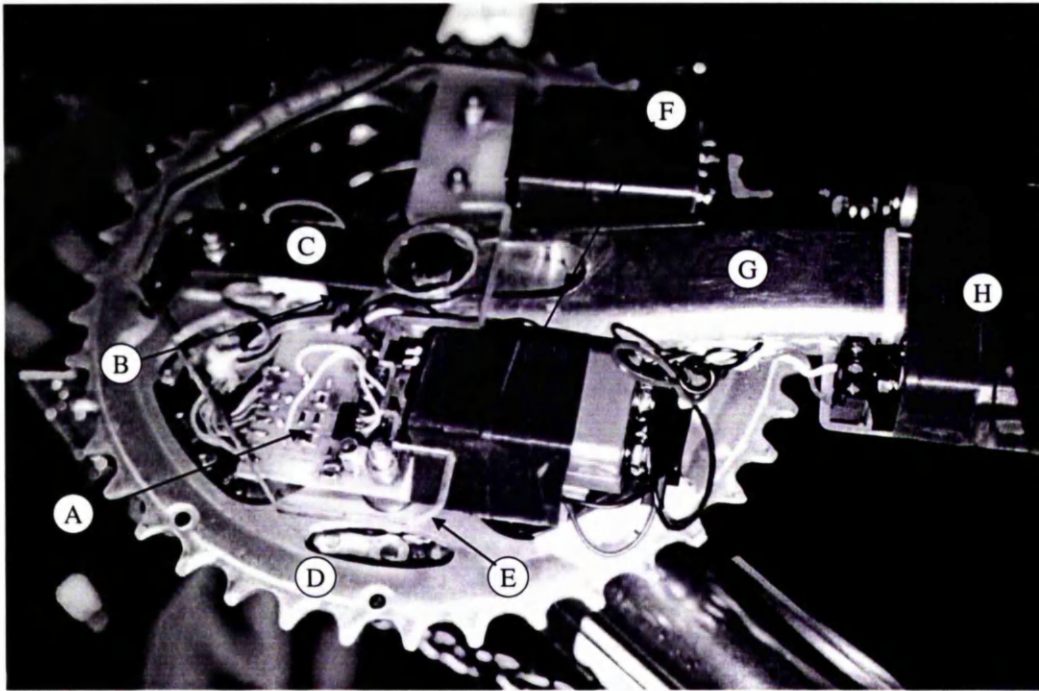
Figure 3.7: Photograph of pedal force measurement instrumentation. Key:A - strain gauge amplifier, B - Wheatstone bridge, C - cantilever beam, D - chain rings, E - perspex protective cover, F - 9 volt bridge supply , G - crank arm, H - 1.5 volt amplifier supply.

To the author's knowledge, the only commercially available equipment used for measuring the torque transmitted by and the rotational speed of the crank set was the SRM Training System (http://www.srm.de). This was available at prohibitive cost and therefore it was decided to design and build a torque and speed measurement system for an existing crank set (Shimano, STXrc).

The crank set used was chosen because it had solid crank arms[4]. A slot was machined into the right crank arm so that the cantilever beam (C) could be inserted.

The spline of the spider, locking the spider and chain rings to the crank arms and the bottom bracket axle, was machined off and replaced with a bushing. This allowed

---

[4]The new crank set models from Shimano have hollow crank arms, which do not allow for modifications without a large reduction in strength.

the spider and chain rings to rotate freely and independently from the bottom bracket axle and crank arms. (The spider is the unit to which the chain rings are attached and fixes them to the crank arms)

The end of this cantilever beam was bolted to the chain rings, thus fixing the chain rings to the crank arms and bottom bracket axle. All torque generated by the pedals was transmitted through the cantilever beam to the chain rings. This force was calculated from the strain measured using a full Wheatstone bridge (B), as described earlier, attached to the cantilever beam (C). The positive and negative rails of the Wheatstone bridge were supplied by two 1.5 Volt batteries (H), attached to the sides of the crank arm (see Figure H.3 for battery board layout). The bridge voltage was transmitted through slip rings (see Figure 3.8). These were attached to the spider in place of the 22 tooth sprocket. The front derailleur of the HT and SU bicycles was locked so that only the 32 tooth chain ring could be used. This prevented any accidental shifting of the gears which would have damaged attached instrumentation.

The noise generated by the slip rings was found to be similar in amplitude to the voltage output amplitude before signal amplification. The solution was to amplify the signal before the slip rings. The amplifier (A) was attached to the chain rings (see Figure H.2 for circuit board layout). The input signal was amplified 2000 times, thus eliminating the effect of the noise generated by the slip rings. Both the amplifier (A) and the cantilever beam (C) were covered in a clear perspex shield to protect the instrumentation during use.

The signal was transmitted via carbon brushes, from the slip rings, to a circuit board attached to the base of the bottom bracket (see Figure 3.8). All the signals of pedal force, pedal velocity (see Section 3.4.3) and the pedal position indicator switch (see Section 3.4.5) were transferred via this circuit board, up the base of the down
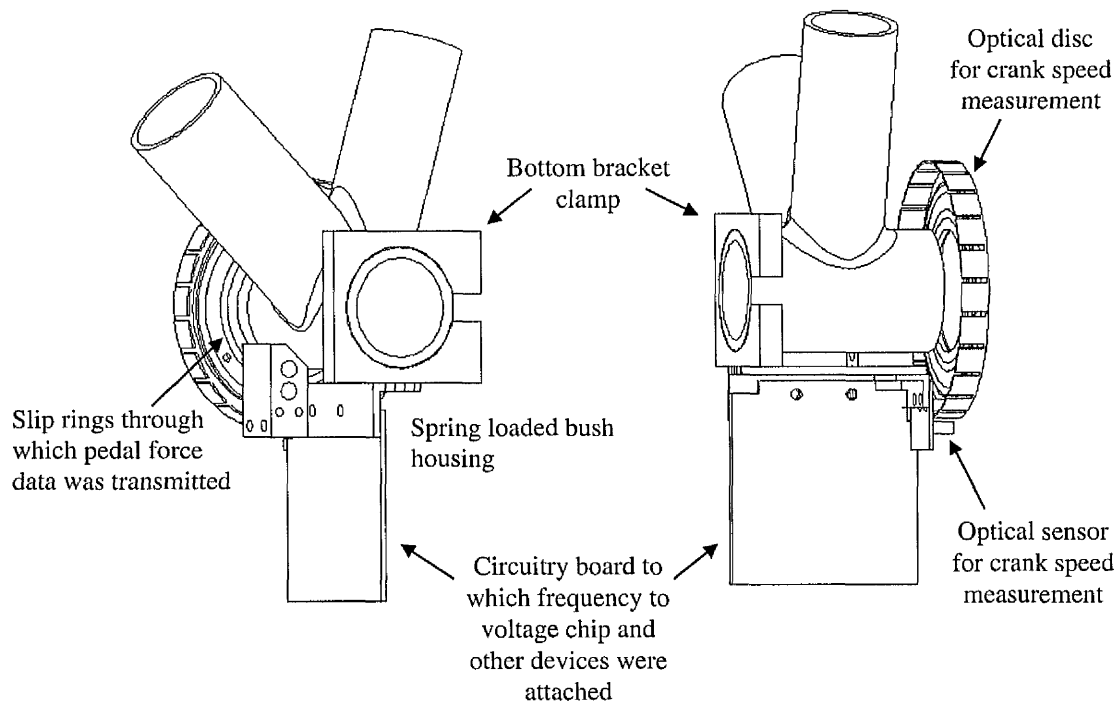
Figure 3.8: Views of the instrumentation attached to the bottom bracket of the bicycle. The left hand view shows the slip rings and the bush housing. The right hand view shows the optical sensor use to measure the rotational velocity of the crank arms.

tube of the frame of the bicycle and to the acquisition box (National Instruments, DACPad-6020E) (see Figure 3.16)(see Figure H.1 for circuit board layout).

3.4.3 Velocity Measurement

The rotational velocity of the roller and the crank set was measured using an optical sensor and disc (see Figure 3.8). The output frequency from the disc was converted to a voltage using a frequency to voltage converter chip, attached to the circuit board mounted on the base of the bottom bracket. This voltage was in turn converted to the tangential velocity of the pedals (see Section 3.4.4 for pedal speed calculation).
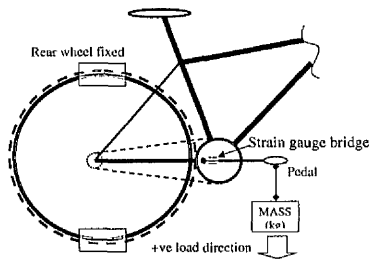
Figure 3.9: Schematic of pedal force calibration set-up.
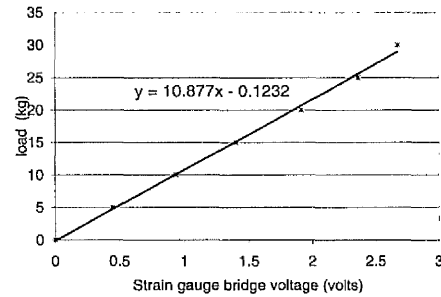
Figure 3.10: Plot of the pedal load versus output voltage.

3.4.4 Calibration

Hung mass was used to calibrate the strain gauges for both the pedal force and the front bracket force.

Pedal Force Calibration The crank arms were placed in a horizontal position and the rear wheel was fixed. Mass units (kg) were hung from the pedal and the corresponding bridge output voltages were recorded (see Figure 3.9). These values were then plotted to determine their linear relationship (see Figure 3.10). A positive force produces a clockwise moment around the bottom bracket

Front Bracket Force Calibration Horizontal force was applied with the aid of a pulley to the mounting point of the bicycle forks of the front bracket using hung mass units (kg) (see Figure 3.11). The corresponding strain gauge bridge output voltage was plotted against the applied load to determine the linear relationship (see Figure 3.12).
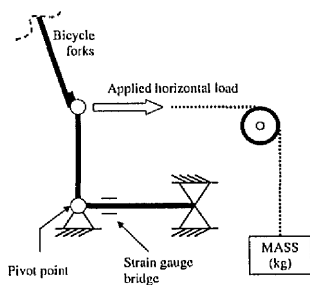
Figure 3.11: Schematic of front bracket force calibration setup
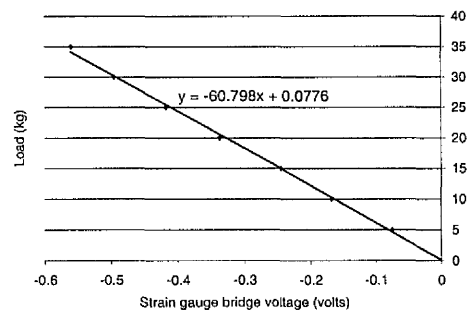
Figure 3.12: Plot of the front bracket load versus output voltage

Velocity Calibration

To measure the rotational velocity (ν) of the crank arms and the roller a 58 slot optical disc and sensor were used. The pulse frequency (f) from the sensor was used to determine the velocity.

$$\nu = \frac{f}{58} \cdot 2 \cdot \pi \cdot r_{pdl/roller} \qquad (m \cdot s^{-1}) \qquad (3.1)$$

The pulse frequency was converted to a voltage with a frequency to voltage converter. This was calibrated using known input frequencies from a frequency generator.

The voltage was plotted against the calculated velocity (equation 3.1) of the corresponding frequency (see Figure 3.13) to determine their linear relationship. The pedal position data was adjusted so that there was a drop in the data value when the switch was on.
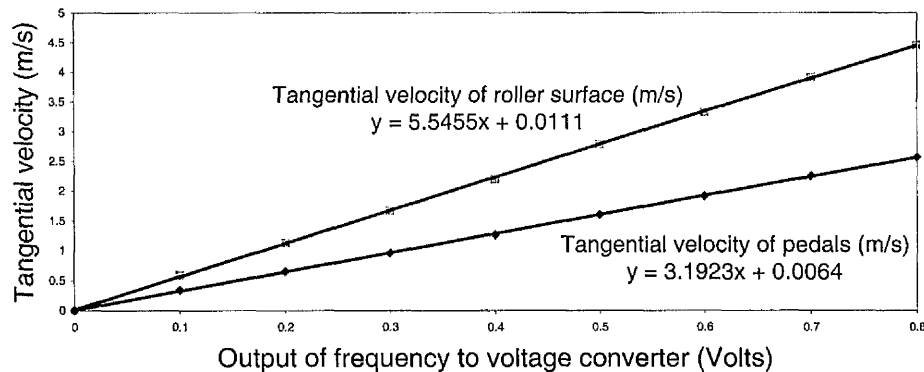
Figure 3.13: Plot of frequency to voltage output versus pedal velocity and roller surface velocity.

Strap Brake Calibration

During the no bump test, a brake was applied to the roller (see Figure 3.2) so that the work rate of the subjects during the no bump test would be matched to that during the bump tests. The brake was calibrated by cycling on both the HT and SU bicycles, with a subject of average mass (73 kg), at a speed of 15 $km \cdot h^{-1}$ for a set time, and then removing all torque from the crankset. The roller was allowed to roll to a stop, with the subject seated. This test was repeated a number of times to ensure that consistent braking was applied under all brake temperatures. The deceleration of the roller during the no bump test was matched to the average deceleration of the roller with the HT and SU bicycles, when ridden by a subject of average mass (73 kg), during the bump test.

3.4.5 Position Indicator Switches

The bump position was determined using a magnetic switch situated on the front face of the bump. It was switched on when the centre of the bump passed vertically above
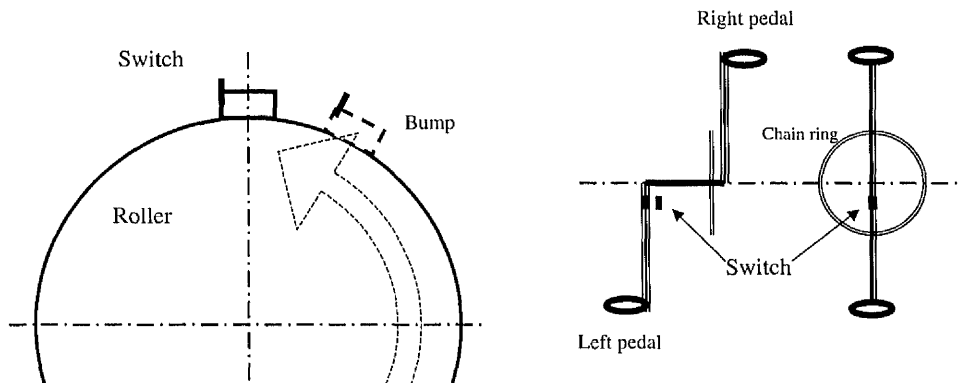
Figure 3.14: Indicator switch locations for indicating pedal and bump positions.

the centre of the roller (see Figure 3.14). The magnetic activator was attached to only one of the two bumps, which means that there is an impact half way between each pulse in the bump indicator data set.

The pedal position was also determined using a magnetic switch which was switched on when the left pedal was at the bottom of its stroke (see Figure 3.14).

3.4.6   Cable management

All cables from attached instrumentation were directed to the front of the bicycle, and from there to the respective amplifiers and acquisition boxes. The cable originating from the instrumentation attached to the bottom bracket was spiral wrapped in one half of a strip of velcro tape. The other half was attached along the under side of the down tube of the bicycle. This allowed for rapid and neat cable management when moving instrumentation between bicycles. All other cables were taped to the frame. No cable routing affected the operation of the bicycle.

3.5 Test Program

3.5.1 Subjects

Eight male subjects participated in each set of tests. They were aged between 19 and 27 years (mean 22.3, standard deviation 2.54) and were all active in either cycling or some other physical sport. They all signed a consent form and the study was approved by the local ethics committee.

3.5.2 Bicycles

The HT bicycle used in the testing was typical of HT bicycles available on the market and the SU bicycle was typical of most single swing arm suspension system mountain bicycles. Two mountain bicycles were acquired on loan for the tests. For the purpose of these investigations the bicycles were the same apart from one having a rear suspension system (Marin Mt. Vision) and one having a rigid frame (Marin Rocky Ridge)(see Figures 4.1 and 4.2 and Appendix F for geometry). The same front shock absorbers (Manitou Magnum R) were attached to both bicycles with the setting for pre-load and damping kept constant throughout the tests. The same rear wheel (Shimano XT hub, Mavic 222 rim and Marin Quake 7.1 tyre) was used in all the tests and the tyre pressure was a constant 50 psi, as in Wang & Hull's (1996) treadmill study.

3.5.3 Testing Routine

Each subject was tested on both the SU and the HT bicycles, both with and without bumps on the roller. The first tests were conducted with bumps on the roller but

without any additional braking effect. The tests were then repeated without bumps but with a brake applied to the roller and adjusted so that the time to "free roll" to rest was similar with and without bumps (see Section 3.4.4, p 26). This ensured that the work rate and heart rate of the subjects during the bump tests and the no bump tests were at comparable levels.

Each subject attended the laboratory at the same time of day for all his tests. The order in which the two bicycles were ridden was randomly assigned to each subject. The saddle height was set so that the subject's leg was straight when at maximum extension with his heel on the pedal. To allow for different riding styles, the subjects were permitted to ride in the rear gear of their choice, but the attachment of measuring equipment restricted them to the middle front chain ring (32 teeth)(see 3.4). The first test included a familiarisation session during which the subject was instructed to cycle at a speed, between $10 \, \mathrm{km \cdot h^{-1}}$ and $15 \, \mathrm{km \cdot h^{-1}}$, that he could maintain comfortably for ten minutes. This was to ensure that the subject exercised at a sub-maximal level. The subjects were then asked to use their chosen gear and to match this speed to within $\pm 0.5 \, \mathrm{km \cdot h^{-1}}$ during all their tests.

3.5.4 Test Structure

The subject was instructed to remain seated on the bicycle at all times during the tests to ensure that the effects of the suspension were being measured and not the ability of the legs to absorb bumps, and to reduce the effect of the cyclist's inertia on the horizontal force measured at the front bracket. This is described as a passive mode of riding. It also prevented the subjects from transferring their centre of gravity from the pedals onto the handlebars, which would affect the operation of the suspension

and the horizontal impact force applied by the bumps on the roller. The subjects were instructed to remain motionless and not apply any load to the pedals for the first approximately 10 seconds of the first minute (this was to take zero load readings). They then had the remainder of the first minute to attain their chosen test speed at the start of each test. The test started at the end of the first minute and continued for a further ten minutes during which readings and samples were taken. The subjects were then instructed to allow the bicycle to come to a halt and remove all load on the pedals and remain motionless for a further approximately 10 seconds (this was to take further zero load readings). Data acquisition was then stopped. See Figure 3.15 for schematic of test structure.
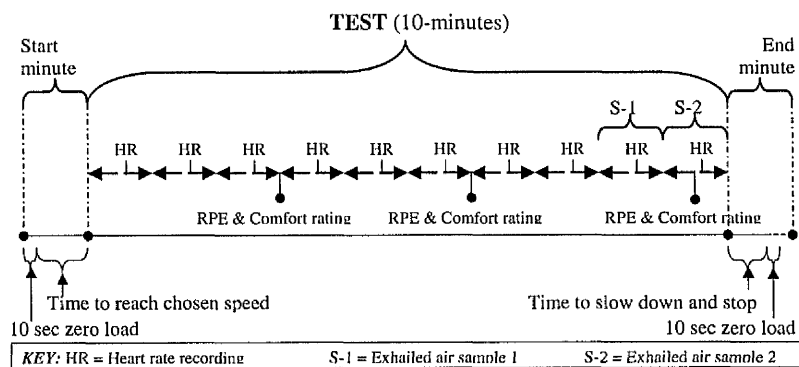
Figure 3.15: Schematic of the test structure for both the bump and no bump tests.

3.5.5 Measurements

Heart Rate

A Polar Favor heart rate monitor (Polar Heart Rate Monitor, Kempele, Finland) was used to monitor the heart rate, which was recorded 45 seconds into each minute of the test. The mean value of the last two recordings was taken as the representative value

Subject

RPE and
Comfort rating

Heart Rate

Gas
Analysis

Manual
data input

Data
Storage

**Cycling
Rig**

Real time data
storage

Data Acquisition

| 1 | 2 | 3 | 4 | 5 | 6 | 7 | 8 |

Position indicator signal

Signal
Amplification
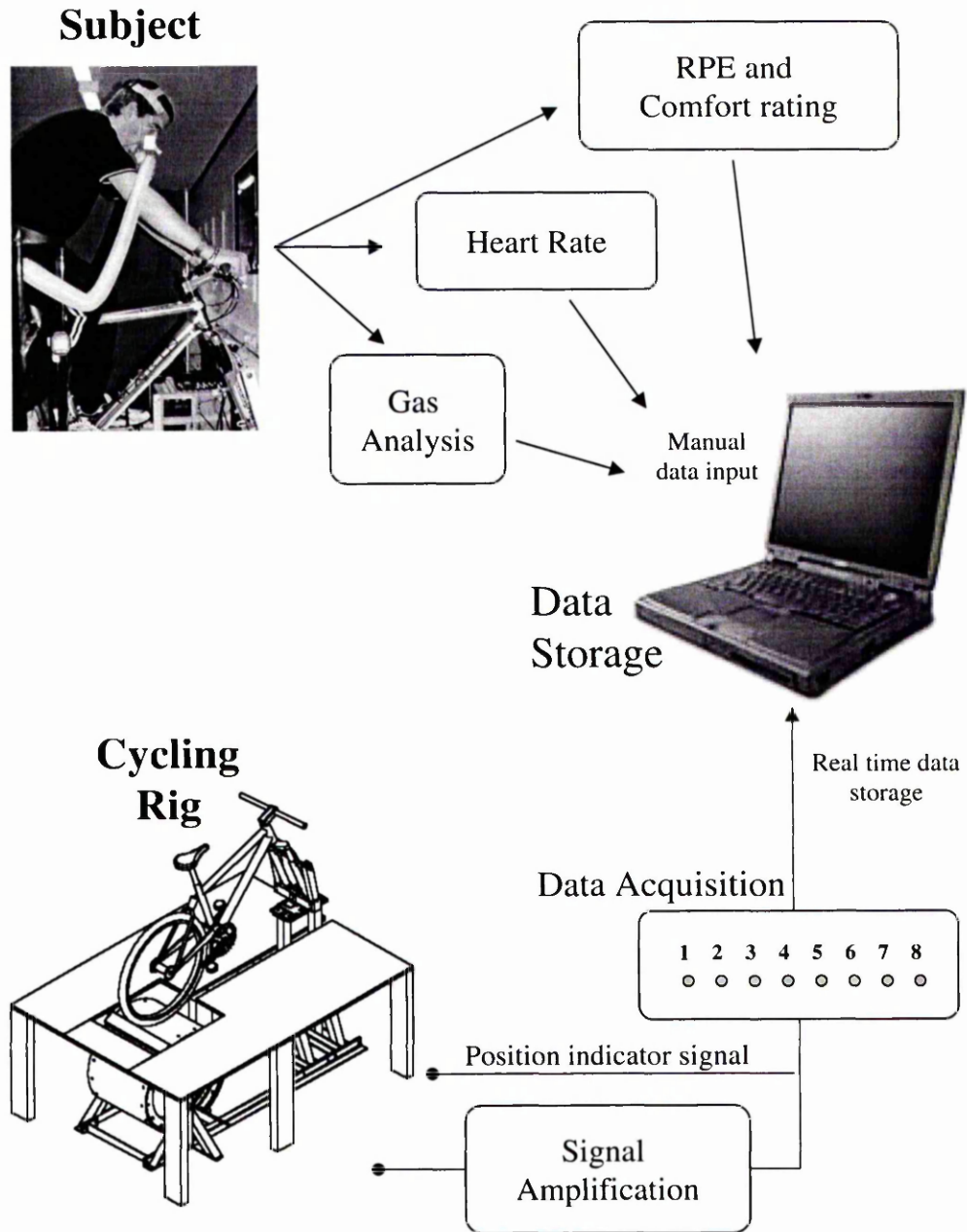
Figure 3.16: Schematic of the data measurement and storage process.

for each test(see Table A.2).

Oxygen Consumption

One minute samples of expired air were taken in the 9th and 10th minutes of the test. These were collected using a two-way Hans Rudolph 2770 mouthpiece, tubing and Douglas bags. All the subjects wore a nose clip. The expired air was analysed using a Servomex 570 A O_2 analyser (Servomex, Crowborough, UK) and a PK Morgan TD 801 A CO_2 analyser (Morgan 801B, Morgan, Rainham, UK). Both analysers were calibrated before testing with gases of known concentrations. Gas volumes were measured using a Parkinson Cowan (Cranlea, Birmingham, UK) meter calibrated against a Tissot spirometer (Collins, Massachusetts, USA). Standard formulae were used to calculate O_2 consumption and CO_2 production (McArdle et al. 1996) (see Section D for physiological data analysis code).

Subject Power Output: The energy expended by the cyclist was calculated in the 9th minute and the 10th minute of the test using the Weir formula (1949) (equation 3.2).

$$E_{exp} \; (J \cdot min^{-1}) \;\; = \;\; VO_2 \; (litres \cdot min^{-1}) \; \cdot X_{RQ} \cdot 4186.8, \qquad (3.2)$$

where X_{RQ} is a tabulated value that is derived from the respiratory quotient (RQ) where $RQ = \frac{VCO_2}{VO_2}$ (McArdle et al. 1996).

RPE and Comfort ratings

During the tests at the 3rd minute, the 6th minute and the 9.5^{th} minute, the subjects were asked to indicate their ratings of perceived exertion (RPE) using the 6-20 scale (Borg 1998) (see Figure G.1, and their rating of comfort using a scale rated from 1 (very uncomfortable) to 5 (very comfortable), as in Seifert et al. (1997)(see Figure G.2).

Zero Load Readings

Zero load readings were taken in the first 10 seconds of the first minute of the test and the last ten seconds of the last minute of the test (see Figure 3.15). This was done to determine the strain gauge offsets (see Section 3.6.3) at the beginning and end of each test.

Data Sets

A total of eight sets of data were recorded from the instrumentation on the bicycle rig and bicycle. These data sets were stored in an eight column matrix:

Column 1: Handlebar acceleration

Column 2: Saddle acceleration

Column 3: Strain gauge readings from the front bracket

Column 4: Strain gauge readings from the crank arms

Column 5: Rotational velocity of the crank arms

Column 6: Rotational velocity of the roller
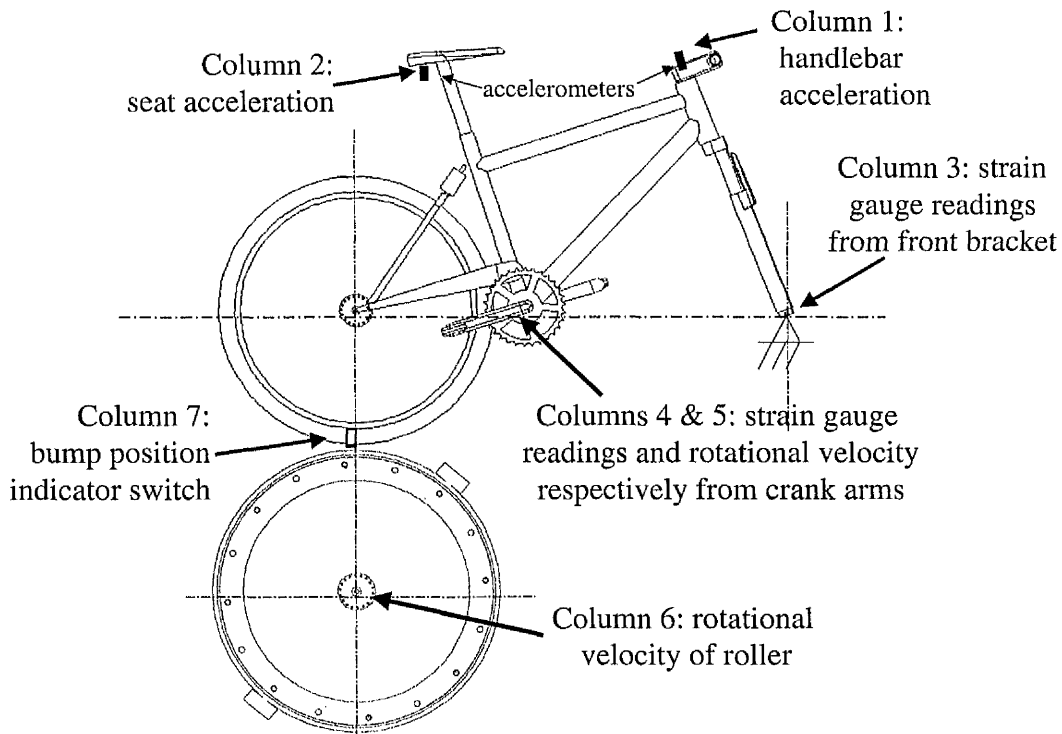
Figure 3.17: Schematic showing location from which data sets have been recorded on the cycling rig.

Column 7: Bump position indicator signal

Column 8: Pedal position indicator signal

The location from which these reading have been recorded on the cycling rig can be seen in Figure 3.17.

Sampling Frequency

A sampling frequency of 100 Hz was used. From power spectral density plots, the frequency range for saddle and handlebar acceleration was 0 to 30 Hz (see Figure 3.18), which was the largest frequency range and maximum frequency of any of the measure-
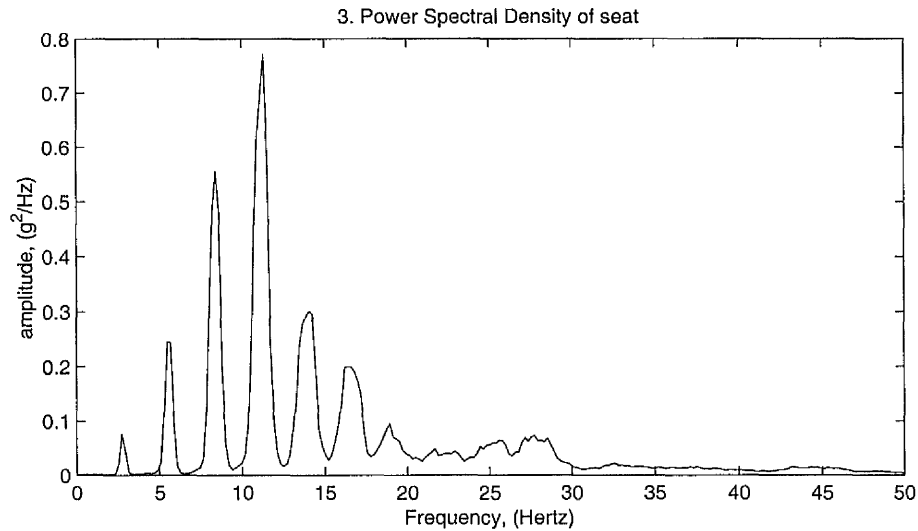
Figure 3.18: Power spectral density plot of the saddle acceleration during the bump test.

ments. The lowest sampling frequency that would avoid aliasing was used so that data file sizes remained reasonable and manageable. The same sampling frequency was used for all data sets so that each set of data was the same length for analysis purposes.

Data Points

Each complete data set consisted of more than 72000 data points. Test data started at the end of the 1st minute of the test (see Section 3.5.4) which corresponded to data point 6000 of the data sets. The test data ended at the end of the 11th minute of the test (see Section 3.5.4) which corresponded to data point 66000 of the data sets.

3.6 Mechanical Data Processing

3.6.1 Analysis Software

Matlab (Matlab, Version 5.3, http://www.mathworks.com) was used to analyse the data that was obtained from the cycling rig. The code was checked using data with known results.

3.6.2 Signal Filtering

The acceleration signal had a small offset which needed to be removed before velocity and subsequent displacement could be derived. Therefore a high pass Butterworth filter with a cutoff frequency of 1.5 Hz was used to filter the acceleration, velocity and displacement data sets for the handlebars and the saddle. The cumulative sum technique used to derive the velocity, and subsequently the displacement, also generated a small offset on the velocity and displacement which needed to be removed by the filter. A cutoff frequency of 1.5 Hz, which is the lowest frequency of interest in the acceleration signal, was applied. See Appendix C, Section C.1 for an example of the effects of applying the low pass filter.

3.6.3 Strain Gauge Offset and Drift Removal

To remove strain gauge offset and drift a zero load average of the first and last 300 points of the strain data sets were calculated (see Figure 3.15 for periods of zero load). A linear offset was calculated for each data point from the first and the last data averages and subtracted from the original data set. It was found that a linear drift

approximation between the average of the zero readings at the beginning of the test and at the end of the test was sufficient to remove drift.

$$Drift = offset_{zero\ load\ end} - offset_{zero\ load\ start} \tag{3.3}$$

$$offset(n) = \frac{Drift}{N} \cdot n + offset_{zero\ load\ start} \tag{3.4}$$

where $N = number\ of\ data\ points$ and $n = (1 : N)$

3.6.4 Calculation of Bicycle Dynamics

Saddle and Handlebar Acceleration

The accelerometer charge amplifier was calibrated to output 1 volt for 1 g of acceleration. A low pass zero phase shift filter was applied to the acceleration data to remove any DC shift.

Saddle and Handlebar Velocity

The vertical velocities (ν) of the saddle and the handlebars were derived from their vertical accelerations using a cumulative sum to approximate the integrations.

$$\nu_n = \sum_{i=1}^{n} \frac{(a_i - a_{mean}) \cdot g}{Sampling\ frequency} \ (m \cdot s^{-1}), \tag{3.5}$$

The low pass filter was then applied to the velocity data to remove any offset

that resulted from the cumulative sum. Any offset would be compounded when the displacement is calculated from the displacement.

Saddle and Handlebar Displacement

The vertical displacements (d) of the of the saddle and the handlebars were derived from the vertical velocity of the saddle and handlebars using a cumulative sum.

$$d_n = \sum_{i=1}^{n} \frac{(\nu_i - \nu_{mean})}{Sampling\ frequency}\ (m),\tag{3.6}$$

The low pass filter was then applied to the displacement data to remove any DC drift that resulted from the cumulative sum.

Tangential Pedal Velocity

$$\nu_{pedal} = 3.1923 \cdot V_{crank\ instrumentation} + 0.006\ (m \cdot s^{-1}),\tag{3.7}$$

(See Section 3.4.4 p 25 for the calibration of the velocity measurement instrumentation.)

Surface Velocity of the Roller

$$\nu_{roller\ surface} = 5.5455 \cdot V_{roller\ instrumentation} + 0.011\ (m \cdot s^{-1}),\tag{3.8}$$

(See Section 3.4.4 p 25 for the calibration of the velocity measurement instrumentation.)

Tangential Pedal Force

The pedal force (F_{pedal}) data was corrected by subtracting offset and drift as described in Section 3.6.3 p 36.

$$F_{pedal} = (10.877 \cdot (V_{pedal \ strain} - offset) - 0.1232) \cdot 9.806 \ (N), \qquad (3.9)$$

(See Section 3.4.4 p 24 for the calibration of the pedal force measurement instrumentation.)

Front Bracket Force

The front bracket force ($F_{frt \ brk}$) is a measure of the horizontal force applied at the front hub of the bicycle. It was hoped that this force would be a measure of the reactive force between the roller and the rear wheel and the horizontal force of the impact of the bump. However, critical analysis of the data showed that horizontal force applied by the inertia of the cyclist was far larger than expected. The front bracket force did, however, still give sufficient information for the comparison of the HT and SU bicycles during the bump and no bump tests (see Section 6.2.3 for the discussion of the front bracket force).

The front bracket force data was corrected by subtracting offset and drift as described in Section 3.6.3 p 36.

$$F_{frt\ brk} = (0.0776 - 60.798 \cdot (V_{frt\ brk\ strain} - offset)) \cdot 9.806\ (N), \quad (3.10)$$

(See Section 3.4.4 p 24 for the calibration of the front bracket force measurement instrumentation.)

During some of the tests the front bracket strain gauge reading had large sharp spikes which came from outside interference of which the source was unknown. The interference appeared to be dependent on the time of day. These were removed post data analysis and all affected variables were corrected accordingly.

Force Separation The front bracket force was separated out into; (1) the predicted reaction force, between the tyre and the surface of the roller, ($F_{frt\ brk\ pedal}$) on the front bracket exerted by force on the pedals and (2) other forces ($F_{frt\ brk\ other}$) which consisted of the inertial forces generated by the cyclist and the impact forces from the bumps on the roller during the bump tests.

$$F_{frt\ brk\ pedal} = F_{pedals} \cdot \frac{V_{pedals}}{V_{roller\ surf.}}\ (N) \quad (3.11)$$

$$F_{frt\ brk\ other} = F_{frt\ brk} - F_{frt\ brk\ pedal}\ (N) \quad (3.12)$$

Power Transmitted through the Pedals

The power transmitted through the pedals (P_{pedal}) was calculated by multiplying the tangential pedal force by the tangential pedal velocity.

$$P_{pedal} \quad = \quad F_{pedals} \cdot \nu_{pedals} \ (Watts), \tag{3.13}$$

Estimated Power Transmitted to the Roller

The estimated power transmitted ($Est. \ P_{frt \ brk}$) to the roller was calculated by multi-plying the force measured at the front bracket ($F_{frt \ brk}$) and the roller speed ($\nu_{roller \ surface}$). This is only an estimate power as the force measured at the front bracket is affected by the movement of the cyclist and not just by the force between the rear wheel and the roller surface (see Section 3.6.4 p 39).

$$Est. \ P_{frt \ brk} \quad = \quad F_{frt \ brk} \cdot \nu_{roller \ surface} \ (Watts), \tag{3.14}$$

3.6.5 Statistical Analysis

Difference between HT and SU Bicycles

The null hypothesis was applied to the mean of the differences measured between the HT and the SU bicycles and the single tailed upper confidence limits calculated to obtain the probability (P) that the population mean of the difference is zero. Low probabilities indicate that the null hypothesis is false and that the measured differences are evidence of a real difference in the underlying population.
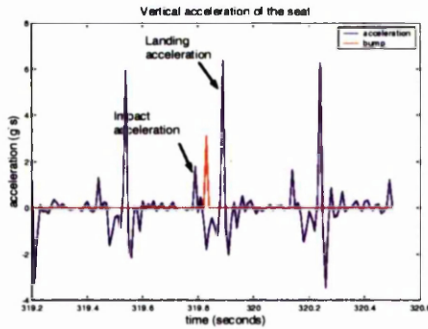
Figure 3.19: Plot of the vertical saddle acceleration and the bump impact indicator during the bump test. The acceleration from bump impact and that from the rear wheel landing on the roller after impact are marked.
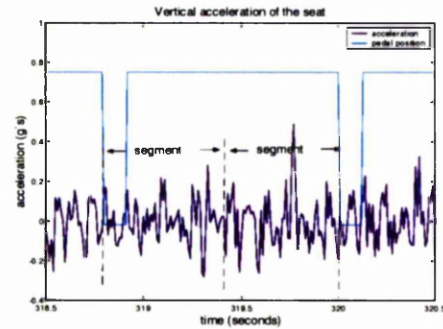
Figure 3.20: Plot of the vertical saddle acceleration and the pedal position indicator during the no bump test. The figure indicates the segments in which the maximum and minimum values have been determined.

Maximum and Minimum Values

The maximum and minimum values of acceleration for the saddle and handlebars during the tests were determined by finding the mean value of the individual means of each subject as described below. A similar method was used to determine the maximum and minimum values of force in Tables A.13 and A.16 and power in Tables A.14 and A.17.

For the bump tests, individual mean maximum acceleration values of bump impact and of the rear wheel landing on the roller surface were calculated from every second maximum value. The acceleration resulting from bump impact and landing is labelled in Figure 3.19. Every second maximum value was used because the bump impact indicator was used to determine the point of impact. This was a mean value of more than 1000 points which was considered sufficient for an accurate representation of the mean maximum and minimum values calculated during the bump test. The maximum acceleration resulting from bump impact (indicated on Figures 3.19 and by an (I) in Table 5.4 and Table A.9) occurred just before the indicator and the maximum acceler-

ation from the wheel landing (indicated on Figure 3.19 and by an (L) in Table 5.4 and Table A.9) occurred just after the indicator. The minimum values were also determined using the bump impact indicator.

For the no bump tests results, the pedal position indicator was used as a marker for segmenting the data into complete cycles. Individual means of each subject were determined from the maximum and minimum values for each segment (see Figure 3.20).

Results are presented in Chapter 5.

Chapter 4

Simulation

The reason for developing a dynamic model to simulate the rig was to help analyse the data from the experiments and to determine the difference between having a bicycle fixed at the front as it is on the rig and a bicycle that is allowed freedom of horizontal movement at the front hub. The model was constructed with the view to optimisation of rear suspension systems in the future.

The frame coordinates (cg of frame tubes and components, tube ends and angles, hinge points and points for applied constraints) were determined by inputting the coordinates of wheel axles, bottom bracket and angles of the head tube and seat tube provided by Marin Bicycles Web Page (2000) into a spreadsheet. The dynamic model was constructed using DADS (Dynamic Analysis and Design Systems) (http://www.lmsintl.com/).

44

4.1   Model Construction

4.1.1   Physical Properties

The geometric centres and end coordinates of both the HT and the SU frames were determined using a spreadsheet. The use of a spreadsheet allows for different frame geometries to be put into the model for analysis. The spreadsheet requires critical variables to be entered from the frame geometry and the geometric data required by the dynamic model is determined.

Figure 4.1: Marin Rocky Ridge (HT bicycle)

Figure 4.2: Marin Mount Vision (SU bicycle)

Hard tail Bicycle

The HT geometry was based on the Marin Rocky Ridge frame (Marin cycles, (Marin Bicycles Web Page 2000)) as used in the testing (see Figure 4.1 and Appendix F for geometry).

Suspension Bicycle

The SU geometry was based on the Marin Mount Vision frame (Marin cycles, (Marin Bicycles Web Page 2000)) as used in the testing (see Figure 4.2 and Appendix F for geometry).

Human Body
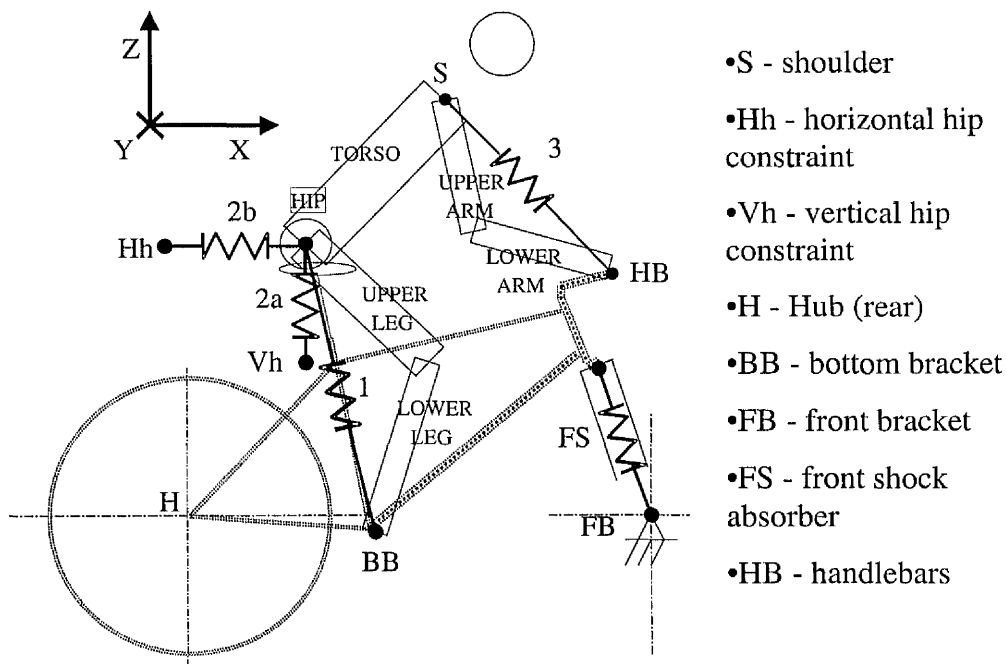
Figure 4.3: DADS human body model schematic.

The human body was adapted from the model used by Wilczynski & Hull (1994) for estimating surface induced frame loads during off-road cycling. They constructed the body from five body segments, the torso, upper and lower arm, and the upper and lower leg, and their model was configured for two different simulations, a rider standing up and a rider seated. During the current testing the subjects were seated

Body section properties		
Body Section	Length (m)	mass (kg)
Torso	0.51	38.25
Upper Leg	0.42	11.59
Lower leg	0.47	9.40
Upper Arm	0.32	4.10
Lower Arm	0.35	2.60
Body spring properties		
	Length (m)	Stiffness ($N \cdot m^{-1}$)	Damping (N)
Leg Spring (1)	0.82	40000	1200
Vert. Saddle Spring (2a)	0.06	50000	500
Horiz. Saddle Spring(2b)	0.08	8000	1200
Arm Spring (3)	0.60	6000	1000

Table 4.1: Table of simulated human body properties

(see Section 3.5.4 for reasoning), so the seated model was modified for rig simulations (see Figure 4.3). The same body segments were used in the current model with the addition of a sixth hip element, which was massless, but allowed a common point of connection for the saddle forces, the torso and the upper leg.

The saddle forces were simulated by a vertical compression only spring (2a), a horizontal bi-directional spring (2b) and a bi-directional leg spring (1) between the bottom bracket (BB) and the hip. The base of vertical spring 2a translated horizontally with the hip so that it always applied a vertical force.

Spring 1 holds the hip just above the top of spring 2a by a few millimetres. This means that the hip was held just above the saddle by the legs. The saddle on a bicycle applies unidirectional force with no force resistance to movement of the cyclist in the vertical before it is sat on. This is what the model is simulating and this configuration provides the closest simulation results to the test results.

The arm support was applied by spring 3 (see Table 4.1)

4.1.2 Tyre Simulation
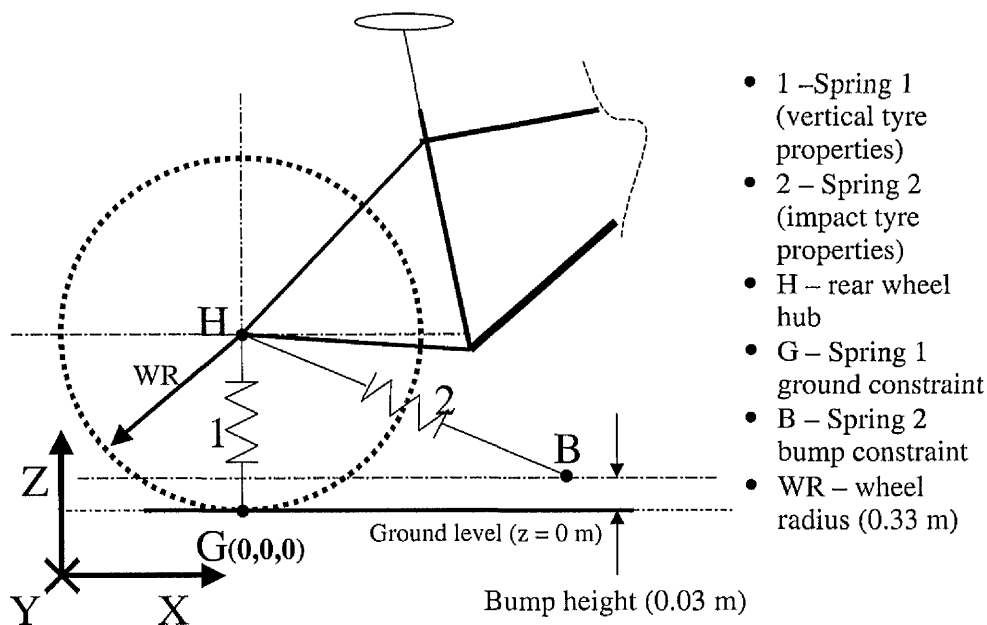
Figure 4.4: Sprung tyre simulation schematic.

The DADS software comes with a tyre model. However this installed tyre model could not be used in a stationary cycling rig model because it is designed for use with a moving vehicle and a fixed road. This meant that when the installed tyre model was used the front bracket, to which the bicycle is attached, had to move in the x direction while being constrained in the Y ($Y = 0\ m$) and Z ($Z = 0.03\ m$) directions (see Figure 4.4). The front bracket force could not be measured because there was nothing at the front bracket that could apply a reactive force, for analysis and comparison, and the result was a model that was not a true representation of the stationary cycling rig with a rolling road. For this reason a sprung tyre model (STM) was created to simulate bump impact on the rear wheel for both the stationary and the moving rig models.

Sprung tyre properties			
	Length (m)	Stiffness ($N \cdot m^{-1}$)	Damping (N)
Spring 1	0.33	100 000	120
Spring 2	0.33	45 000	120

Table 4.2: Table of sprung tyre properties

The STM allowed for the comparison of a moving and a stationary cycling rig simulation and for the measurement of the front bracket force for the stationary rig model simulations.

The STM consisted of two compression only springs which meant that when the tyre left the ground there was no downward force applied by the springs. The springs were of equal length to the radius of an unloaded bicycle tyre (see Figure 4.4) and were attached to the hub of the rear wheel.

The vertical tyre force was simulated by spring 1. The base of the spring (point G in Figure 4.4) was constrained to $Z = 0.0\ m$ and $Y = 0.0\ m$ with reference to the origin (point G in Figure 4.4). The x coordinate of the base of the spring was constrained to the X coordinate of the rear wheel hub ($X_G = X_H$). This ensured that the force applied by spring 1 remain vertical (see Table 4.2 for spring properties).

The bump impact force was applied by spring 2. The base of the spring (point B in Figure 4.4) was constrained to $Z = 0.03\ m$ and $Y = 0.0\ m$ with reference to the origin (point G in Figure 4.4). Bump impact force was applied in three ways. The base of spring 2 was given: (1) a fixed x distance in the moving rig model[1], (2) a velocity in the x direction, set to follow a predetermined[2] spline curve (fixed velocity simulation)[3], (3) or an initial x distance, an initial velocity in the x direction and mass (equivalent

---

[1]The moving rig model was used to compare the DADS tyre model with the STM (see Section 4.2.1).

[2]The predetermined spline cure was generated by a model that allowed for velocity change of the moving body as a result of bump impact. This velocity curve was then modified if required and applied to the bump of the equivalent fixed rig model simulations (see Section 4.2.2).

[3]This simulation was used to measure the bump impact forces (see Section 4.2.2).

momentum simulation)[4]. See Sections 4.2.1, and 4.2.2 respectively for a description of the models that use the 'fixed velocity' and 'equivalent momentum' simulations (see Table 4.2 for spring properties).

4.2   Model Development

The cyclist: Is rigid and fixed to the frame or is constrained using springs

The frame: The frame is either rigid (HT model) or sprung (SU model)

The rear wheel: forces transmitted through tyre or spring combination

The front bracket: free to move along X axis or fixed to ground

Bump: fixed to ground or free to move along X axis
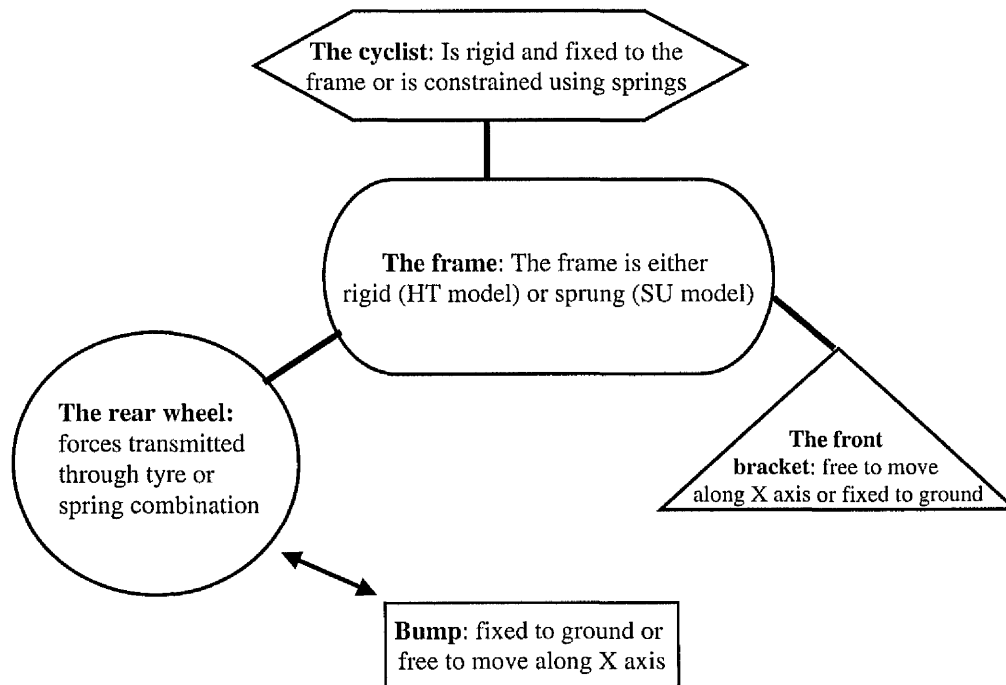
Figure 4.5: A schematic of the DADS model, showing the main elements common to all models.

The DADS model analysed a single impact of a bump. For all the simulations the model was allowed 10 seconds of simulation time before bump impact to allow the model to come to a state of complete equilibrium before impact with the bump. This ensured that the conditions before bump impact for all models were the same.

_____

[4]This simulation was used to measure the velocity change resulting from bump impact (see Section 4.2.2).

Figure 4.5 shows the main elements that are common to all the models and the different possible constraints of each element.
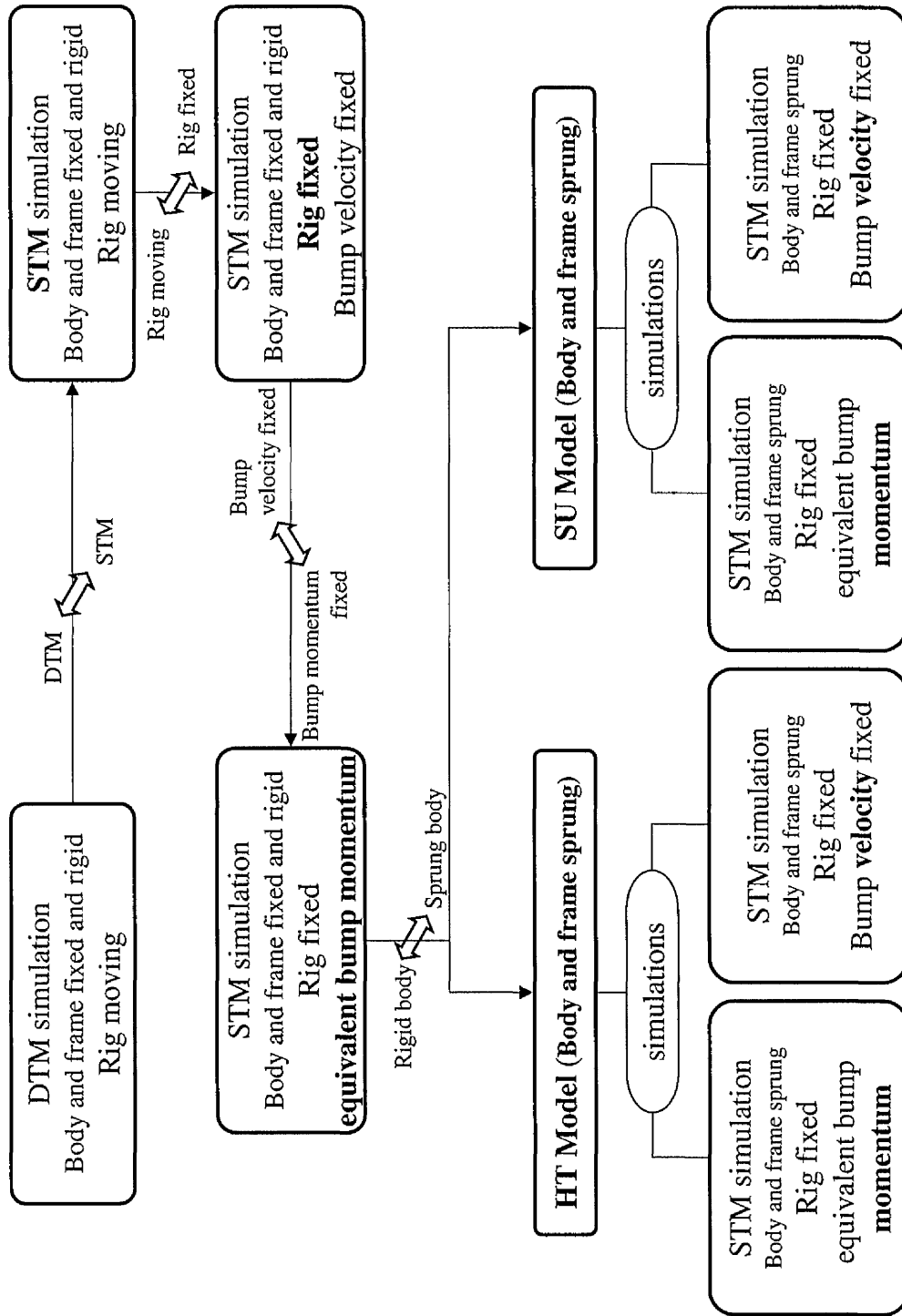
Figure 4.6: Flow diagram plotting the development of the DADS HT and SU models. The changes between each model are shown by the double headed arrow between each model. (Abbreviations: DTM, DADS Tyre Model; STM, Sprung Tyre Model.)

4.2.1 DADS Tyre Model
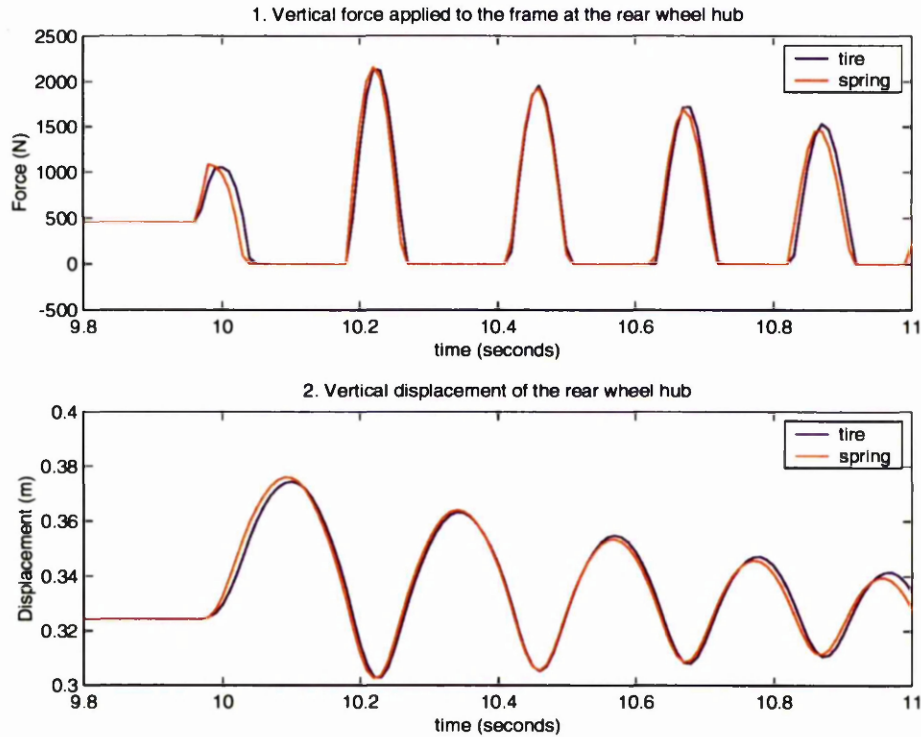
Figure 4.7: Plot of the vertical force on the frame at the rear hub and the vertical displacement of the rear wheel of the DADS HT model with the DADS tyre model and sprung tyre model with the rig moving (Body rigid and fixed to bicycle frame).

To determine the correct tyre characteristics for bump impact and landing the tyre model within DADS (DTM) was used. This model could not be used for simulating the rig because it is required to roll on a stationary road. For the simulation of the rig a tyre model was created using springs (see Section 4.1.2) of set stiffness and damping (see Table 4.2). This was compared to the DTM by applying the same initial conditions before bump impact in the simulation of both the models. The spring stiffness and damping values of the STM were set so that the vertical force at, and the vertical displacement of the rear wheel hub were the same as those for the DTM (see Figure 4.7).

This confirmed that the STM could give the same results at the DTM and could then be used as a new tyre model. For the tyre model comparisons the body of the cyclist was held rigid and fixed to the frame of the bicycle.

4.2.2 Sprung Tyre Models

The STM had two advantages over the DTM for the purpose of the cycling rig simulation. It allowed comparison of the results from the moving front bracket and the fixed front bracket and the comparison of the results from a bump with fixed velocity and equivalent momentum, in other words giving the bump a set mass equivalent to that of the cyclist/bicycle and an initial velocity.

The comparison of the results from the moving front bracket and the fixed front bracket (fixed bump velocity) showed a difference in the dynamic behaviour of the body (see Figure 4.8). That meant that a fixed rig model needed to be used for the analysis of the cycling rig result, because it resembled more closely the experimental rig.

The results from the equivalent momentum and the fixed velocity simulations, conducted using fixed front brackets and rigid subjects (fixed to frame to form a single unit), are shown in Figure 4.9.

Fixing the momentum of the bump, so that it was the equivalent of the cyclist and bicycle, allowed for analysis of the effect of bump impact on the velocity changes of the bump. This is in effect the analysis of the changes of velocity of the cyclist and bicycle, since the inertia is the same. There is a consequent loss in useful energy because of the drop in velocity. (Useful energy is discussed in Section 6.3 and is defined as energy that contributes to forward motion of the bicycle.)

The ability to fix the velocity of the bump allowed for the full duration of the force
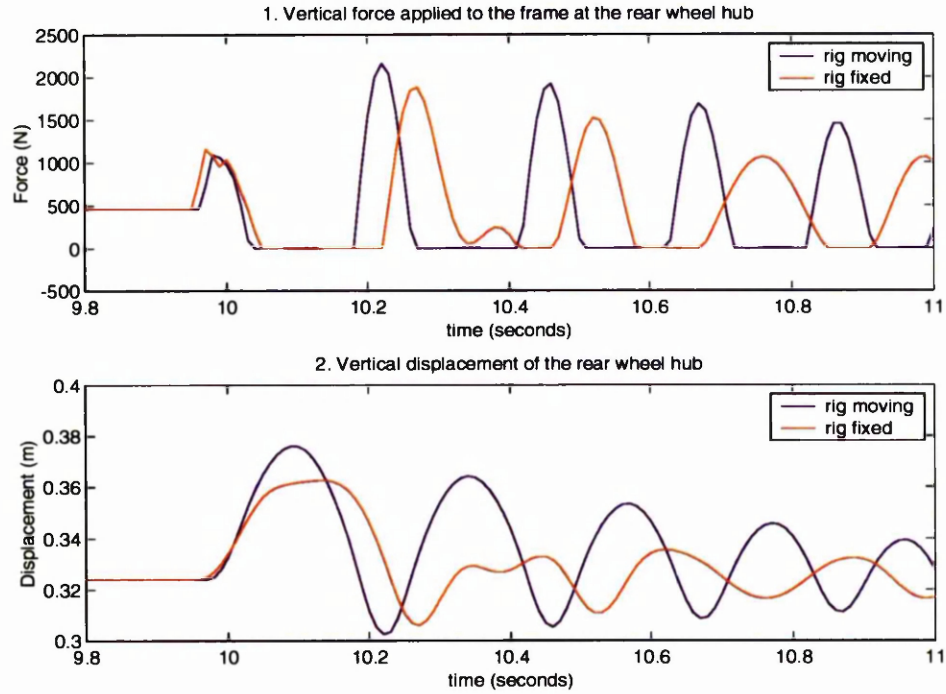
Figure 4.8: Plot of the vertical force on the frame at the rear hub and the vertical displacement of the rear wheel of the DADS HT moving rig and fixed rig models using the sprung tyre model (Body rigid and fixed to bicycle frame).

applied by the bump, because the bump impact is applied by a point force (see Section 4.1.2, Figure 4.4, point B), thus allowing the measurement of more accurate vertical and horizontal forces, than the equivalent momentum simulation, for comparison of the HT and SU models (see Section 4.3 and 4.4). If this bump impact force results from a bump with a mass and velocity, instead of a fixed velocity, and the wheel remains in contact with the bump after the initial impact, then the time duration of force applied between the bump and the tyre is incorrect (see Figure 4.10). When the bump impacts the tyre, the tyre and suspension system deflect. If the time of bump impact (t_{bump}) is too short, then the recovery of the tyre and suspension system does not apply a vertical force for long enough.
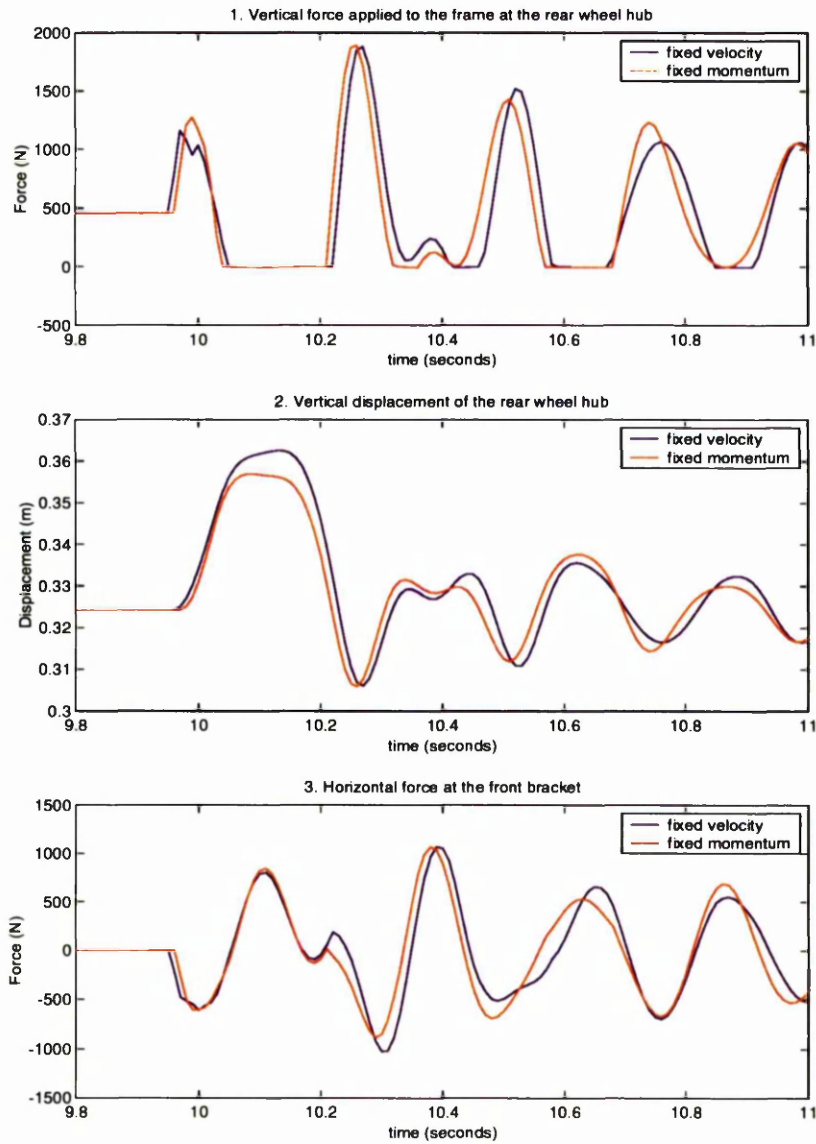
Figure 4.9: Plot of the vertical force on the frame at the rear hub, the vertical displacement of the rear wheel and the horizontal force at the front bracket of the DADS HT model with the fixed velocity and the equivalent momentum simulations (Body rigid and fixed to bicycle frame).
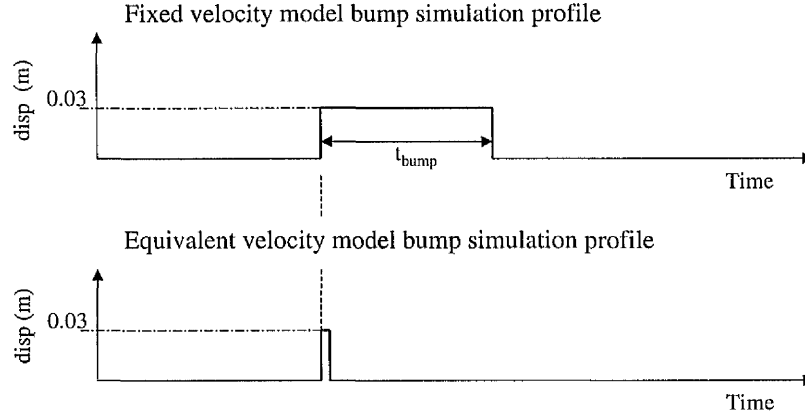
Figure 4.10: Schematic of the bump profiles with respect to time for the fixed velocity and the equivalent momentum models.

There is no difference in the HT model simulations of fixed velocity and equivalent momentum (see Section 4.3) because the rear wheel gets knocked into the air by the initial impact. However, there are differences in the SU model simulations (see Section 4.4). The time duration added to the fixed velocity simulations was applied when the bump reached $X = 0$ (see Figure 4.4) for the duration of the time t_{bump} (see Figure 4.10) where $t_{bump} = \frac{w_{bump}}{\nu_{bump}}$.

The *bump velocity* (ν_{bump}) was determined from the equivalent momentum simulations (see Figure 4.11). Inserting t_{bump} at $X = 0$ does not apply the correct tyre force during this time. This is because the impact force of the bump is applied with spring 2 which has a lower stiffness (see Table 4.2). During this time the tyre is pushed upwards by the flat top surface of the bump, and that force should be simulated by spring 1 of the sprung tyre simulation. The force applied by the impact spring (spring 2) is, however, sufficient for a more accurate simulation of the rear wheel bump impact than that applied by the equivalent momentum model.
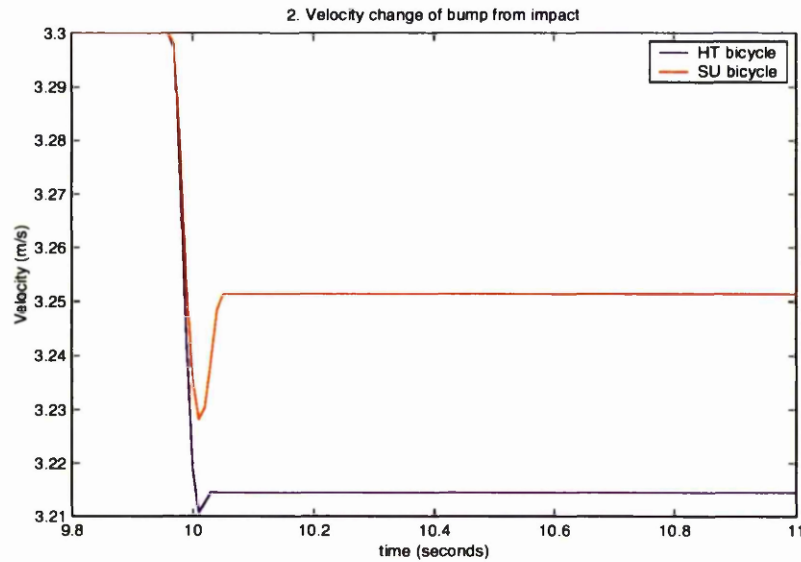
Figure 4.11: Plot of the velocity of the bump of the DADS HT and SU model equivalent momentum simulations

A fixed velocity and the equivalent momentum simulation was done for both the HT and the SU models using both the sprung tyre and sprung body (see Section 4.2.2 and 4.1.1 respectively). The values of tyre and body spring stiffnesses were adjusted to achieve similar results to those of the testing (see Section 6.2.3).

4.3 HT Model

The HT model simulated the cycling rig and the HT bicycle. The front bracket was fixed to ground and the body sprung for all simulations of the model and the results compared to the test results(see Section 6.2.3). The velocity values for the bump of the equivalent momentum HT model simulation were applied to the bump in the fixed velocity simulation with an inserted pause period for the duration of the width of
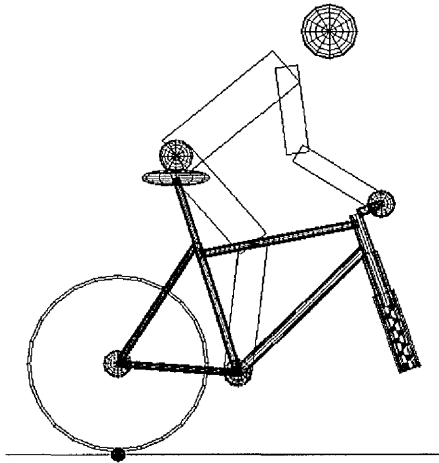
Figure 4.12: DADS HT model   Figure 4.13: DADS SU model
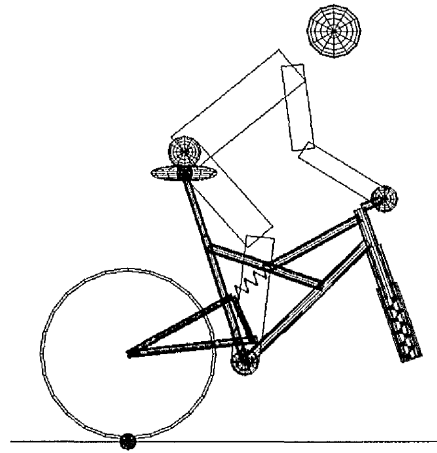
the top of the bump surface (see Section 4.2.2). The results of both the equivalent momentum and the fixed velocity simulations were the same for the vertical force at the rear wheel, the vertical acceleration of the saddle and the horizontal force at the front bracket (see Figure 4.14).

4.4 SU Model

The SU model simulated the cycling rig and the SU bicycle. The front bracket was fixed and the body sprung for all simulations of the model and the results compared to the test results(see Section 6.2.3). The velocity values for the bump of the equivalent momentum SU model simulation were applied to the bump in the fixed velocity simulation with an inserted pause period for the duration of the width of the top of the bump surface (see Section 4.2.2). The results of both the equivalent momentum
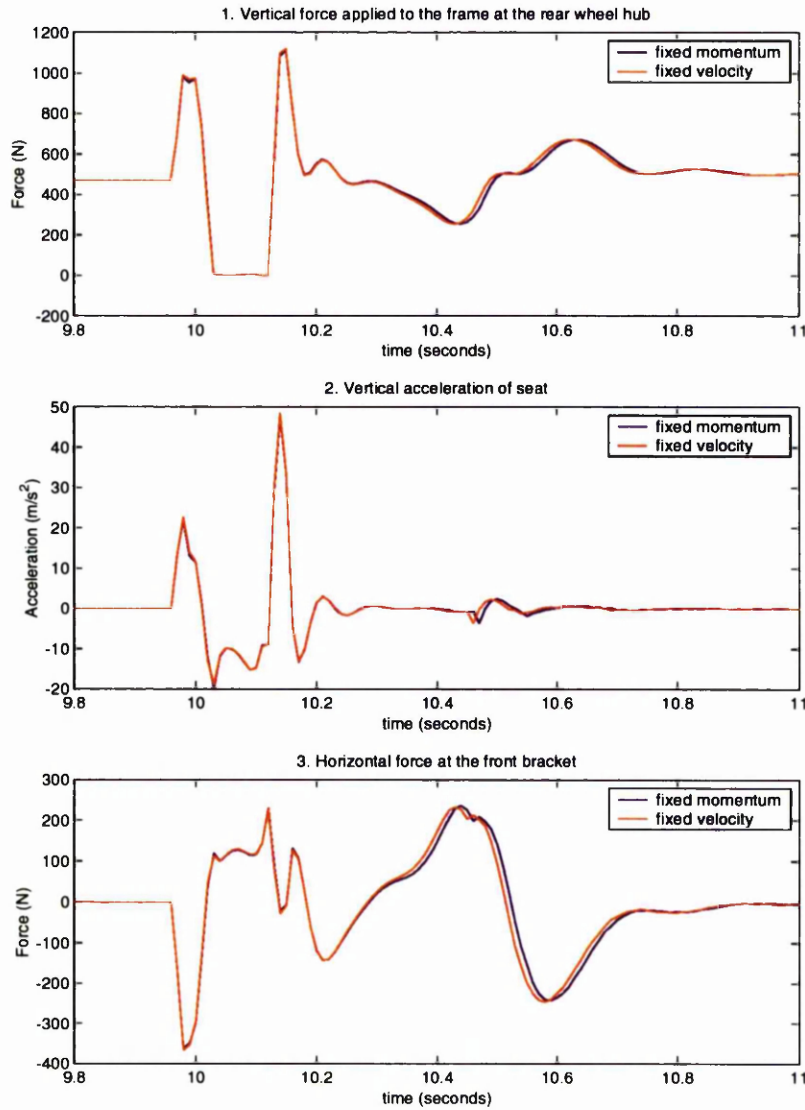
Figure 4.14: Plot of the vertical force on the frame at the rear hub, the vertical displacement of the rear wheel and the horizontal force at the front bracket of the DADS HT model with the rig fixed (body sprung) and an impact bump with an initial momentum and with fixed velocity.
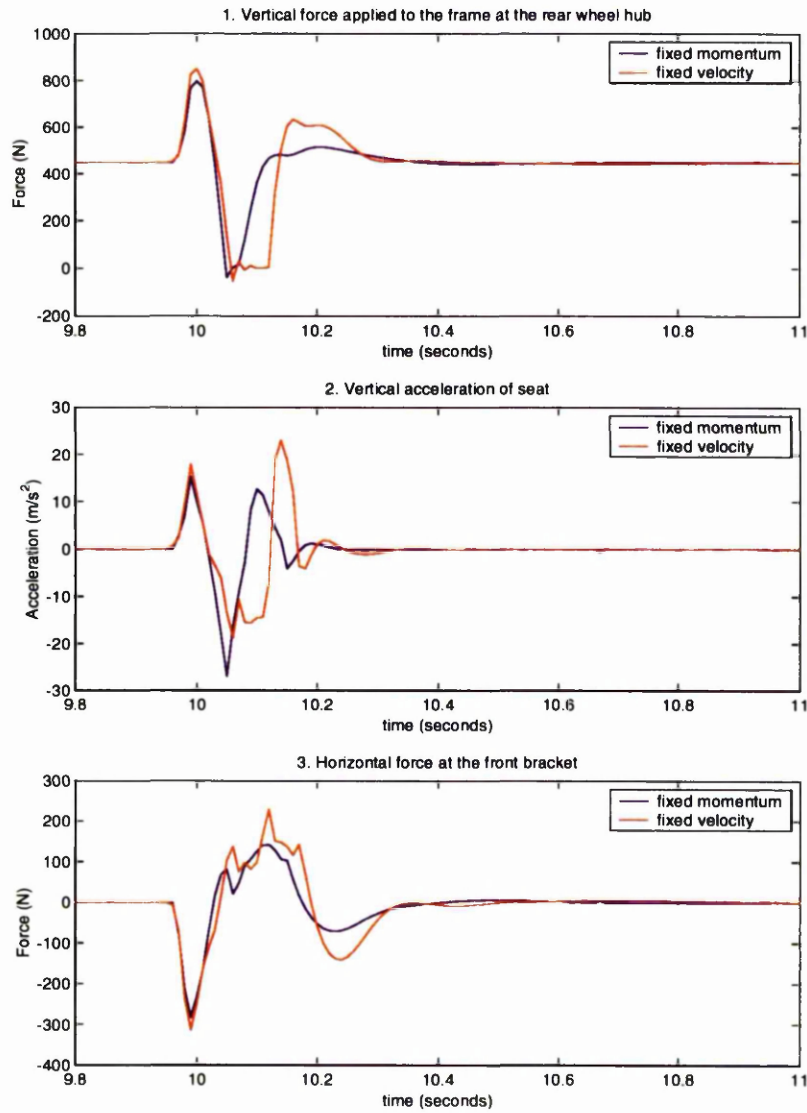
Figure 4.15: Plot of the vertical force on the frame at the rear hub, the vertical displacement of the rear wheel and the horizontal force at the front bracket of the DADS SU model with the rig fixed and an impact bump with an initial momentum and with fixed velocity (Body of the subject sprung).

and the fixed velocity simulations differed for the vertical force at the rear wheel, the vertical acceleration of the saddle and the horizontal force at the front bracket (see Figure 4.15). This is attributed to the rear wheel remaining in contact with the bump for a greater length of time because of the rear suspension system.

Chapter 5

Results

5.1 Physiological Results

To ensure that the results of the physiological testing were reliable, a limit was set on the percentage difference between the $\dot{V}O_2$ values, for the 9th and the 10th minutes, of 5%.

Eighteen subjects took part in the testing, of which 15 did the bump tests and 12 did the no bump tests. Eight subjects for both the bump test and the no bump test had a $\dot{V}O_2$ difference of 5% or less. Six subjects took part in both the bump and no bump tests.

The physiological results that follow are for the subjects that satisfied the above mentioned criteria.

Scatter plots of the $\dot{V}O_2$, heart rate and energy expenditure results are provided to give a visual impression of the differences between the HT and SU bicycles. The null hypothesis was applied to the mean of the differences measured between the HT and

the SU bicycles and the single tailed upper confidence limits calculated to obtain the probability (P) that the population mean of the difference is zero. Low probabilities indicate that the null hypothesis is false and that the measured differences are evidence of an actual difference in the underlying population.

5.1.1 Bump Tests

The mean $\dot{V}O_2$ difference between the HT and SU bicycles was 9.14 ml $\cdot$ kg^{-1} $\cdot$ min^{-1} (standard deviation (s)=2.57, $P < 0.001$), the mean heart rate difference was 34 beats $\cdot$ min^{-1} (s=10.8, $P < 0.001$) and the mean energy expenditure difference was 14.42 KJ $\cdot$ min^{-1} (s=3.87, $P < 0.001$). These results show a significant advantage for the SU bicycle.

The mean difference between the RPE ratings for the HT and the SU bicycles was 1.83 (s=2.02, $P < 0.025$), and the mean difference between the comfort ratings was -1.87 (s=0.96, $P < 0.001$), both measures indicating a preference for the SU bicycle.

5.1.2 No Bump Tests

The mean $\dot{V}O_2$ difference between the HT and the SU was -2.18 ml $\cdot$ kg^{-1} $\cdot$ min^{-1} (s=1.69, $P < 0.005$), the mean heart rate difference was -3 beats $\cdot$ min^{-1} (s=6.35, $0.1 < P < 0.25$) and the mean energy expenditure difference was -2.98 KJ $\cdot$ min^{-1} (s=2.42, $P < 0.025$). These results indicate an advantage for the HT bicycle.

The mean difference between the RPE ratings for the HT and the SU bicycles was -0.54 (s=1.22, $0.1 < P < 0.25$), and on the comfort scale there was a mean difference of 0.25 (s=0.38, $0.1 < P < 0.25$), both measures indicating a slight preference for the HT bicycle.

5.1.3 Figures

Figure 5.1 shows a plot of $\dot{V}O_2$ values from the HT bicycle plotted against those of the SU bicycle. It shows two clear groupings of values above and below the equality line for the bump and no bump tests respectively. Figure 5.2 and 5.3 show results for the heart rate and energy expenditure respectively using the same format.
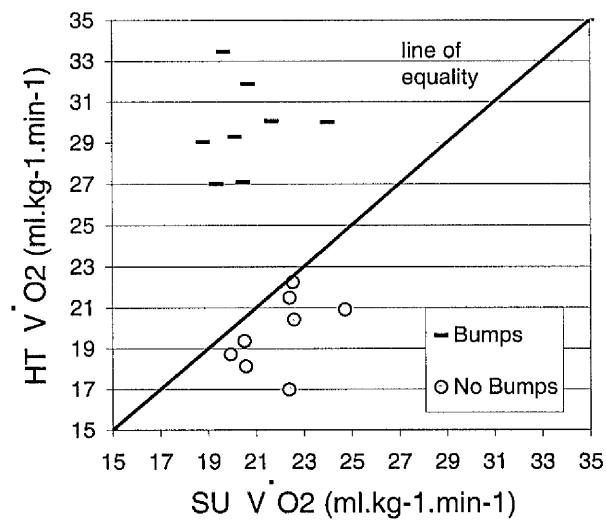
Figure 5.1: Comparison of VO_2 values between the HT and SU bicycles during the bump and no bump tests.

Figure 5.4 shows the range of RPE ratings given by the subjects for each bicycle at the 3rd, 6th and 9.5^{th} minute of the bump and no bump tests. Figure 5.5 shows the comfort data in the same format.
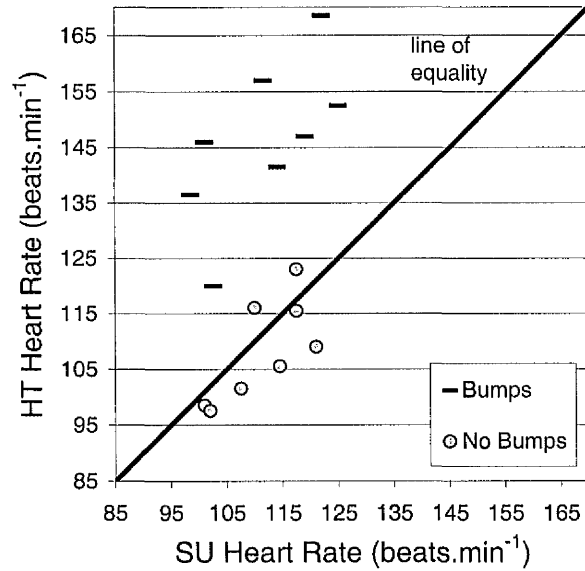
Figure 5.2: Comparison of heart rate values between the HT and SU bicycles during the bump and no bump tests.
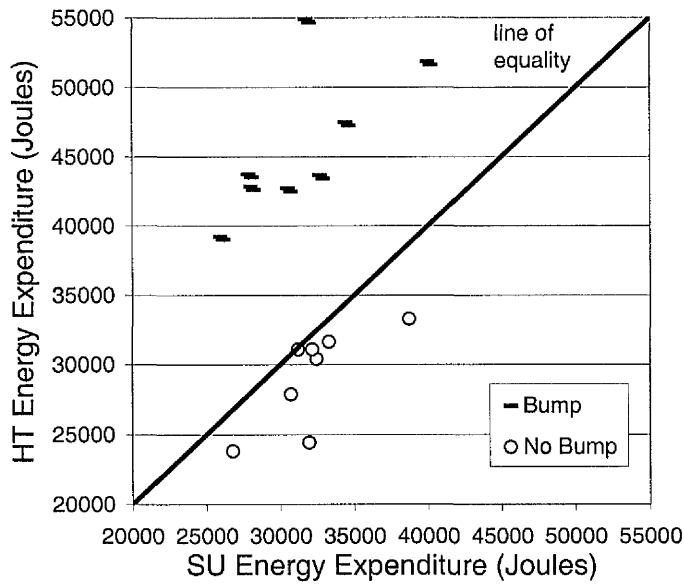
Figure 5.3: Comparison of energy expenditure values between the HT and SU bicycles during the bump and no bump tests.
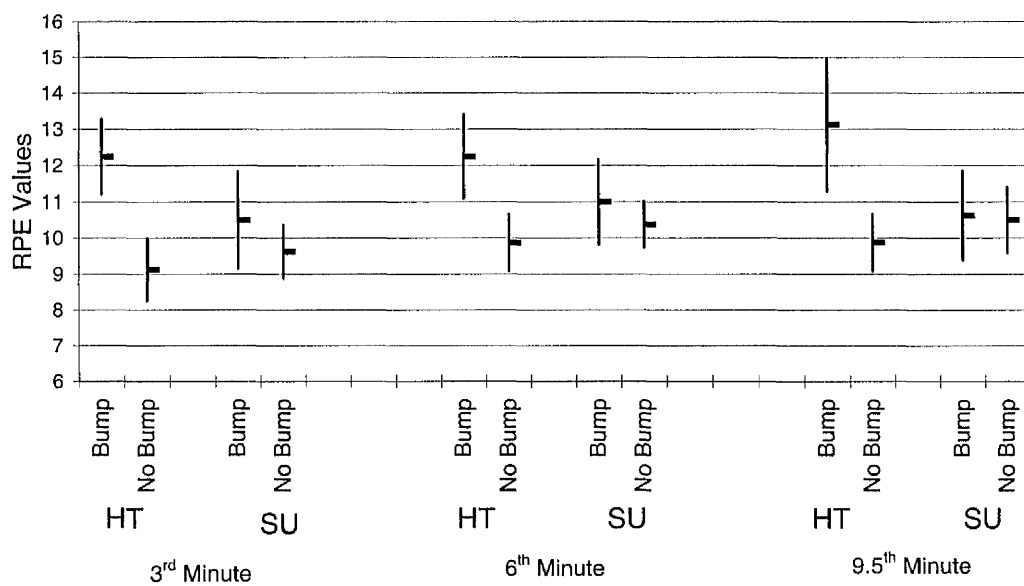
Figure 5.4: Comparison of RPE rating ranges between the HT and SU bicycles during the bump and no bump tests.
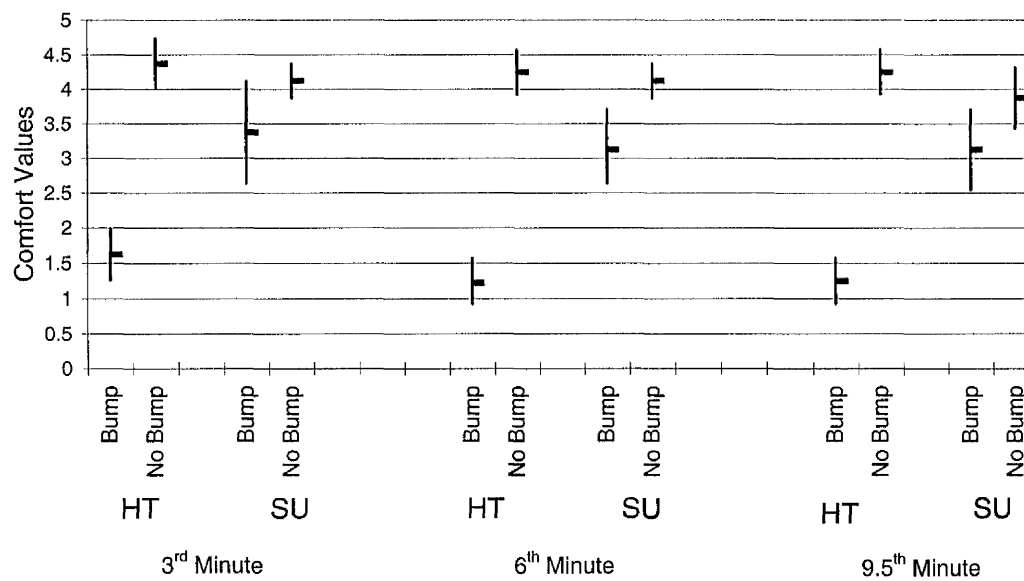
Figure 5.5: Comparison of comfort rating ranges between the HT and SU bicycles during the bump and no bump tests.

5.1.4 Tables

Table 5.1 shows the mean values and standard deviations for $\dot{V}O_2$, heart rate, RPE and comfort ratings recorded during the bump and no bump tests. Table 5.2 shows the mean differences between the HT and the SU bicycles for the RPE and comfort ratings during the 3rd, 6th and 9.5^{th} minutes of the bump tests and the no bump tests. This shows that the subject's response varies with time through the test. It should be noted that SU values have been subtracted from HT values, i.e. a positive difference for RPE ratings means that there is less perceived exertion on the SU bicycle but a negative difference for comfort ratings means that the SU bicycle is more comfortable.

	Bump		No Bump	
	HT	SU	HT	SU
VO_2 ($ml \cdot kg^{-1} \cdot min^{-1}$)	29.73 ± 2.19	20.59 ± 1.64	19.77 ± 1.79	21.96 ± 1.55
Heart Rate ($beats \cdot min^{-1}$)	146 ± 14.4	111 ± 10.1	108 ± 9.2	111 ± 7.5
Energy Expenditure ($KJ \cdot min^{-1}$)	45.81 ± 5.24	31.39 ± 4.46	29.20 ± 3.48	32.17 ± 3.30
RPE (Borg scale, 6-20 scale)	12.54 ± 1.87	10.7 ± 1.6	9.62 ± 1.11	10.16 ± 0.99
Comfort rating (1 to 5)	1.33 ± 0.44	3.2 ± 0.85	4.29 ± 0.45	4.04 ± 0.42

Table 5.1: Mean values and standard deviations (mean±s) for VO_2, heart rate, energy expenditure, RPE and comfort ratings during the bump and no bump tests.

5.2 Mechanical Systems Results

The mechanical results presented are from the tests in which the subjects $\dot{V}O_2$ difference between the 9th and the 10th minutes was equal to or less than 5% (see Section 5.1 p. 63 for set criteria).

	Minute	3rd	6th	9.5^{th}
RPE	Bump Test Difference of means between HT and SU	1.75	1.25	2.50
RPE	No Bump Test Difference of means between HT and SU	−0.5	−0.5	−0.625
Comfort	Bump Test Difference of means between HT and SU	−1.75	−2.00	−1.875
Comfort	No Bump Test Difference of means between HT and SU	0.25	0.125	0.375

Table 5.2: Difference of means of RPE and comfort ratings between HT and SU bicycles during the 3rd, 6th and 9.5^{th} minutes.

5.2.1 Tables

All the mechanical data for the HT and SU tests have been tabulated in this section. Plots of the mechanical data are in Section 6.2. As with the physiological results the SU values have been subtracted from HT values where differences between the bicycles have been tabulated.

For the method of calculating the averaged values in Tables 5.3, 5.4, 5.5 and 5.6 see Section 3.6.5, p 42.

Table 5.3 shows the averaged maximum and minimum values of vertical handlebar acceleration, velocity and displacement of the HT and SU bicycles, showing the difference between the maximum values and the difference between the minimum values during the bump and no bump tests. The table further shows the total displacement of the handlebars and the difference in displacement for the HT and SU bicycles during these tests.

Table 5.4 shows the averaged maximum and minimum values of vertical saddle acceleration, velocity and displacement of the HT and SU bicycles, showing the difference between the maximum values and the difference between the minimum values

during the bump and no bump tests. The table further shows the total displacement of the saddle and the difference in displacement for the HT and SU bicycles during these tests.

Table 5.5 shows the averaged maximum and minimum values of the force applied perpendicular to the crank arms at the pedals and the force applied to the front bracket of the HT and SU bicycles, showing the difference between the maximum values and the difference between the minimum values during the bump and no bump tests. The table further shows the range and mean of the force applied perpendicular to the crank arms at the pedals and the force applied to the front bracket and the differences in force range and mean force for the HT and SU bicycles during these tests.

Table 5.6 shows the averaged maximum and minimum values of the power generated at the pedals and the estimated power generated at the roller of the HT and SU bicycles, showing the difference between the maximum values and the difference between the minimum values during the bump and no bump tests. The table further shows the range and mean of the power generated at the pedals and the estimated power generated at the roller and the differences in power range and mean power for the HT and SU bicycles during these tests.

Individual subject results of handlebar and saddle vertical acceleration (Table A.6 and Table A.9 respectively), vertical velocity (Table A.7 and Table A.10 respectively), displacement (Table A.8 and Table A.11 respectively), pedal and roller velocity (Table A.12 and Table A.15 respectively), pedal force and power (Table A.13 and Table A.14 respectively) and front bracket force and power (Table A.16 and Table A.17 respectively) can be found in Appendix A.

5.2.2   Impact Time Intervals

For analysis of bump impact data plotted against time, time intervals were calculated for specific events. The mean velocity of the roller surface, 3.38 $m \cdot s^{-1}$, during the tests was used for all calculations. At this speed, the point of impact of the wheel with the bump occurs approximately 0.03 seconds before the front of the bump reaches the vertical position, and the last possible point of contact of the wheel and the bump is 0.081 seconds after impact. The time taken to traverse the top of the bump is 0.021 seconds (see Appendix B.1). At 3.38 m·s^{-1} the frequency of bump impact was 3.53 Hz.

Track	Bump		No Bump	
Bicycle	Hard tail	Suspension	Hard tail	Suspension
Max accel. (g's)	1.534	0.997	0.081	0.066
Min accel. (g's)	-1.292	-0.844	-0.086	-0.065
Diff in max. accel. (g's)	0.537 s =0.142 P < 0.001		0.015 s =0.010 P < 0.005	
Diff in min. accel. (g's)	-0.448 s =0.209 P < 0.001		-0.021 s =0.012 P < 0.001	
Max vel. $(m \cdot s^{-1})$	0.225	0.076	0.012	0.009
Min vel. $(m \cdot s^{-1})$	-0.164	-0.085	-0.011	-0.009
Diff in max. vel. $(m \cdot s^{-1})$	0.149 s =0.031 P < 0.001		0.003 s =0.002 P < 0.001	
Diff in min. vel. $(m \cdot s^{-1})$	-0.078 s =0.020 P < 0.001		-0.002 s =0.002 P < 0.005	
Max displ. (mm)	6.686	2.089	0.467	0.308
Min displ. (mm)	-5.265	-2.404	-0.456	-0.312
Total displ. (mm)	11.950	4.493	0.923	0.620
Diff in max. displ. (mm)	4.596 s =1.260 P < 0.001		0.160 s =0.080 P < 0.001	
Diff in min. displ. (mm)	-2.860 s =0.709 P < 0.001		-0.144 s =0.083 P < 0.001	
Diff in total displ. (mm)	7.457 s =1.841 P < 0.001		0.304 s =0.163 P < 0.001	

Table 5.3: Table of the averaged maximum and minimum values of vertical handlebar acceleration, velocity and displacement of the HT and SU bicycles, showing the difference between the maximum values and the difference between the minimum values during the bump and no bump tests. The table further shows the total displacement of the handlebars and the difference in displacement for the HT and SU bicycles during these tests.

Track	Bump		No Bump	
Bicycle	Hard tail	Suspension	Hard tail	Suspension
Max accel.(I) (g's)	2.615	1.161	0.293	0.286
Max accel.(L) (g's)	6.481	5.090	0.000	0.000
Min accel. (g's)	-2.900	-2.675	-0.311	-0.308
Diff in max.(I) accel. (g's)	1.454 s =0.109 P < 0.001		0.007 s =0.022 P > 0.100	
Diff in max.(L) accel. (g's)	1.391 s =0.853 P < 0.005		no landing acceleration	
Diff in min. accel. (g's)	-0.225 s =0.424 P < 0.100		-0.002 s =0.026 P > 0.100	
Max vel. $(\mathrm{m \cdot s^{-1}})$	0.536	0.322	0.044	0.045
Min vel. $(\mathrm{m \cdot s^{-1}})$	-0.693	-0.344	-0.047	-0.047
Diff in max. vel. $(\mathrm{m \cdot s^{-1}})$	0.214 s =0.041 P < 0.001		-0.001 s =0.004 P > 0.100	
Diff in min. vel. $(\mathrm{m \cdot s^{-1}})$	-0.349 s =0.061 P < 0.001		0.001 s =0.004 P > 0.100	
Max displ. (mm)	16.876	7.063	1.678	1.792
Min displ. (mm)	-7.588	-5.560	-1.565	-1.685
Total displ. (mm)	24.464	12.623	3.242	3.477
Diff in max displ. (mm)	9.812 s =1.753 P < 0.001		-0.114 s =0.148 P < 0.050	
Diff in min displ. (mm)	-2.029 s =1.064 P < 0.001		0.121 s =0.182 P < 0.050	
Diff in total displ. (mm)	11.841 s =2.661 P < 0.001		-0.235 s =0.321 P < 0.050	

Table 5.4: Table of the averaged maximum and minimum values of vertical saddle acceleration, velocity and displacement of the HT and SU bicycles, showing the difference between the maximum values and the difference between the minimum values during the bump and no bump tests. The table further shows the total displacement of the saddle and the difference in displacement for the HT and SU bicycles during these tests. Key: (I) is the maximum acceleration resulting from bump impact (for bump test only). (L) is the maximum acceleration resulting from ground impact (landing) after leaving the bump (for bump test only).

Track	Bump		No Bump	
Bicycle	Hard tail	Suspension	Hard tail	Suspension
Pedal force data (Newtons)				
Max pedal force	253.814	131.323	126.318	92.153
Min pedal force	-0.310	-2.947	23.646	26.334
Force range	254.124	134.270	102.672	65.819
Mean pedal force	124.238	65.238	80.195	63.968
Diff in max pedal force	122.491 s =32.602 P < 0.001		34.165 s =36.964 P < 0.025	
Diff in min pedal force	2.637 s =8.146 P > 0.100		-2.688 s =6.315 P > 0.100	
Diff in force amplitude	119.854 s =28.095 P < 0.001		36.853 s =35.837 P < 0.025	
Diff in mean pedal force	59.000 s =19.320 P < 0.001		16.228 s =20.551 P < 0.050	
Front bracket force data (Newtons)				
Max frt brk force	291.977	247.011	99.884	104.648
Min frt brk force	-469.526	-271.618	-44.483	-48.193
Force range	761.503	518.629	144.367	152.841
Mean frt brk force	34.318	20.840	26.982	28.249
Diff in max frt brk force	44.966 s =29.339 P < 0.005		-4.764 s =11.069 P > 0.100	
Diff in min frt brk force	-197.907 s =35.090 P < 0.001		3.709 s =12.399 P > 0.100	
Diff in force range	242.874 s =49.762 P < 0.001		-8.473 s =21.486 P > 0.100	
Diff in mean frt brk force	13.479 s =15.442 P < 0.025		-1.267 s =4.644 P > 0.100	

Table 5.5: Table of the averaged maximum and minimum values of the force applied perpendicular to the crank arms at the pedals and the force apply to the front bracket of the HT and SU bicycles, showing the difference between the maximum values and the difference between the minimum values during the bump and no bump tests. The table further shows the range and mean of the force applied perpendicular to the crank arms at the pedals and the force applied to the front bracket and the differences in force range and mean force for the HT and SU bicycles during these tests.

Track	Bump		No Bump	
Bicycle	Hard tail	Suspension	Hard tail	Suspension
Pedal power data (Watts)				
Max pedal power	275.2	141.5	140.1	107.9
Min pedal power	-0.4	-2.9	26.5	30.9
Power range	275.6	144.4	113.6	77.0
Mean pedal power	134.1	70.1	88.8	74.9
Diff in max pedal power	133.7 $s = 25.4$ $P < 0.001$		32.3 $s = 26.5$ $P < 0.025$	
Diff in min pedal power	2.5 $s = 8.6$ $P > 0.100$		-4.4 $s = 8.1$ $P < 0.100$	
Diff in power range	131.2 $s = 25.3$ $P < 0.001$		36.6 $s = 28.6$ $P < 0.005$	
Diff in mean pedal power	64.0 $s = 12.1$ $P < 0.001$		13.9 $s = 13.6$ $P < 0.025$	
Estimated roller power data (Watts)				
Max est roller pwr	954.0	835.6	347.1	363.1
Min est roller pwr	-1558.0	-925.0	-154.5	-167.1
Est roller pwr range	2512.0	1760.6	501.6	530.2
Mean est roller pwr	113.8	72.7	93.8	98.5
Diff in max est roller power	118.4 $s = 103.2$ $P < 0.025$		-16.0 $s = 37.0$ $P > 0.100$	
Diff in min est roller power	-633.0 $s = 136.3$ $P < 0.001$		12.6 $s = 40.5$ $P > 0.100$	
Diff in est roller pwr range	751.4 $s = 188.0$ $P < 0.001$		-28.7 $s = 70.5$ $P > 0.100$	
Diff in mean est roller pwr	41.1 $s = 53.3$ $P < 0.050$		-4.7 $s = 15.5$ $P > 0.100$	

Table 5.6: Table of the averaged maximum and minimum values of the power generated at the pedals and the estimated power generated at the roller of the HT and SU bicycles, showing the difference between the maximum values and the difference between the minimum values during the bump and no bump tests. The table further shows the range and mean of the power generated at the pedals and the estimated power generated at the roller and the differences in power range and mean power for the HT and SU bicycles during these tests.

5.3 Simulation Results

In all simulation results presented the front of the bump is situated 10 seconds into the simulation.

5.3.1 Tables

Table 5.7 shows the velocity of the bump in the DADS HT and SU model equivalent momentum simulations. The plot of the velocity of the bump in the DADS HT and SU model equivalent momentum simulations can be seen in Figure 4.11 p 58. Table 5.8 shows the maximum, minimum and mean vertical acceleration, velocity and displacement results for the saddle from the DADS HT and SU model fixed velocity simulations. Table 5.8 shows maximum, minimum and mean force results calculated at the front bracket and the rear axle from the DADS HT and SU model fixed velocity simulations.

As with previous tabulated differences between the HT and SU bicycles the difference values in Tables 5.8, and 5.9 have been calculated by subtracting the SU values from that of the HT values (HT - SU).

Velocity Results Before and After Bump Impact		
	HT model	SU model
Velocity Before Impact $(m \cdot s^{-1})$	3.300	3.300
Velocity After Impact $(m \cdot s^{-1})$	3.215	3.251
Velocity Range $(m \cdot s^{-1})$	0.085	0.049
Difference in Velocity Range	0.036 $m \cdot s^{-1}$	

Table 5.7: Table of velocity results for the bump before and after rear wheel impact from the DADS HT and SU model, equivalent momentum simulations.

Saddle Acceleration, Velocity and Displacement Results		
	HT model	SU model
Maximum Acceleration (impact) (g's)	2.31	1.84
Maximum Acceleration (landing) (g's)	4.94	2.35
Minimum Acceleration (g's)	-1.95	-1.91
Difference in Max Accel (impact)	0.47 g's	
Difference in Max Accel (landing)	2.59 g's	
Difference in Min Accel (landing)	0,04 g's	
Maximum Velocity $(m \cdot s^{-1})$	0.60	0.47
Minimum Velocity $(m \cdot s^{-1})$	-0.77	-0.68
Difference in Max Velocity	$0.134\ m \cdot s^{-1}$	
Difference in Min Velocity	$-0.082\ m \cdot s^{-1}$	
Maximum Displacement (mm)	33.05	28.61
Minimum Displacement (mm)	-6.06	-4.72
Total Displacement (mm)	39.11	33.33
Difference in Max Displacement	$4.44\ mm$	
Difference in Min Displacement	$-1.34\ mm$	
Difference in Total Displacement	$5.78\ mm$	

Table 5.8: Table of maximum, minimum and mean vertical acceleration, velocity and displacement results for the saddle from the DADS HT and SU model, fixed velocity simulations.

Front Bracket Force Results		
	HT model	SU model
Maximum Force (N)	228.0	229.5
Minimum Force (N)	-366.5	-313.6
Force Range (N)	594.5	543.2
Difference in Max Force	-1.5 N	
Difference in Min Force	-52.9 N	
Difference in Force Range	51.3N	
Rear Axle Force Results		
	HT model	SU model
Maximum Force (N)	249.4	207.0
Minimum Force (N)	-29.5	-24.6
Force Range (N)	279.0	231.6
Difference in Max Force	42.5 N	
Difference in Min Force	-4.9 N	
Difference in Force Range	47.4 N	

Table 5.9: Table of maximum, minimum and mean force results from the DADS HT and SU model, fixed velocity simulations.

Chapter 6

Discussion

The tests in this study were conducted with a fixed bump size and a constant impact frequency of between 2.9 Hz and 4.3 Hz, which represents severely bumpy conditions. However, this provided only a single sample of the actual bump sizes and impact frequencies that are encountered when mountain cycling in practice. Also, speeds of the roller surface during the testing did not reflect race speeds. Many of the subjects felt that travelling faster over the bumps would have improved relative comfort, but the lower speed had been set so that the effects of the impact force from one bump had dissipated before impact with the next bump. During the bump tests, the majority of the subjects also felt that it was far easier to maintain a constant speed on the SU bicycle than on the HT bicycle.

6.1 Physiological and Psychological Results

The physiological and psychological results can be found in Section 5.1.

The results show that the SU bicycle places lower physiological and psychological

demands on the subject than the HT bicycle during sub-maximal laboratory tests over bumps, as evidenced by the significantly lower $\dot{V}O_2$, heart rate and RPE, and the significantly higher comfort rating. However, when the same bicycles were compared during the tests without bumps, there was a small but significant difference in $\dot{V}O_2$, with the HT bicycle having the lower value, while differences in heart rate, RPE, and comfort rating also tended to favour the HT bicycle, but were not significant and very small. These differences are consistent with results obtained by Nielens & Lejeune (2001) who found no significant difference between $\dot{V}O_2$ and heart rate values of subjects riding seated on a fully suspended, front suspended and a fully rigid mountain bicycle on a smooth surface.

While the physiological results indicate similar trends to those reported by Berry et al. (1993) and Seifert et al. (1997), it is not possible to draw specific conclusions from comparisons between the different studies because of a number of differences in the way the tests were conducted. Berry et al. (1993) recorded significant differences in $\dot{V}O_2$ between no suspension and full suspension bicycles, with the suspension bicycle having lower values. However, unlike the current study, their observations did not show any significant difference between front suspension and full suspension bicycles. Their bump impact frequency of 42 impacts per minute was approximately 2.5 times lower than in this study. In the study by Berry et al. (1993), the subjects expended energy to cycle on a constant 4% slope, to balance on the treadmill and to overcome front wheel impact. The characteristics of the drive motor of the treadmill and the inertia of the belt and bump will also have influenced the test subjects. A direct comparison cannot therefore be made with the current tests where energy was primarily expended to control and overcome rear wheel bump impacts. Seifert et al. (1997) recorded no significant difference in oxygen consumption between the bicycles tested

on an artificial track with regular bumps, but, as in this study, they did observe a significantly ($P < 0.04$) lower heart rate for the SU bicycle. During their study the subjects rode over a flat track at a rate of 30 bumps per minute for a much longer period of over 60 minutes. Seifert et al. (1997) also carried out time trials on actual trails. There were no significant differences in time on the ascent and descent trails, but on a cross country trail the fastest times were achieved with their HT bicycle, which suggests that the advantage of the suspension system under sub-maximal laboratory conditions may not translate directly to full exertion trail conditions. The preference of most professional cyclists for HT bicycles also suggests that care is needed in translating test results to time trial and race conditions.

The cycling rig was designed to focus on the dynamics of the bicycle and a largely passive rider when the rear wheel impacts with bumps. It does not simulate the effort that the cyclist must exert to control the bicycle on a rough trail. However, since the suspension system acts to attenuate the impact forces, it might be expected that it will also improve the controllability of the bicycle. The physiological and psychological advantages that the full suspension system provides over regular and quite large bumps can be expected to translate to free riding on a trail with similar bumps. However, actual trails have irregular bumps with long stretches of quite smooth surface and possibly some soft ground with much higher rolling resistance. The tests show that in the absence of bumps there is a slightly higher $\dot{V}O_2$ cost when using the SU bicycle (see Section 5.1.2). Thus, the trail must exceed a certain level of roughness before the SU bicycle can provide an advantage. In reality there will be sections of trail where the SU bicycle may provide an advantage, and sections where it imposes a performance penalty. With the advent of bicycles with adjustable suspension systems this crossover point is of importance. When determined, it will allow riders and team mechanics to

set up the bicycle before a race for optimum performance, or to tune the suspension to suit different parts of the trail during the race, for continuous optimisation.

Results from time trials and races suggest an advantage for the HT bicycle. This is somewhat surprising given the advantages of the SU bicycle in tests. The finding of MacRae et al. (2000) that more energy is transmitted through the chain on an SU bicycle than on the HT bicycle can perhaps be explained by the technique adopted by the rider on the different bicycles. On the SU bicycle, impacts are softened, as described later on page 6.2.2, so that a more sustained transmission of energy though the transmission system is possible. On the HT bicycle, the higher accelerations over the bumps, and loss of contact between the wheel and the road, may cause the rider to adopt a technique where energy is transmitted not only through the transmission system, but also by use of the hands through the handlebars, and by effectively and efficiently lifting up the bicycle by applying zero force to the pedals, by using the shock absorption of their legs, and allowing the impact to lift the bicycle so as to achieve as smooth a progress as possible. A skilled cyclist does achieve high efficiencies on an HT bicycle with good timing of his movement on the bicycle, as evidenced by the UCI world cup results (see Section 1).

The relationship between input power and output power of a bicycle can be written as; $P_{out_{bicycle}} = P_{in_{cyclist}} * Eff_{cyclist} * Eff_{bicycle}$, where P stands for power and Eff for efficiency. It is possible that highly trained professional cyclists can adapt their style when riding over bumps so that their efficiency does not change much between the HT or SU bicycles. Wang & Hull (1997) claim that no bicycle frame with a suspension system will ever be as efficient as a rigid frame without a lockout device on the suspension. (A lockout device is a mechanism that, when activated, locks the shock absorber so that it becomes incompressible. The effect is to make the rear suspension system of

a suspension bicycle rigid, and therefore emulating a hard tail bicycle.) If this is the case, the better efficiency of a rigid frame would improve the overall efficiency of the cyclist/bicycle system over that of a suspension system, provided that the cyclist can alter his or her riding style so as not to change their own efficiency. However, Burrows (2001) claims that there is an SU bicycle without a lockout device that is as efficient as an HT bicycle. This means that the benefits of a full suspension system can be utilised without any loss in efficiency, thus allowing for an improvement in the efficiency of the cyclist without the cyclists having to change their riding style when riding over bumps.

6.2   Mechanical Results

To aid in the discussion of the mechanical results, plotted data has been presented in this discussion.

6.2.1   Graphical Data Presentation: A Brief Explanation

The graphs for the HT and SU data have been presented side by side so that they can be compared. The SU and HT values were not superimposed on the same graph because of the unknown initial conditions before each bump impact.

The DADS HT and SU model simulation results are plotted on the same graph for comparison since the conditions just before impact are the same. When test data and simulation data have been plotted for comparison they have also been plotted on the same graph. Although the initial conditions are not the same the superposition of the different results allows for easier comparison of the time axis.

Acceleration plots of multiple impacts have been presented to show the effect of

rear wheel bump impact on the saddle and handlebars in Figures 6.1 6.2, 6.3 and 6.4. For analysis of single impacts three consecutive impacts have been plotted in Figures 6.5, 6.6, 6.8 and 6.9.

Individual subjects have not been compared to one another and the data plotted is all from the same subject and is of a typical nature.

Where pedal and bump positions (as described in Section 3.4.5) have been plotted on the graphs, they have been plotted in red for bumps and cyan for pedal position unless otherwise stated on the figure. A rough indicator for the width of the bump impact on the graphs is the width of the base of the bump indicator spikes

In plot 1 and 2 of Figure 6.19 the rapid drop of tangential force on the crank arms at the pedal just after 303.5 seconds is as a result of a momentary accidental disconnection of the slip rings mounted to the chain rings. For further detail see Appendix C.

6.2.2 Vertical Acceleration, Velocity and Displacement: Saddle and Handlebars

Results for this section can be found in Table 5.3.

The results show that the SU bicycle had lower vertical saddle and handlebar acceleration than the HT bicycle, as measured by the acclerometers during the sub-maximal laboratory tests over bumps. The vertical velocity and displacement, which were derived from the acceleration, of the SU bicycle were also lower than those of the HT bicycle. However, when the same bicycles were compared during the no bump test there was no significant difference in the saddle acceleration and velocity. There was a significant difference in the saddle displacement but this was very small and would have been very difficult for a subject to detect. The SU bicycle had a significantly

lower handlebar acceleration, velocity and displacement than the HT bicycle during the no bump test, but again, the differences were very small and difficult for a subject to detect.

On the cycling rig, the saddle moves through a theoretical distance of 20 mm when the rear wheel goes over the bump, assuming that the wheel is rigid and stays in contact with the bump (see Appendix B Section B.1). It was expected, from observation of the tests, that the saddle would move through a distance greater than 20 mm on the HT bicycle and less than 20 mm on the SU bicycle. This observation is confirmed by the saddle displacement results in Table 5.4. During the no bump test the total displacement of the saddle for both the HT and SU bicycles was 3.24 mm and 3.4 mm respectively, which corresponds to the radial run out of the roller (see Section 3.3.3).

Figures 6.1 and 6.2 are plots of the vertical acceleration, velocity and displacement of the saddle and the handlebars during the bump tests. Pedalling positions have not been included in these plots because they have little effect on the vertical acceleration of the saddle and handlebars during the bump tests. It is apparent how less violent the acceleration of the saddle and the handlebars of the SU bicycle is compared to the HT bicycle, which correlates with the psychological results of RPE and comfort rating.

The magnitude of the vertical saddle acceleration and displacement affects the subjects RPE and comfort ratings. The differences between the HT and SU bicycles in vertical saddle acceleration on impact and landing, and the displacement of the saddle, correlate with the change in RPE and comfort ratings of the subject. For a difference in acceleration of 1.45 g's (impact) and 1.39 g's (landing) and a displacement of 11.84 mm there is a corresponding difference of 1.83 in the RPE rating and -1.87 in the comfort rating. During the no bump test there is no significant difference in the RPE and comfort ratings which corresponds with the small differences in the acceleration and
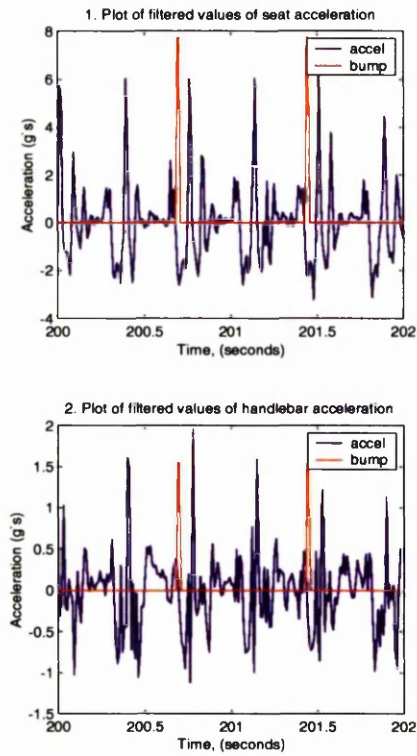
Figure 6.1: Saddle and handlebar acceleration with the pedal position indicator for the HT bicycle during a bump test.
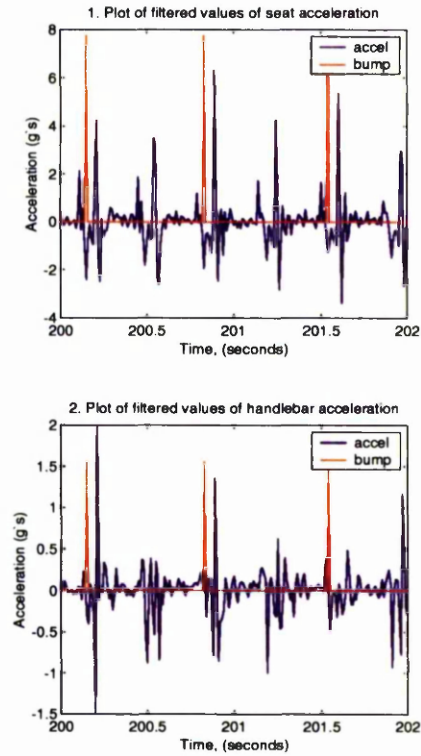
Figure 6.2: Saddle and handlebar acceleration with the pedal position indicator for the SU bicycle during a bump test.

displacement values.

More energy is lost through the front shock absorber during bump tests with the HT bicycle than the SU bicycle. This is deduced from the fact that there is a significant difference ($P > 0.001$) between the HT and the SU bicycle in both the maximum and minimum values of accelerations, velocities and displacements of the handlebars during the bump tests. The total displacement of the shock absorbers during the HT bump tests was 7.457 mm greater than that of the SU bicycle. This shows that during the

HT tests there is a significantly greater rate and amount of compression and extension of the front shock absorbers than in the SU tests.

The maximum vertical saddle acceleration from bump impact of the HT bicycle is 1.454 g's ($p < 0.001$) greater than the SU bicycle during the bump tests. The impact acceleration has a horizontal component that opposes the forward motion of the bicycle. The greater the vertical impact acceleration the greater the horizontal force and the consequent deceleration. This increase can be seen in the test results of front bracket force in Table 5.5 and the DADS simulation results in Table 5.9. There is a 1.391 g difference in the maximum landing acceleration between the HT and the SU bicycle. This means that there will be a higher normal force between the rear tyre and the roller with the HT bicycle resulting in a greater rolling resistance on landing. Grappe et al. (1999) measured an increase in the coefficient of rolling resistance with increased normal force. This further decelerates the bicycle and cyclist. The increase cannot be quantified from the current test results and is highly dependent on the nature of the track surface and tyre tread, build and pressure. Further work is needed to quantify these effects to determine if the effects are significant (see Section 7.4).

During the no bump test (Figures 6.3 and 6.4) there is still an amount of vibration at the saddle and the handlebars which appears to be marginally worse for the HT bicycle.

Figures 6.5 and 6.6 show the vertical acceleration, velocity and displacement of three impacts of a bump on the rear wheel of the bicycle. Visual analysis of the acceleration in plot 1 of both impact acceleration and landing acceleration agrees with the results in Table 5.4.

The measurement of the displacement during the bump tests is not accurate enough
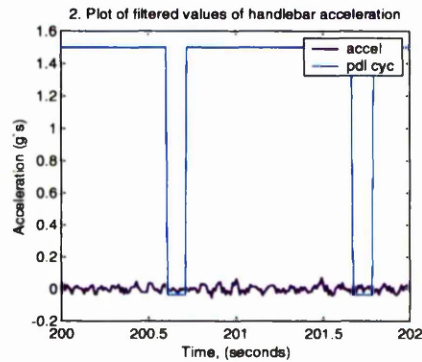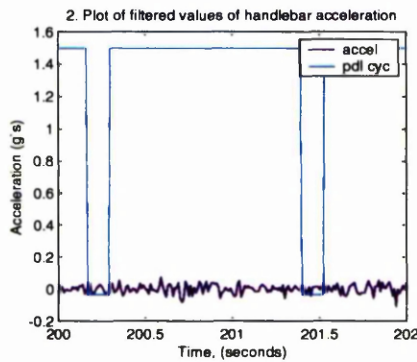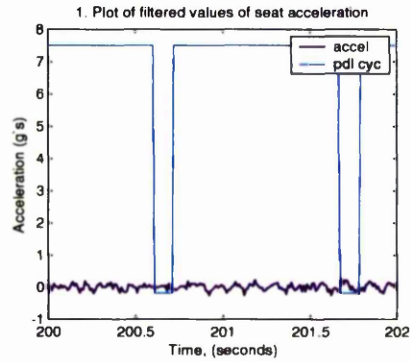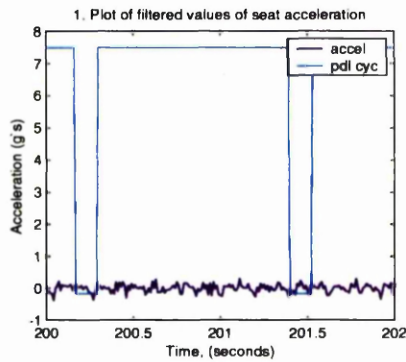
Figure 6.3: Saddle and handlebar acceleration with the pedal position indicator for the HT bicycle during a no bump test.

Figure 6.4: Saddle and handlebar acceleration with the pedal position indicator for the SU bicycle during a no bump test.

to determine that the wheel has left the bump on impact but the DADS model does show that the rear wheel of the HT bicycle does leave the bump impact. The rear wheel of the SU bicycle stays in contact with the bump for longer although the Z force on the wheel does drop to zero for a short duration while travelling over the bump (see Figure 6.10). This would indicate that the wheel does leave the bump and is discussed further on page 94.

Figure 6.7 plots the vertical acceleration, velocity and displacement of the saddle
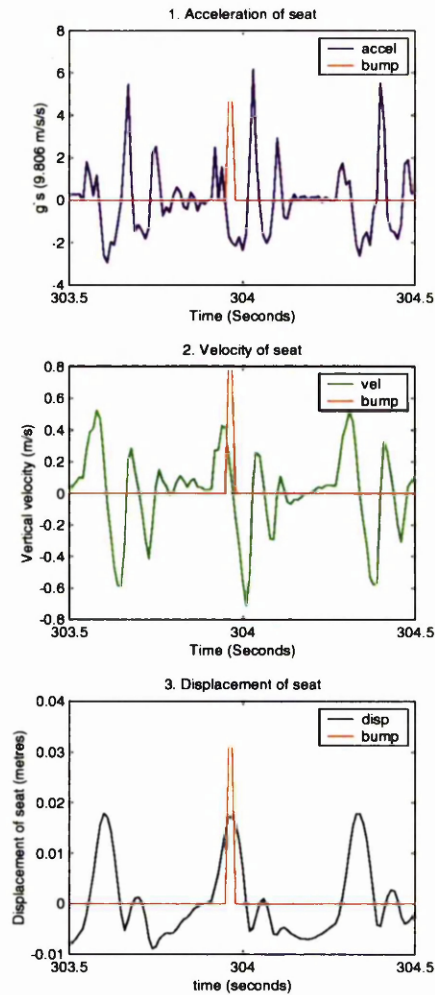
Figure 6.5: A single impact cycle for vertical saddle acceleration, velocity and displacement of HT bicycle during a bump test.
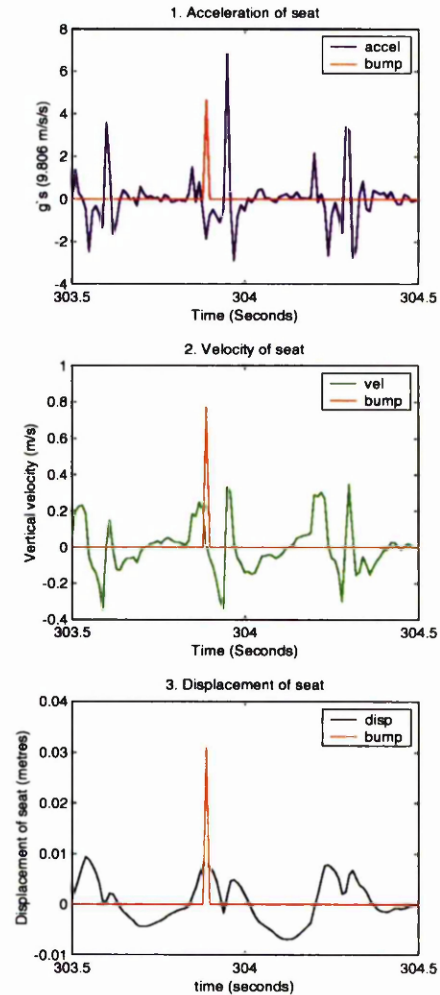
Figure 6.6: A single impact cycle for vertical saddle acceleration, velocity and displacement of SU bicycle during a bump test.

of the fixed velocity simulation of the DADS HT and SU models. The model shows

increases in the landing acceleration over impact acceleration for both the DADS HT
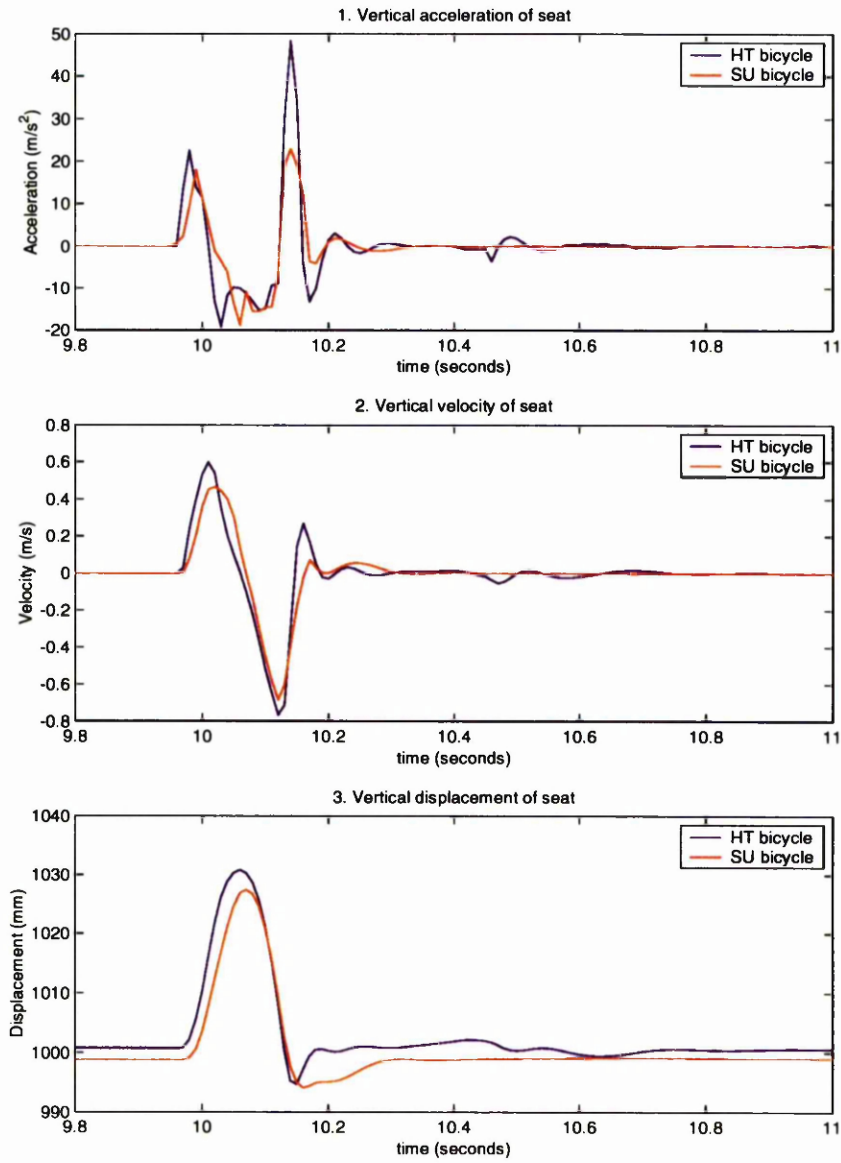
Figure 6.7: Plot of the vertical acceleration, velocity and displacement of the saddle of the DADS HT and SU models with fixed bump velocity (rig fixed).

and SU models similar to the test saddle acceleration data, although there is not as much difference for the DADS SU model. A possible explanation for this, considering that the DADS HT model has an impact and landing acceleration close to the test data, is the fact that the body used in the model was constrained using springs. This is by no means an accurate representation of the human body, which is an incredibly complex, intelligent control system impossible to simulate.

Figures 6.8 and 6.9 show the acceleration, velocity and displacement for a single pedal cycle during the no bump test. Visual analysis does indicate that there is more movement on the HT bicycle than the SU bicycle but, as mentioned earlier, these differences are very small.

6.2.3 Force Results from the Crank Arms and the Front Bracket

Results for the pedal and front bracket can be found in Table 5.5.

The results show that the SU bicycle had a lower maximum pedal force, a lower force range and a lower mean force than the HT bicycle during sub-maximal laboratory tests over bumps, as measured by the pedal force measurement instrumentation (see Section 3.4.2). There is no significant difference in the minimum pedal force between the HT and the SU bicycles, but the force is negative for both bicycles during the bump test. During the no bump test the SU bicycle still has a lower maximum pedal force, a lower force range and a lower mean force than the HT bicycle. However, the difference between the two bicycles was much lower. Again, there was no significant difference between the minimum pedal forces measured for the two bicycles during the no bump test, but the minimum force was always positive, unlike the bump test. This difference between the bump and no bump tests is discussed further on page 101.
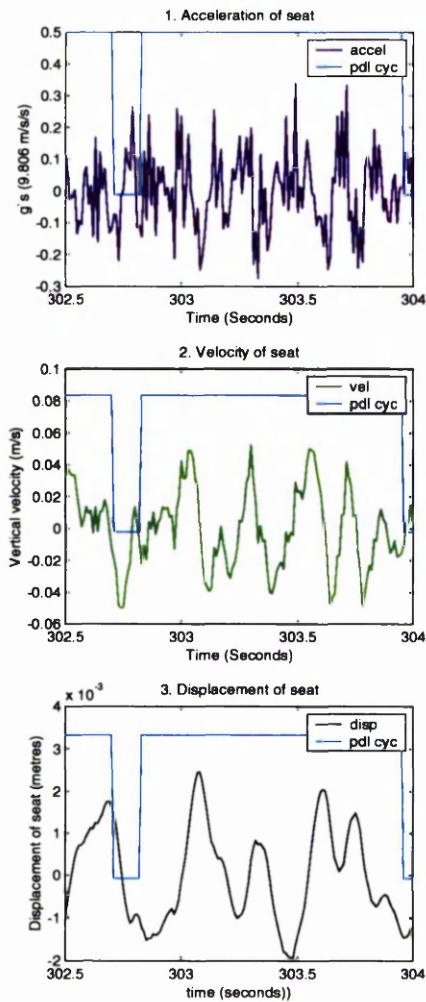
Figure 6.8: A single pedal cycle for vertical saddle acceleration, velocity and displacement of HT bicycle during a no bump test.
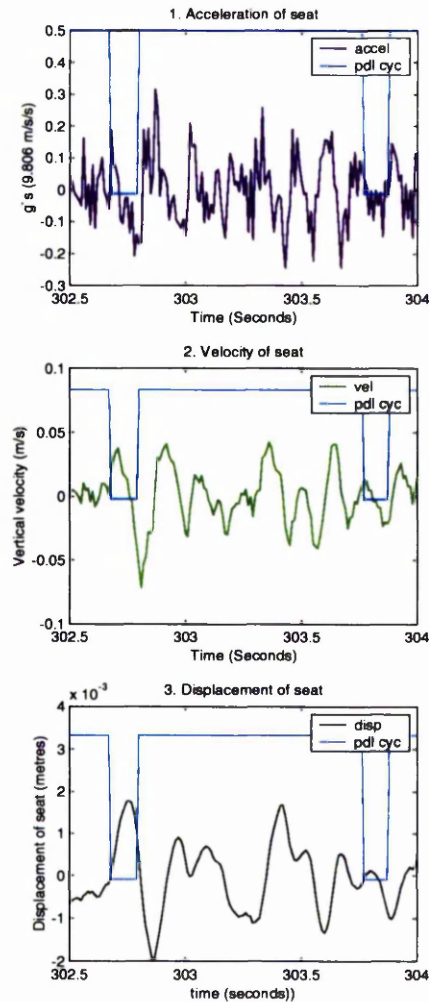
Figure 6.9: A single pedal cycle for vertical saddle acceleration, velocity and displacement of SU bicycle during a no bump test.

The mechanical results of the pedal force for the no bump test suggest that less work is being done on the SU bicycle than on the HT bicycle, as evidenced by the lower

mean pedal force and lower maximum pedal force. This conflicts with physiological results which suggest that more work is required on the SU bicycle than on the HT bicycle as evidenced by the small but significant differences in the $\dot{V}O_2$ and energy expenditure in favour of the HT bicycle. It must, however, be remembered that these are only small differences.

As mentioned previously, it was hoped that the front bracket force would be a measure of the reactive force between the roller and the rear wheel. However, analysis of the data, with the aid of the DADS model, showed that the horizontal force applied to the front bracket by the inertia of the cyclist was far larger than expected. The front bracket force did however still give sufficient information for the comparison of the HT and SU bicycles during the bump and no bump tests. Intriguingly, the inertia forces measured do indicate the amount that the cyclist is thrown about on the bicycle, which was not a variable that was originally intended to be measured. They can only be used as a very rough measure of the force of movement, but can be used for comparison of the two bicycles, during the bump and no bump tests, as all other variables are the same. It can be seen in Table 5.5 and in Figures 6.17 and 6.18 that the maximum force applied to the front bracket on the HT bicycle is much higher than that on the SU bicycle. This would indicate that the subject is thrown about more on the HT bicycle which is to be expected and the results correlate with the larger saddle acceleration and displacement values.

The results from the front bracket show that the HT bicycle had a larger maximum force, force range and mean force than the SU bicycle during sub-maximal laboratory tests over bumps. During the no bump test there was no significant difference between the HT and SU bicycles for maximum force, force range, and mean force as measured at the front bracket. The maximum force and force range are largely influenced by the

inertial forces that result from the movement of the subject on the bicycle during the tests.

The influence of the inertial forces was confirmed by the DADS computer simulation, which provided data to compare the results at the front bracket and the rear hub of the bicycle (see Figure 6.10 for plotted results). This demonstrated that the horizontal force at the rear hub occurred only at impact for both the DADS HT and SU models. However, the horizontal force at the front bracket varies greatly after impact. This results from the body of the cyclist moving after bump impact. This movement is visible on the dynamic animation of the DADS HT and SU models.

Figure 6.10 plots the vertical and horizontal forces on the frame at the rear hub and the horizontal force at the front bracket of the DADS HT and SU models with fixed bump velocity. The maximum vertical force applied to the rear wheel hub was 1130 N which is reasonable. De Lorenzo & Hull (1999b) measured vertical forces of up to 4000 N for the rear wheel hub while trail riding.

From plot 1 of Figure 6.10 it can be seen that the bump impact results in a zero Z force at the rear hub for both the DADS HT and SU models. This implies that the rear wheel has left the bump surface. The horizontal force at the rear wheel hub in plot 2 spikes at impact, which is expected, but drops back to zero the moment the Z force drops to zero and there is no further change in the horizontal force. This indicates that the wheel has been knocked so high into the air that it does not land before the bump has passed, and therefore does not roll off the bump converting some of the potential energy gained back into forward velocity, as described in Section 6.3.1. Plot 3 shows the difference between the DADS HT and SU models in reaction force at the front bracket.
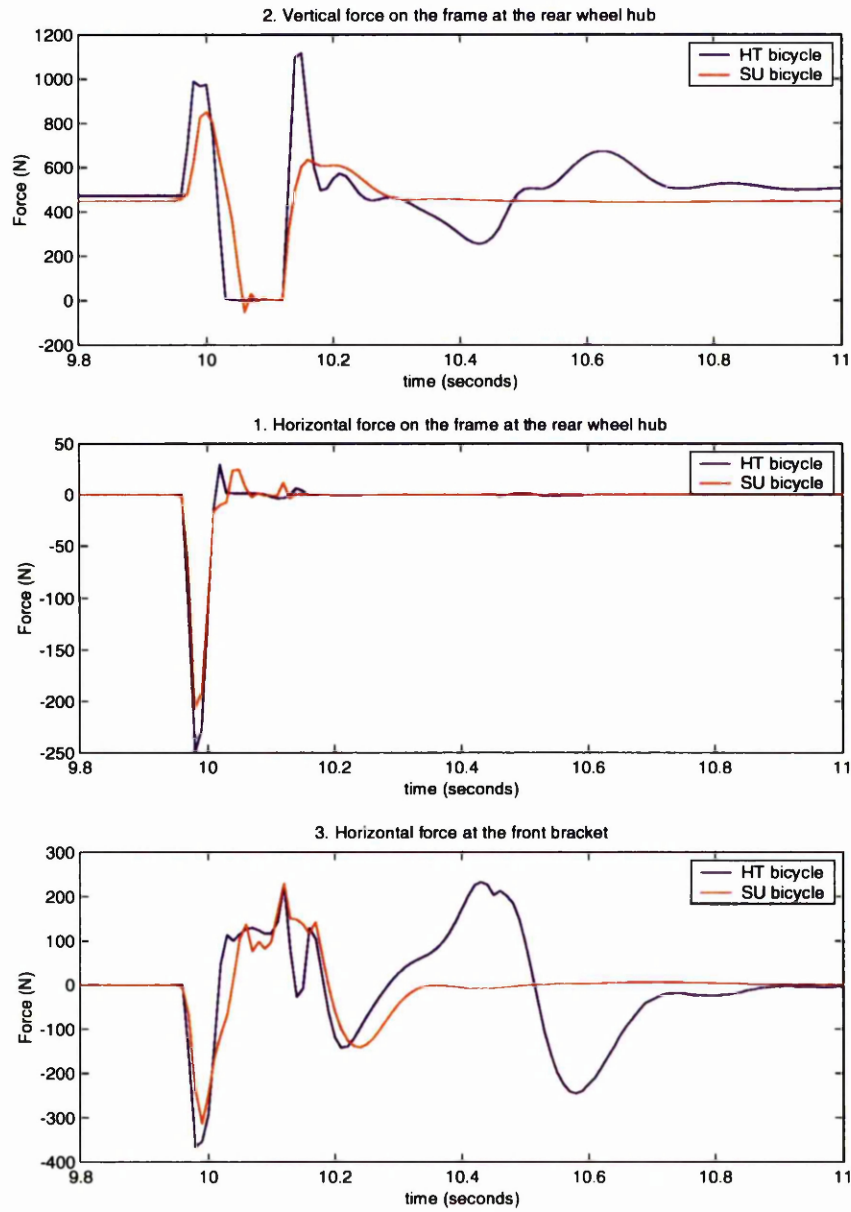
Figure 6.10: Plot of the vertical and horizontal force on the frame at the rear hub, and the horizontal force at the front bracket of the DADS HT and SU models with fixed bump velocity.
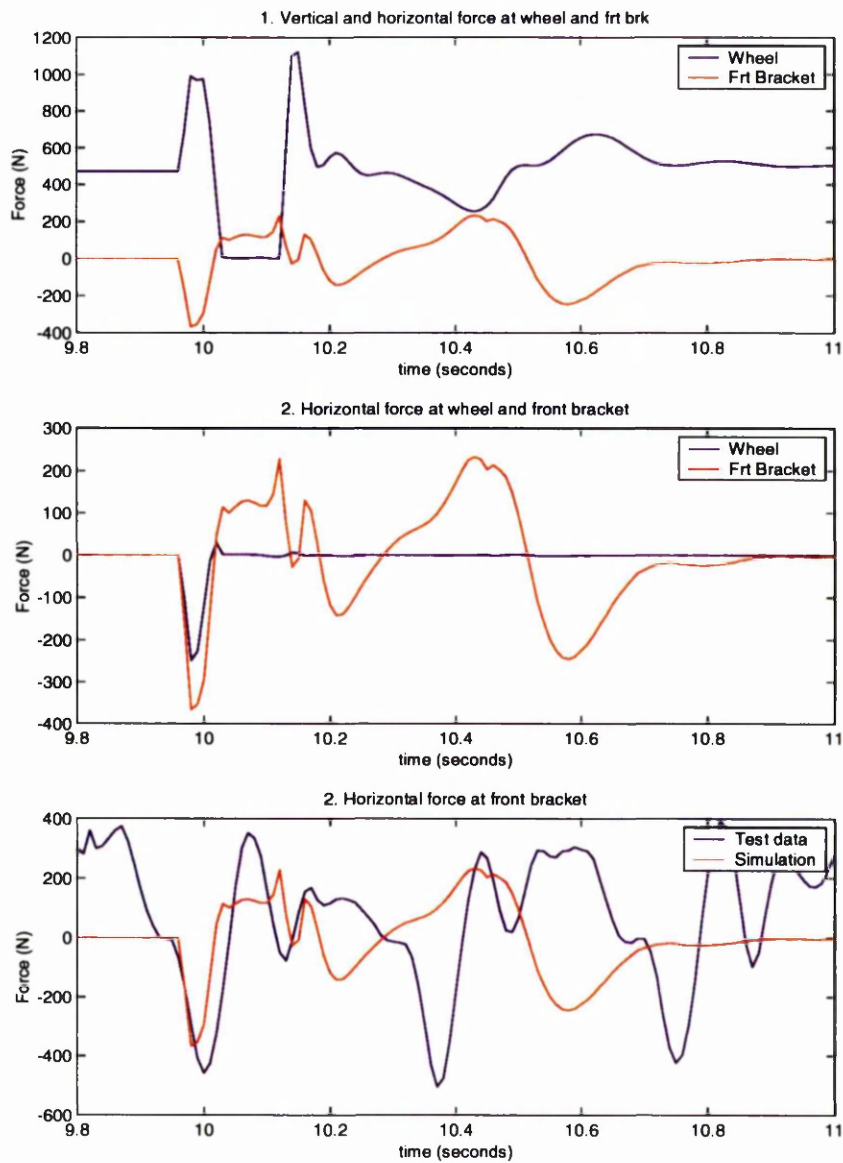
Figure 6.11: Plot of the vertical force and horizontal forces, at the wheel and the front bracket of the DADS HT models with fixed bump velocity, and the front bracket force from the HT bicycle and the DADS HT model.

Plot 1 of Figure 6.11 shows that the negative horizontal force of bump impact measured at the front bracket correlates with the positive vertical force of bump impact

applied to the rear wheel. However, the subsequent positive horizontal force measured at the front bracket correlates with the period of zero vertical force which implies that the positive front bracket force is a reaction to the movement of the subject on the bicycle. Plot 2 shows that the horizontal force at bump impact measured at the front bracket is greater than the horizontal force measured at the rear wheel. The forces are, however, proportional and the front bracket forces of the HT and SU bicycles can be compared (see Figures 6.11 and 6.12).

Plot 3 of Figures 6.11 and 6.12 show the comparison of the front bracket force measured on the rig and the simulated model, for the HT and SU bicycles. This shows the similarity of the negative bump impact force measured at the front bracket on the rig and DADS models.

Plot 1 and 2 of Figures 6.13 and 6.14 show the major frequencies of the forces applied to the front bracket and the tangential force applied to the crank arms at the pedal during the bump test respectively. The largest peak of plot 1 of Figures 6.13 and 6.14 corresponds to the bump impact frequency. The largest peak of plot 2 corresponds to the pedalling frequency which is roughly 1.5 Hz. Plot 3 of Figures 6.13 and 6.14 shows a sample of the pedalling and front bracket force from which the PSD plots were generated. Both figures show that the energy from the front bracket force and the pedal force is concentrated in the band 0-15 Hz.

Plots 1 and 2 of Figures 6.15 and 6.16 show the major frequencies of the forces applied to the front bracket of the bicycle and the tangential force applied to the crank arms at the pedal during the no bump test respectively. The largest peak of plot 1 of the figures corresponds to the pedalling frequency, of roughly 1.5-2 Hz, which is the same as the largest peak of plot 2. Plot 3 of Figures 6.15 and 6.16 shows a sample of the pedalling and the front bracket force. The energy from the front bracket force and
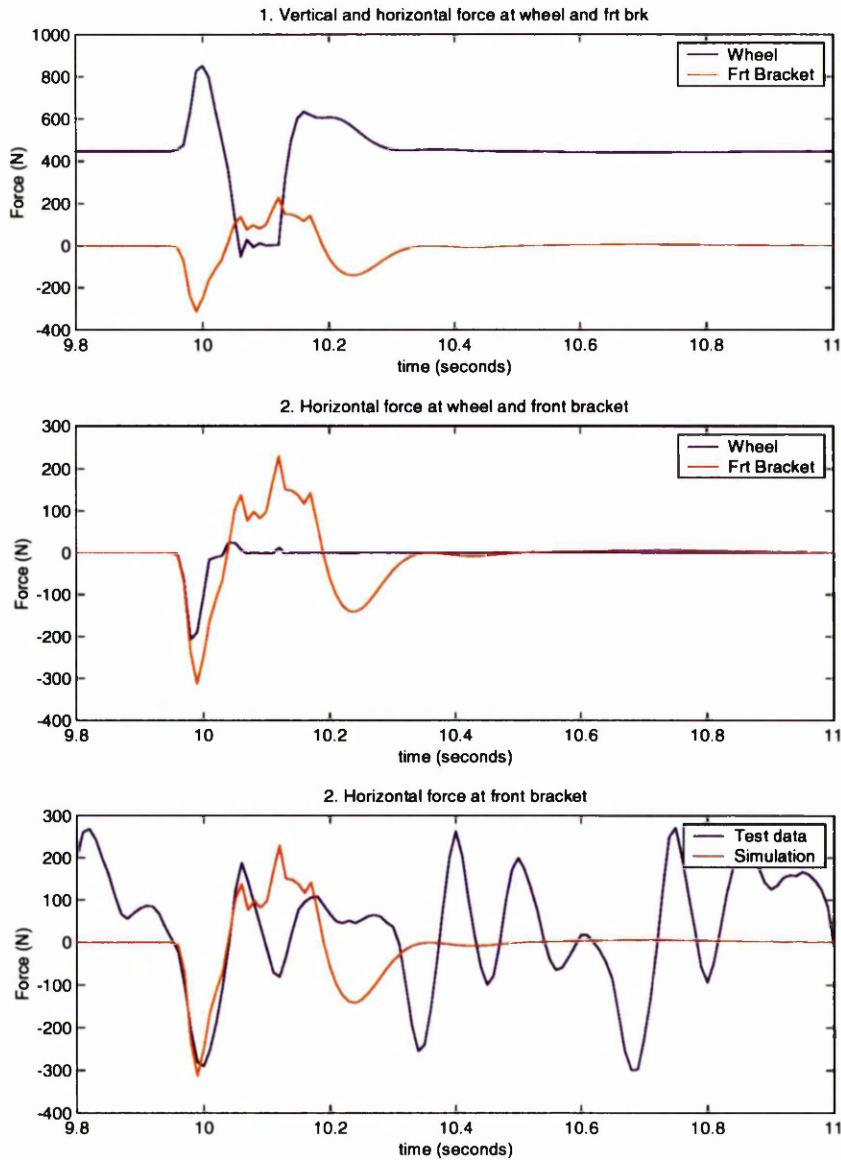
Figure 6.12: Plot of the vertical force and horizontal forces, at the wheel and the front bracket of the DADS SU models with fixed bump velocity, and the front bracket force from the SU bicycle and the DADS SU model.

pedal force are, however, concentrated only in the band 0-5 Hz.

Figures 6.17 and 6.18 show a 3 second sample of the front bracket and the pedal
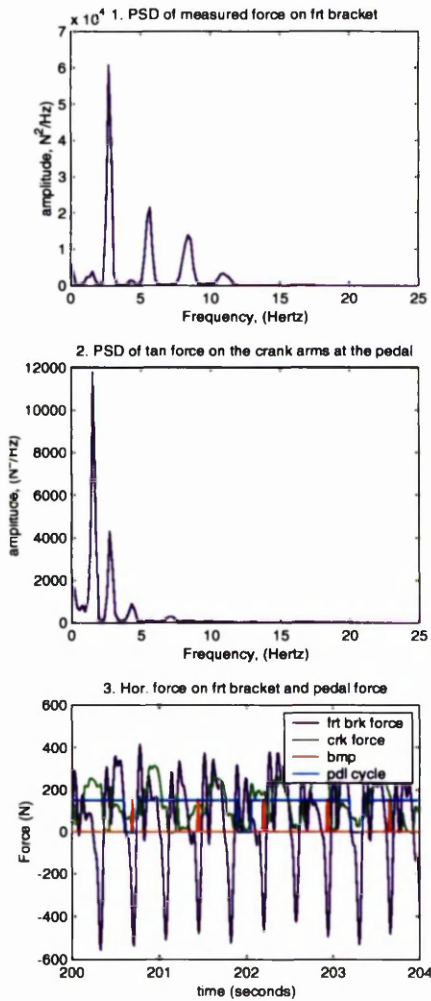
Figure 6.13: PSD plots of the forces applied to the pedals and to the front bracket and a plot of the forces on the HT bicycle during a bump test.
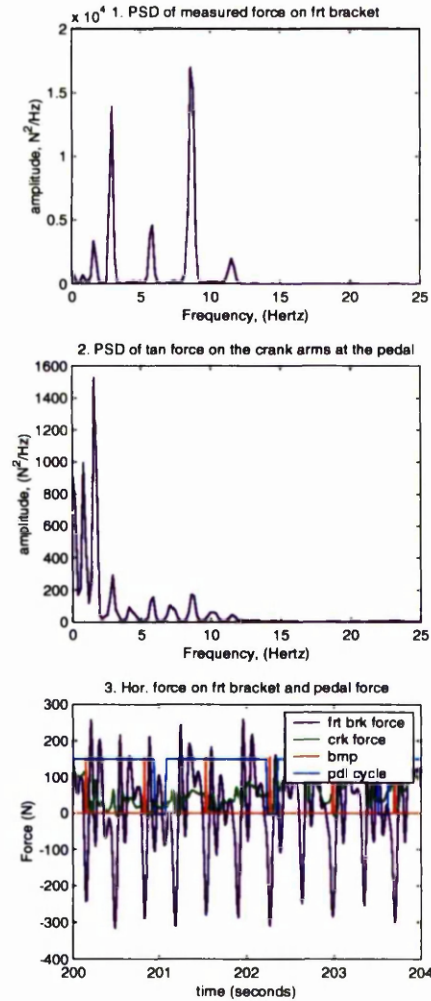
Figure 6.14: PSD plots of the forces applied to the pedals and to the front bracket and a plot of the forces on the SU bicycle during a bump test.

forces and a 3 bump impact sample of pedal forces and front bracket force. There is a consistent drop, of variable amount, in the torque transmitted to the chain just after
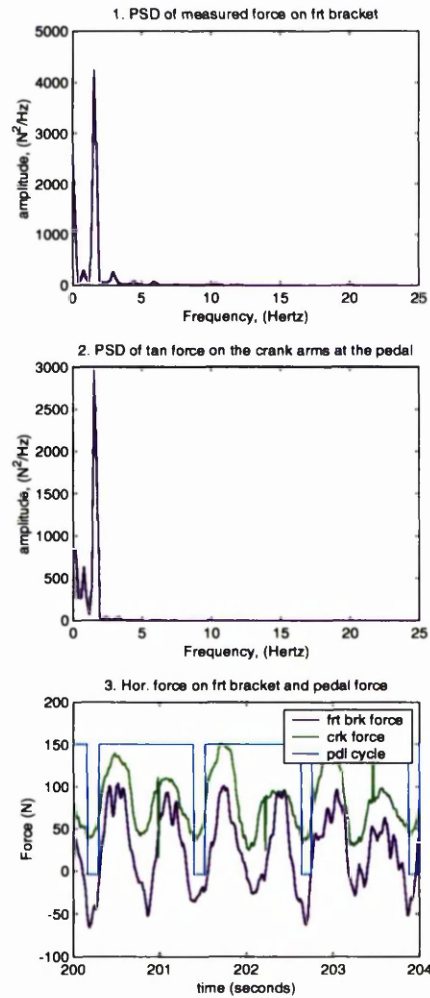
Figure 6.15: PSD plots of the forces applied to the chain and to the front bracket and a plot of the forces on the HT bicycle during a no bump test.
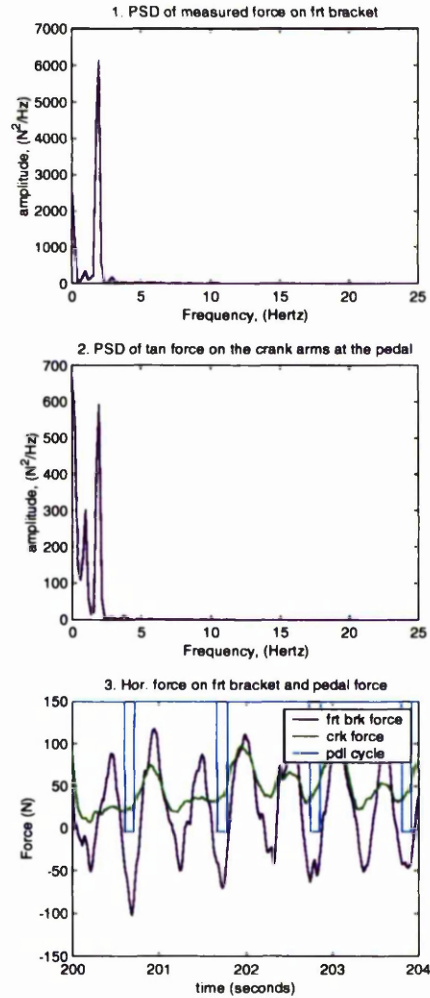
Figure 6.16: PSD plots of the forces applied to the chain and to the front bracket and a plot of the forces on the SU bicycle during a no bump test.

bump impact, which suggests that the bump impact disrupts the torque transmitted to the rear wheel. Plot 2 of Figure 6.17 is a good example of this drop immediately

after the bump impact which occurs in the middle of the subject's downward stroke with his right leg. The only way this can occur is for the chain tension to drop. Two things can affect the chain tension, first, the cyclist can stop applying torque to the chain rings, thus disrupting the pedalling cycle, and secondly, the rear wheel can leave the roller surface thus rapidly reducing the reactive force applied by the roller surface to the chain tension. The latter is the more likely explanation because of the evidence that already shows that the rear wheel does leave the roller surface. The drop is not always as large as that of plot 2 of Figure 6.17.

The impact force of the bump during the HT bicycle test is greater than the impact force during the SU bicycle test. This can be seen in plot 1 of Figure 6.17 and 6.18 and table 5.5.

In Figures 6.19 and 6.20, it can be seen that the maximum force that is applied to the pedals is applied when the crank arms are horizontal, which is to be expected.

Figures 6.21 and 6.22 have been plotted to show the effect that the pedals have on the front bracket and the effect that the other forces have on the front bracket, such as inertial forces generated by the cyclist and the force of bump impact during the bump tests (see Section 3.6.4).

If one separates the force measured at the front bracket into its individual components (predicted reaction force from the pedals between the rear tyre and the roller surface and the inertia force from the cyclist's movement) during the no bump test, then the force resulting from the movement of the cyclist is roughly double that of the reaction force from the pedals (see Figure 6.23 and 6.24). Both these forces are in phase with each other suggesting that the movement of the cyclist resulted from their application of a force to the pedals. From Figure 6.23 it can be seen that the
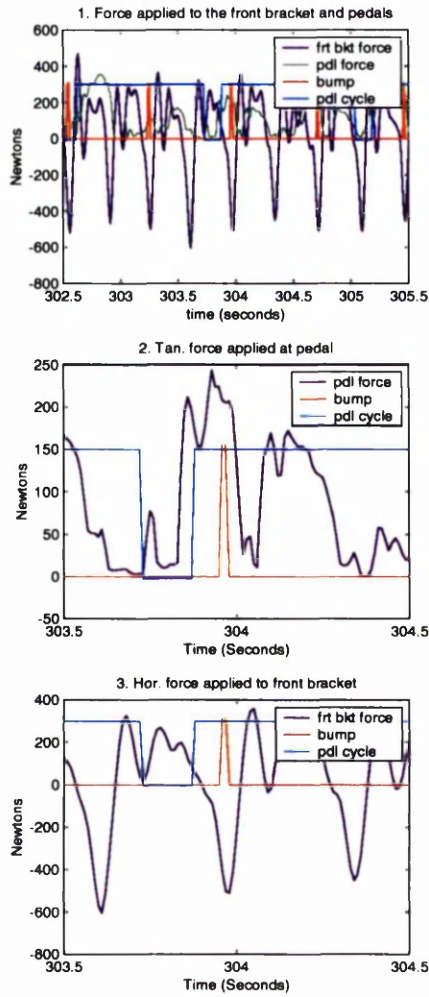
Figure 6.17: Tangential force applied to the crank arms at the pedal and front bracket for the HT bicycle during the bump test.
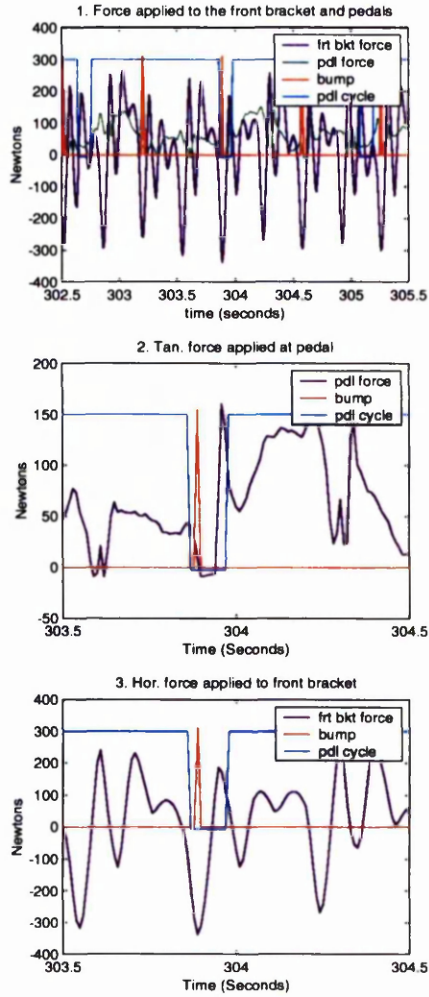
Figure 6.18: Tangential force applied to the crank arms at the pedal and front bracket for the SU bicycle during the bump test.

maximum inertial force is roughly 50 N. To achieve a force of 50 N, the cyclist's torso has to move 1 cm twice a second, which is the frequency of the applied force, 1.5-2 Hz
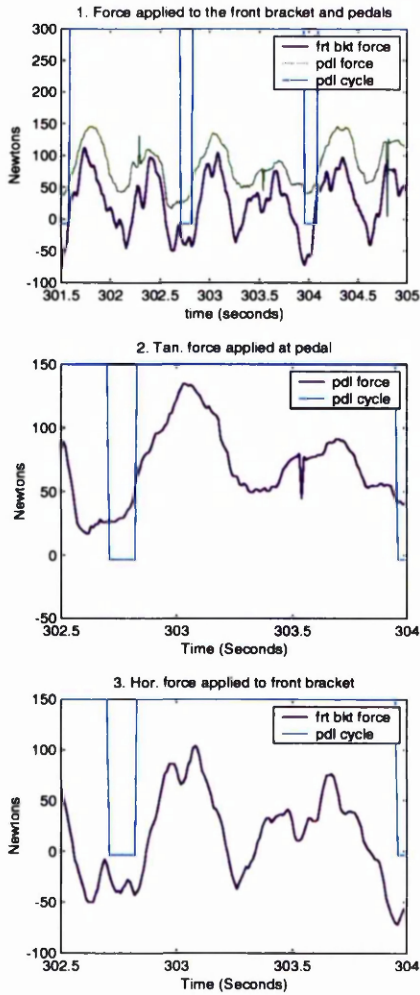
Figure 6.19: Tangential force applied to the crank arms at the pedal and front bracket for the HT bicycle during the no bump test.
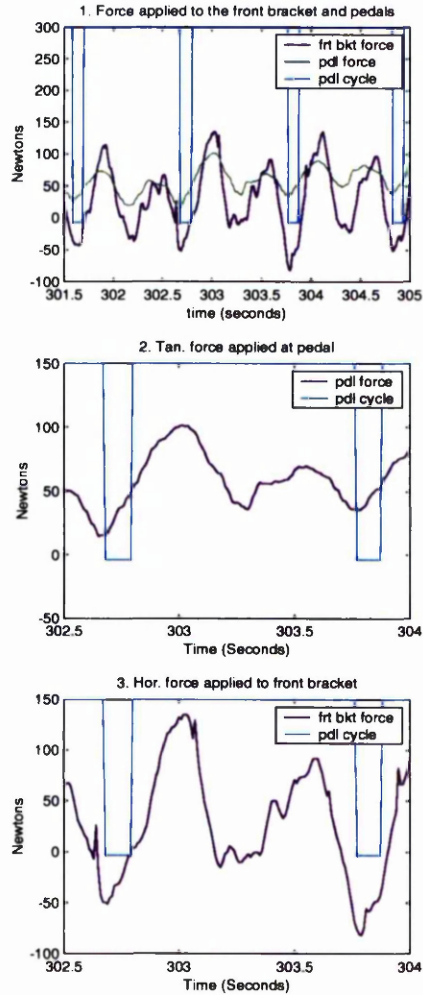
Figure 6.20: Tangential force applied to the crank arms at the pedal and front bracket for the SU bicycle during the no bump test

(see Figures 6.23 and 6.24). This amount of movement is reasonable to expect. See Appendix B Section B.1.3 for calculations of body movement.
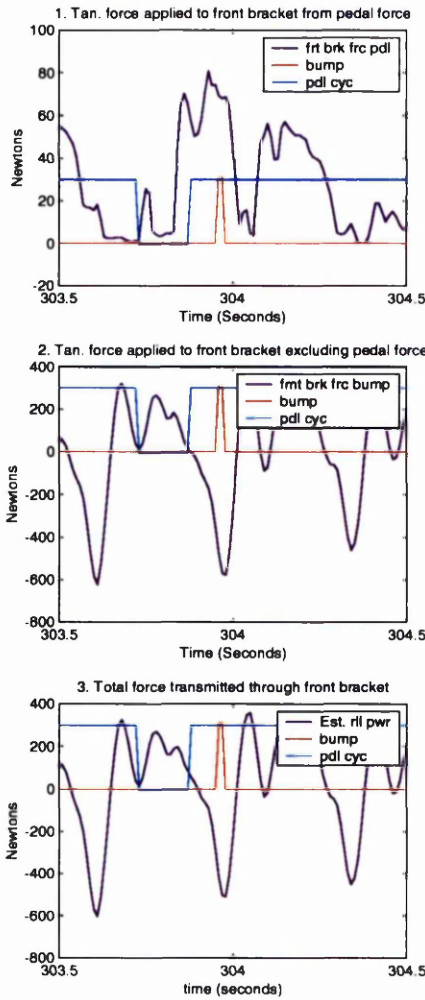
Figure 6.21: The component forces applied by the pedal component and other effects to the front bracket for the HT bicycle during the bump tests.
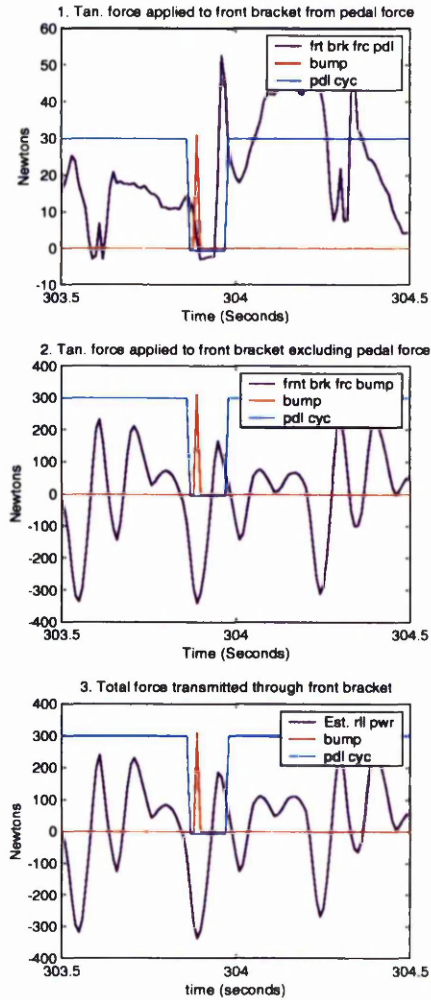
Figure 6.22: The component forces applied by the pedal component and other effects to the front bracket for the SU bicycle during the bump tests.

In Figures 6.25 to 6.28, as expected, the instantaneous power generated by the pedals follows the tangential force applied to the pedals as a result of the constant
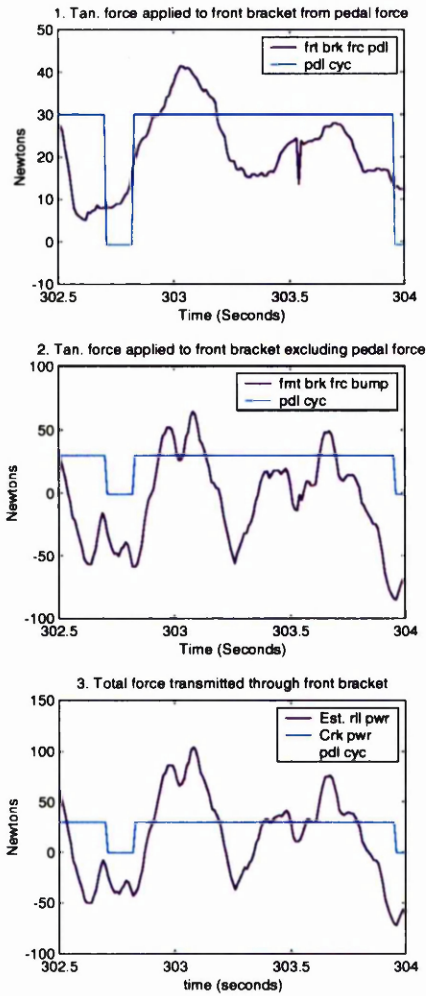
Figure 6.23: The component forces applied by the pedal component and other effects to the front bracket for the HT bicycle during the no bump tests.

rotational velocity of the pedals.
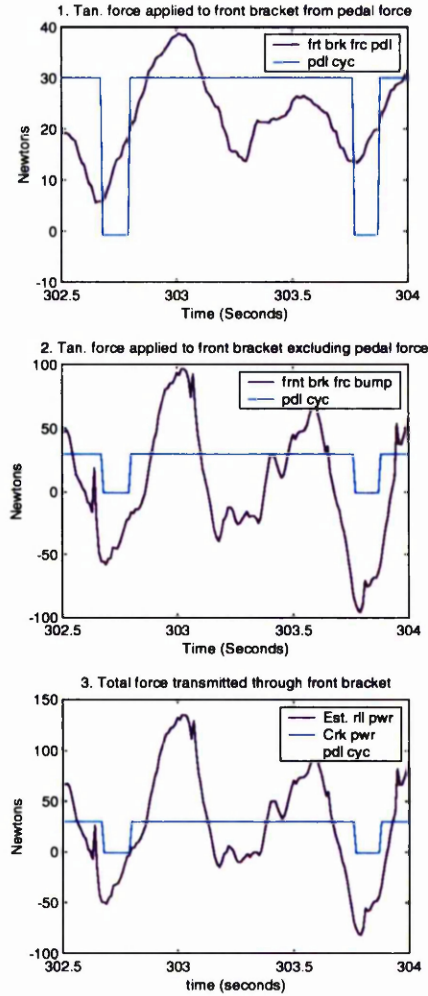
Figure 6.24: The component forces applied by the pedal component and other effects to the front bracket for the SU bicycle during the no bump tests.
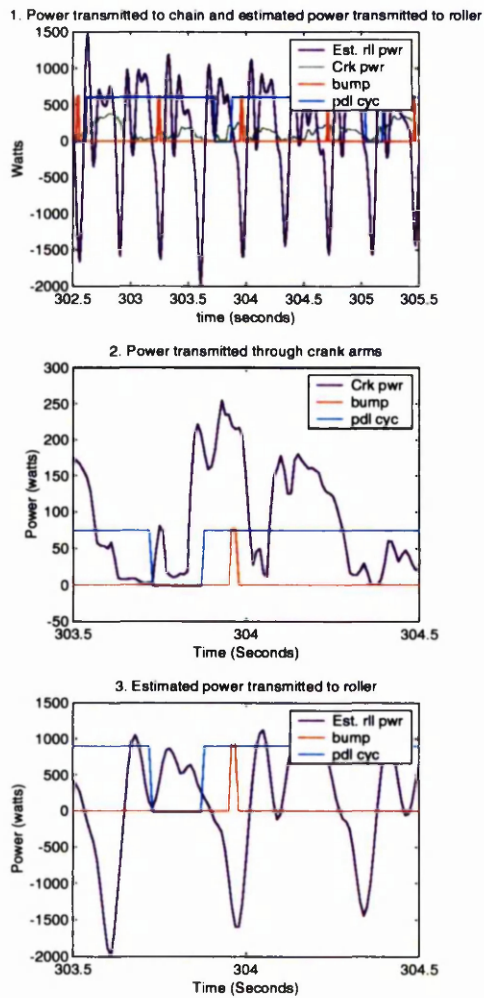
Figure 6.25: Power transmitted through the cranks and front bracket for the HT bicycle during the bump test.
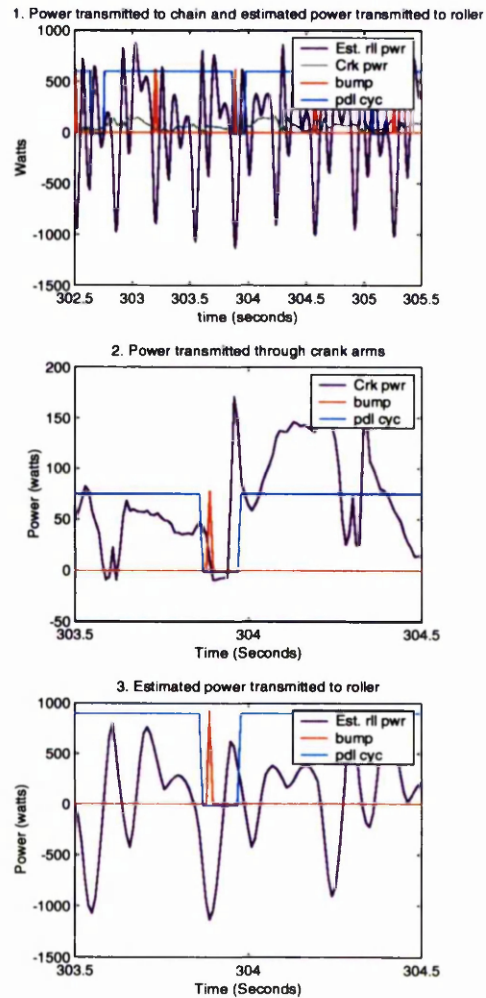
Figure 6.26: Power transmitted through the cranks and front bracket for the SU bicycle during the bump test.
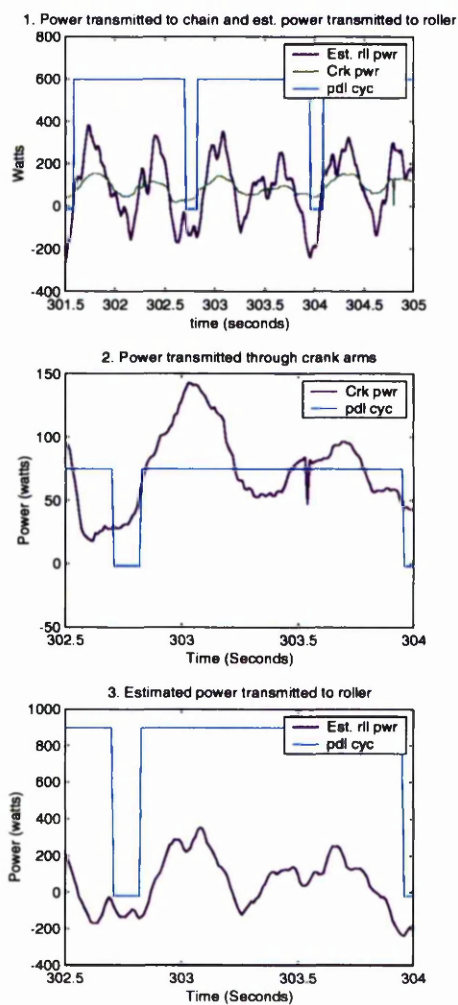
Figure 6.27: Power transmitted through the cranks and front bracket for the HT bicycle during the no bump test.
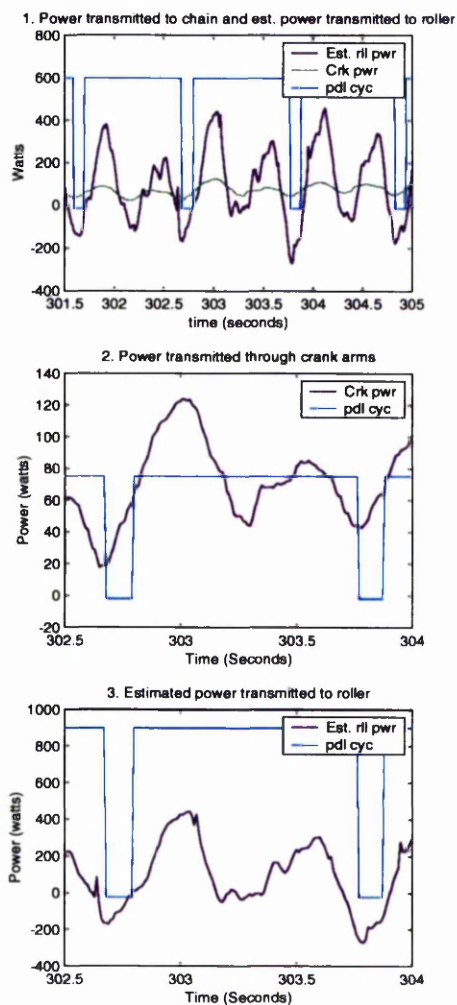
Figure 6.28: Power transmitted through the cranks and front bracket for the SU bicycle during the no bump test.

Three efficiencies can be calculated from the results of energy expended by the subject per minute ($E_{subject}$), the energy transmitted through the pedals per minute ($E_{pedals} = F_{pedals} \cdot \nu_{pedals} \cdot 60 \ KJ \cdot min^{-1}$) and the energy transmitted to the roller per minute ($E_{roller} = F_{frt \ brk} \cdot \nu_{roller \ srf} \cdot 60 \ KJ \cdot min^{-1}$). The efficiency of the subject ($Eff_{subject} = \frac{E_{pedals}}{E_{subject}}$), the efficiency of the bicycle ($Eff_{bicycle} = \frac{E_{roller}}{E_{pedals}}$), and the efficiency of the bicycle/cyclist system ($Eff_{system} = \frac{E_{roller}}{E_{subject}}$). Unfortunately, as explained earlier, the reactive force between the roller and the rear wheel was not measured accurately enough for the efficiency of the bicycle or system to be calculated.

The subject requires energy for fundamental body processes which is on average, 1.2 $kcal \cdot min^{-1}$ or 5 $KJ \cdot min^{-1}$ (McArdle et al. 2000). This was subtracted from the mean calculated energy expenditure of the subjects during the testing. The efficiency of the subject during the bump test is 19.7% ($Eff_{subject \ HT} = \frac{8.04}{45.8-5}$) and 15.0% ($Eff_{subject \ SU} = \frac{4.20}{31.4-5}$) for the HT and SU bicycles respectively. The lower efficiency can possibly be explained by the fact that during the bump test the SU bicycle had a lower rolling resistance than the HT bicycle, which results in a drop in energy per minute transmitted through the pedals. The energy expended by the subject is determined by the energy required at the pedals ("pedal energy") and the energy associated with the upper body movement, e.g. in response to bump impact ("upper body energy"). If the percentage drop in the upper body energy is not as large as the percentage drop in pedal energy on the SU bicycle, the efficiency of the subject will be lower, despite the overall drop in the energy expended by the cyclist.

The efficiency of the subject during the no bump test was 21.9% ($Eff_{subject \ HT} = \frac{5.3}{29.2-5}$) and 16.5% ($Eff_{subject \ SU} = \frac{4.5}{32.2-5}$) on the HT and SU bicycle respectively. Again, the subject has a lower efficiency on the SU bicycle, as with the bump test, however the reason for this is different. The resistance at the roller was consistent

between the two bicycles, therefore the energy required at the pedals was similar. The difference in efficiency results mostly from the higher energy expended by the subject during the SU bicycle tests.

6.3   Energy Analysis

One of the aims of suspension that Olsen (1996) identifies is to keep the wheels on the ground. His reasons are to improve traction, when driving and braking, and steering. However, there is one more. By keeping the wheel on the ground the loss of forward velocity from bump impact is partially regained when the wheel rolls back off the bump.

When the bicycle/cyclist travels over a bump, energy is used against gravity to go up onto the bump. A percentage of this energy only goes back into the forward motion if the bicycle rolls off the bump (see Section 6.3.1) (Burrows 2001). In the DADS HT and SU models there is a clear difference in the speed before and after impact (see Figure 4.11). This shows that energy is lost from traversing a bump, but the figure also shows that the SU bicycle has a greater increase in the velocity as the wheel rolls off the bump. Whitt & Wilson (1982) describe energy lost to bump impact in a similar way:

> "...imagine a very small scale of roughness, with a supposedly rigid machine
> travelling over the surface. Each little roughness could give the machine an
> upward component of velocity sufficient for the wheel(s) to leave the surface. The
> kinetic energy of this upward motion has to be taken from the forward motion,
> just as the rider were going up hill. But when the wheel and machine descend,
> under the influence of gravity as before, the wheel contacts the surface at an
> angle whose magnitude depends upon the speed and the scale of the roughness.

All the kinetic energy perpendicular to the surface at the point of contact can be considered lost."
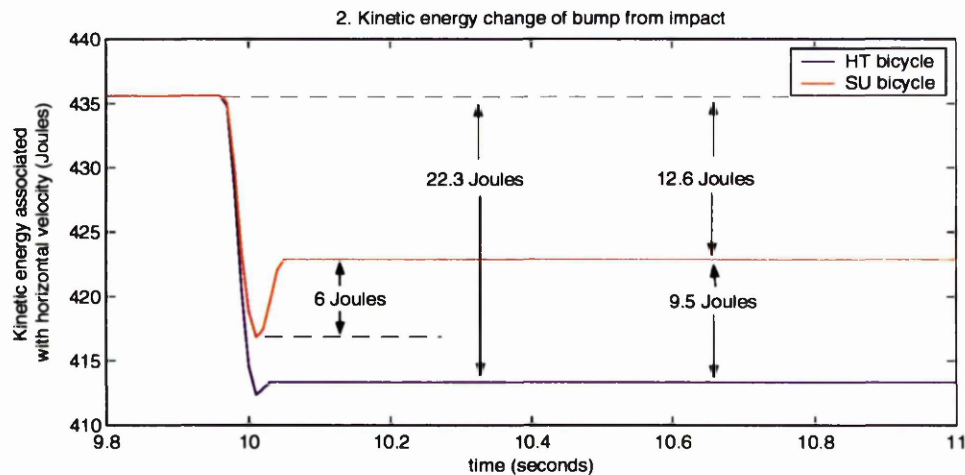
Figure 6.29: Plot of the kinetic energy associated with horizontal velocity of the bump during impact for the DADS HT and SU equivalent momentum models.

If one considers that potential energy gained by travelling over the top of each bump for the HT bicycle is 15.5 Joules for each impact (calculated from DADS HT model results), and the wheel never rolls off the bump (i.e. the wheel returns to the ground without touching the corner of the bump) then all this energy will be lost (the energy will dissipate as heat when the wheel impacts the ground). This is a large percentage of the 22.3 Joules of the kinetic energy associated with horizonal velocity ($Ek_{horizontal}$) lost from traversing the bump in this model (see Figure 6.29). However, the DADS SU bicycle model shows that there is a $0.2 \ m \cdot s^{-1}$ increase in the velocity[1], corresponding to 6 Joules, as the bicycle rolls off the bump (see Figure 4.11). The height gain, going over the bump, is also not as great as that in the DADS HT model. The gain in

---

[1]There is a small increase in velocity for the DADS HT model but this is a result of the way the tyre has been modelled in DADS, and results from the fraction of a second when the base of the impact spring is still compressed, but has passed $X = 0$ (see Figure 4.4) therefore applying a forward force on the rear wheel. This is not the case with a proper tyre.

potential energy is 13.2 Joules, but 6 Joules of this gain in potential is converted back into $Ek_{horizontal}$. Therefore, only 7.2 Joules of $Ek_{horizontal}$ is lost to a gain in potential energy, of the total 12.6 Joules of $Ek_{horizontal}$ lost when traversing the bump in the DADS SU model (see Figure 6.29). This shows that losses in both the impact energy and potential energy are reduced from 6.8 Joules and 15.5 Joules respectively for the HT bicycle to 5.4 Joules and 7.2 Joules respectively for the SU bicycle. The SU bicycle reduces the total losses of $Ek_{horizontal}$ or useful energy per impact by 9.5 Joules. This equates to a reduction of 2000 Joules per minute for the DADS SU model. This is 52% of the difference in energy transmitted through the pedals per minute between the HT and SU bicycles during the bump tests, and can account for the large proportion of the difference in energy expended by the subjects on the two bicycles.

6.3.1 Useful Energy

Useful energy is defined as energy that is used to create horizontal motion.

$$\frac{1}{2}\cdot m \cdot v_a^2 \qquad \frac{1}{2}\cdot m \cdot v_b^2 + m \cdot g \cdot h \qquad \frac{1}{2}\cdot m \cdot v_c^2$$

I v_a v_b $a_{tan\ gent}$ v_c $9.81 m \cdot s^{-1}$

Consider zero friction for both cases

where $v_a = v_c > v_b$ and the kinetic energy converted to potential energy is converted back into kinetic energy with all the velocity of the wheel in the horizontal

$$\frac{1}{2}\cdot m \cdot v_a^2 \qquad \frac{1}{2}\cdot m \cdot v_b^2 + m \cdot g \cdot h \qquad \frac{1}{2}\cdot m \cdot v_c^2 + \frac{1}{2}\cdot m \cdot v_d^2$$

II v_a v_b v_d v_c $9.81 m \cdot s^{-1}$

where $v_a > v_c > v_b$ and the kinetic energy converted to potential energy is converted back into kinetic energy but not all the velocity of the wheel is the horizontal

Figure 6.30: Energy flow of wheel going over two different bump shapes.
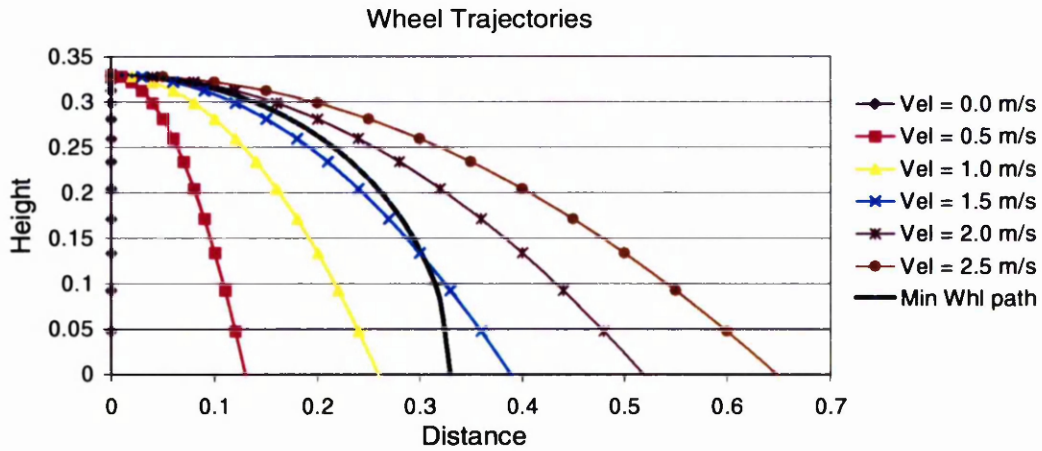
Figure 6.31: Trajectory plots of a rigid wheel going off a bump at different velocities. The downward acceleration is 1 g.
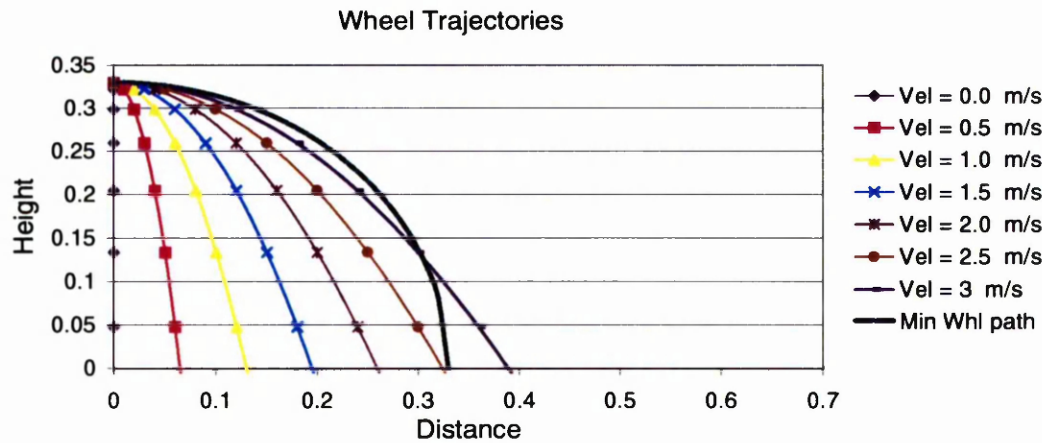
Figure 6.32: Trajectory plots of a suspended wheel, where the mass of the body to which the wheel is attached is far greater than the mass of the wheel, going off a bump at different velocities. The downward acceleration of the wheel is set at 4 g.

When a rigid wheel ramps onto a bump (assuming no impact) there is a loss of kinetic energy that is converted to potential energy. When the rigid wheel goes off the bump that potential energy is converted back into kinetic energy, but only if the wheel rolls off the bump is all the energy converted back into horizontal motion (i.e. useful

energy) (see Case 1 Figure 6.30).

If the horizontal velocity is high enough or the edge of the bump is sharp enough the energy is not converted back into horizontal velocity and is effectively lost to the rigid wheel (see case 2 Figure 6.30). There is a critical horizontal velocity at which the circumference of the wheel will not touch the edge of the bump as it drops to the ground. That critical velocity is approximately 2.5 $m \cdot s^{-1}$ (see Figure 6.31) if the wheel drops with an acceleration of 9.81 $m \cdot s^{-1}$. Any velocity above the critical velocity and none of the potential energy is converted back into useful energy.

Figure 6.32 shows a suspended wheel going off the same bump. The mass to which the wheel is attached, by the suspension system, is presumed to be far greater than the wheel, as with a rear suspended bicycle and cyclist. This means that the wheel will get pushed down at a greater force than just that applied by gravity and the critical velocity will increase proportionally to the increase in downward force on the wheel.

Chapter 7

Conclusions

7.1 Physiological and Psychological Effects

The physiological and psychological results from the tests show that at constant speed, over frequent regular bumps, during sub-maximal exercise, the full suspension bicycle offers a significant advantage over the hard tail bicycle in terms of $\dot{V}O_2$, heart rate, energy expended, R.P.E. and comfort. Without bumps, the HT bicycle offers a small advantage evidenced by a lower $\dot{V}O_2$ and energy expended, backed by a trend to improvement in heart rate, RPE and comfort ratings. These findings indicate that the suspension system has the potential to improve bicycle performance on rough trails, but the better than expected performance of HT bicycles in time trials and off road races suggests that the riding style of the cyclist is an important factor.

7.2 Mechanical Systems Dynamics

7.2.1 Experimental Results

The mechanical results from the tests show that at constant speed, over frequent regular bumps, during sub-maximal exercise and with a passive rider, the full suspension bicycle offers a significant advantage over the hard tail bicycle. The vertical saddle and handlebar acceleration, total saddle and handlebar displacement and the horizontal force applied by the bump impact for the SU bicycle are significantly lower than that for the HT bicycle. During the no bump test there were slight advantages for the HT bicycle in saddle displacement, but this was very small. The SU bicycle had a slight advantage over the HT bicycle in handlebar acceleration and displacement, but again this was very small. There was a small but significant advantage for the SU bicycle, as evidenced by the lower mean force applied to the pedals, in comparison to the HT bicycle during the no bump test.

7.2.2 Simulation Results

The model produced results similar to the test results for bump impact and has shown that a dynamic computer model aids in the understanding of test results. The models have shown that there are definite uses for simulations in future work for both the optimisation of suspension systems and dynamic analysis of testing equipment manufacture, specifically for the placement of instrumentation.

The simulation data shows that there is a drop in the velocity of the bicycle/cyclist when a bump is impacted, and therefore a corresponding drop in the kinetic energy of the bicycle and cyclist. It also showed that the drop in velocity of the HT bicycle is

greater than that of the SU bicycle. This indicates that the SU bicycle will be faster than the HT bicycle when riding over bumps.

7.3 Correlation of Results

The differences measured between the HT and SU bicycle for the physiological results of $\dot{V}O_2$, heart rate and energy expended, and the mechanical results of the horizontal force applied by the bump impact, saddle acceleration and total saddle displacement during the bump test, correlate well.

There is further correlation between the psychological result of RPE and comfort rating and the mechanical results of saddle acceleration and total displacement in both the bump and no bump test. There is, however, a lack of correlation between the $\dot{V}O_2$ result and the mean pedal force during the no bump test, but it should be remembered that all the differences between the HT and SU bicycles during the no bump tests are very small.

The mechanical experimental results correlate with the simulation results of saddle acceleration and bump impact force. This has allowed for the decomposition of the experimental results into their components, using the dynamic model simulation, for better understanding.

The current study has shown that for isolating and measuring the effect of rear wheel impact a rig can be used and a method of laboratory testing has been found that enables consistent results, that correlate well, to be obtained. The results from the research provide a fundamental and solid basis for further research.

7.4 Future Work

So far this study has looked at sub-maximal testing, with low torque applied to the chain rings, which means less shock compression as a result of chain tension. Research needs to be done to improve understanding of the effects of rear suspension systems on race times and elite off-road cyclists. This requires time-trial testing in laboratory conditions the same as the tests conducted in this study, but with elite cyclists. The tests need to be modified to allow for the effects of rear suspension systems to be analysed during high torque and high speed conditions to determine if they are faster than non-suspended systems. The subjects should have no restrictions on riding style and should be allowed to go as fast as they can with an additional braking force on the roller, proportional to air resistance. Testing should also be done with different bump sizes and frequencies. The cycling rig design can be adapted to give satisfactory results under these conditions.

The cycling rig instrumentation can be redesigned to give a more accurate estimate of the force between the rear wheel and the roller surface. Further measurements that should be taken during future testing are the vertical force at the front and rear wheel hubs, for aiding in the analysis of future rear suspension system designs. A separation of the vertical force applied to the pedals and the tangential force applied to the crank arms at the pedals is desirable. This will aid the understanding of how cyclists use their inertia when cycling hard, and compensate for bump impact.

High speed video footage should also be taken on any future testing to view how the different bicycles are controlled by the cyclist, and what happens to the rear wheel during bump impact.

The effects of increased rolling resistance from high landing decelerations after

bump impact, and the significance of this effect, need to be investigated further.

Bibliography

anon (2000). Spanish stroll, *Mountain Biker International* (60): 40–46.

Berry, M., Koves, T. & Benedetto, J. (2000). The influence of speed, grade and mass during simulated off road bicycling, *Applied Ergonomics* **31**: 531–536.

Berry, M., Woodard, C., Dunn, C., Edwards, D. & Pittman, C. (1993). The effects of a mountain biking suspension system on metabolic energy expenditure, *Cycling Science* pp. 8–14.

Borg, G. (1998). *Borg's perceived exertion and pain scale*, 1 edn, Human Kinetics, P.O.Box IW14,Leeds.

Brisswalter, J., Hausswrith, C., Smith, D., Vercruyssen, F. & Vallier, J. (2000). Energetically optimal cadence vs. freely-chosen cadence during cycling: Effect of exercise duration, *International Journal of Sports Medicine* **21**(1): 60–64.

Burrows, M. (2001). *Bicycle Design Towards the Perfect Machine*, 1 edn, Company of Cyclists Publications, 7 Coda Avenue, York.

Candau, R., Grappe, F., Menard, M., Barbier, B., Millet, G., Hoffman, M., Belli, A. & Rouillon, J. (1999). Simplified deceleration method for assessment of resistive force in cycling, *Medicine and Science in Sports and Exercise* **31**(10): 1441–1447.

Candy, L. & Edmonds, E. (1996). Creative design of the lotus bicycle: implications for knowledge support systems research, *Design Studies* **17**(1): 71–90.

Castejon, L., Miravete, A., Ullod, J. & Larrode, E. (1994). Composite monocoque frame for a mountain bicycle: Testing and calculation, *Applied Composite Materials* **1**: 247–258.

De Groot, G., Welbergen, E., Clijsen, L., Clarijs, J., Cabri, J. & Antonis, J. (1994). Power, muscular work, and external force in cycling, *Ergonomics* **37**(1): 31–42.

De Lorenzo, D. & Hull, M. (1999a). A hub dynamometer for measurement of wheel force in off-road bicycling, *Journal of Biomechanical Engineering, Transaction of the ASME* **121**(1): 132–137.

De Lorenzo, D. & Hull, M. (1999b). Quantification of structural loading during off-road cycling, *Journal of Biomechanical Engineering, Transaction of the ASME* **121**(4): 399–405.

Ferraresi, C., Garibaldi, L., Perocchio, D. & Piombo, B. (1998). Dynamic behaviour and optimisation of frames for road and mountain bicycles, *Proceeds of International Modal Analysis Conference* **1**: 387–393.

Good, C. & McPhee, J. (1999). Dynamics of mountain bicycle with rear suspension: design optimisation, *Sports Engineering* **2**: 129–143.

Good, C. & McPhee, J. (2000). Dynamics of mountain bicycle with rear suspension: modelling and simulation, *Sports Engineering* **3**: 49–55.

Gorman, D. & Kennedy, W. (1998). *Applied Solid Dynamics*, Butterworth & Co. (Publishers) Ltd, London. p 6.

Grappe, F., Candau, R., Barbier, B., Hoffman, M., Belli, A. & J.D., R. (1999). Influence of tyre pressure and vertical load on the coefficient of rolling resistance and simulated cycling performance, *Ergonomics* **10**: 1361–1371.

Grappe, F., Candau, R., Belli, A. & Rouillon, J. (1997). Aerodynamic drag in field cycling with special reference to the obree's position, *Ergonomics* **40**(12): 1299–1311.

Graves, P. (2000). Olympic preview, *Mountain Biker International* (61): 62–64.

Han, R., Thomlinson, M. & Tu, Y. (1991). Kinematics and kinetics of a non-circular bicycle drive system, *Mech. Mach. Theory* **26**(4): 375–388.

Harris, T. (1995). Rear wheel suspension for a bicycle equipped therewith, U.S. Patent Documents. patent number 5452910.

Kidd, M., Loch, N. & Reuben, R. (1999). Experimental examination of bicycle chain force, *Experimental Mechanics* **39**(4): 278–283.

Kopka, H. & Daly, P. (1999). *A Guide to LATEX*, 3 edn, Addison-Wesley, Edinbough Gate, Harlow, CM20 2JE.

Kukoda, J. (1992). Impact eaters, *Bicycling* **33**(4): 148–166.

Kyle, C. (1990). Chain friction, windy hills and other quick calculations, *Cycling Science* **2**: 23–26.

Kyle, C. & Burke, E. (1984). Improving the racing bicycle, *Mechanical Engineering* pp. 34–45.

Leitner, H. (1996). Rear suspension for bicycles, U.S. Patent Documents. patent number 5509679.

Lucia, A., Hoyos, J. & Chicharro, J. (2001). Preferred pedalling cadence in professional cycling, *Medicine and Science in Sports and Exercise* **33**(8): 1361–1366.

MacRae, H.-S., Hise, K. & Allen, P. (2000). Effects of front and dual suspension mountain bike systems on uphill cycling performance, *Medicine and Science in Sports and Exercise* **32**(7): 1276–1280.

Marin Bicycles Web Page (2000). 1999 bicycles, World Wide Web. http://www.marinbikes.com/.

Martin, J., Milliken, D., Cobb, J., McFadden, K. & Coggan, A. (1998). Validation of a mathematical model for road cycling power, *Journal of Applied Biomechanics* **14**: 276–291.

McArdle, W., Katch, F. & Katch, V. (1996). *Exercise physiology: energy, nutrition, and human performance*, 4 edn, Williams & Wilkins, London.

McArdle, W., Katch, F. & Katch, V. (2000). *Essentials of Exercise Physiology*, 2 edn, Williams & Wilkins, London.

Needle, S. & Hull, M. (1997). An off-road bicycle with adjustable suspension kinematics, *Journal of Mechanical Design, Transaction of the ASME* **119**(3): 370–375.

Nielens, H. & Lejeune, T. (2001). Energy cost of riding bicycles with shock absorbtion systems on a flat surface, *International Journal of Sports Medicine* **22**(6): 400–404.

Olsen, J. (1992). Bicycle suspension systems meet mr. simple dynamics, *Cycling Science* **4**: 6–12.

Olsen, J. (1996). *Bicycle suspension systems. In High-Tech Cycling*, Human Kinetics, Champaign, IL, USA. pp. 45-64.

Owen, F. & Jones, R. (1994). *Statistics*, 4 edn, Pitman Publishing, 128 Long Acre, London WC2E 9AN.

Ryschon, T. (1994). Physiologic aspects of bicycling, *Clinics in Sports Medicine* **13**(1): 15–38.

Scott, R. (1889). Cycling art, *Energy and Locomotion* . Philadelphia: Lippincott.

Seifert, J., Luetkemeier, M., Spencer, M., Miller, D. & Burke, E. (1997). The effect of mountain bike suspension systems on the energy expenditure, physical exertion, and time trial performance during mountain bicycling, *International Journal of Sports Medicine* **18**(3): 197–200.

Shennum, P. & de Vries, H. (1976). The effect of saddle height on oxygen consumption during bicycling ergometer work, *Medicine and Science in Sport* **8**(2): 119–121.

U.C.I. Web Page (2001). About mountain biking, World Wide Web. http://www.uci.ch/english/mtb/what_is.htm.

Vercruyssen, F., Hausswirth, C., Smith, D. & Brisswalter, J. (2001). Effects of exercise on the choice of an optimal pedaling cadence among triathletes, *Canadian Journal of Applied Physiology* **26**(1): 44–54.

Wang, E. & Hull, M. (1996). A model for determining rider induced energy losses in bicycling suspension systems, *Vehicle System Dynamics* **25**: 223–246.

Wang, E. & Hull, M. (1997). Minimisation of pedaling induced energy losses in off-road rear suspension systems, *Vehicle System Dynamics* **28**: 291–306.

Whitt, F. & Wilson, D. (1982). *Bicycling Science*, 2 edn, The MIT Press, Cambridge, Massachusetts.

Wilczynski, H. & Hull, M. (1994). A dynamic system model for estimating surface-induced frame loads during off-road cycling, *Journal of Mechanical Design, Transaction of the ASME* **116**(3): 816–822.

Williams, H. (2000). Dutch master, *Mountain Biker International* (57): 68–72.

Appendix A

Individual Subject Results

A.1 Physiological Results

Units	Bump				No Bump			
ml·kg^{-1}·min^{-1}	Hard tail		Suspension		Hard tail		Suspension	
Subject	mean		mean		mean		mean	
No.	9th min	10th min	9th min	10th min	9th min	10th min	9th min	10th min
	27.016		19.335		18.120		20.579	
1	26.542	27.490	19.427	19.243	18.493	17.746	20.466	20.691
	29.997		24.015		20.425		22.591	
2	30.111	29.882	23.958	24.071	20.063	20.787	22.479	22.702
	29.056		18.787		18.715		19.944	
3	28.707	29.404	18.299	19.275	18.782	18.647	19.742	20.145
	29.292		20.129		19.316		20.519	
4	29.539	29.044	19.701	20.557	19.405	19.317	20.490	20.547
	27.108		20.457		16.982		22.383	
5	26.867	27.348	20.011	20.903	16.731	17.233	22.024	22.741
	31.881		20.682		22.243		22.548	
6	31.391	32.371	20.760	20.604	22.018	22.468	22.968	22.128
	33.469		19.651		20.912		24.731	
7	34.091	32.847	20.014	19.287	20.969	20.855	25.324	24.138
	30.065		21.668		21.480		22.412	
8	29.749	30.380	21.488	21.848	21.441	21.518	22.872	21.952
aver-	29.735		20.590		19.780		21.963	
age	29.625	29.846	20.457	20.724	19.738	19.821	22.046	21.881

Table A.1: Table of individual results for $\dot{V}O_2$ values for the bump and no bump test.

Units	Bump				No Bump			
beats · min^{-1}	Hard tail		Suspension		Hard tail		Suspension	
Subject	mean		mean		mean		mean	
No.	9th min	10th min	9th min	10th min	9th min	10th min	9th min	10th min
	153		125		116		118	
1	153	152	126	124	115	116	120	115
	120		103		115		110	
2	120	120	103	102	115	116	109	111
	169		122		109		121	
3	166	171	124	120	108	110	118	124
	142		114		99		101	
4	142	141	115	113	100	97	102	100
	147		119		102		108	
5	145	149	119	119	100	103	108	107
	158		112		123		118	
6	158	157	112	111	122	124	118	117
	146		101		106		115	
7	149	143	100	102	108	103	115	114
	137		99		98		102	
8	137	136	99	98	98	97	101	103
aver-	146		112		108		111	
age	146	146	112	111	108	108	111	111

Table A.2: Table of individual results for heart rate values during the 9th and 10th minute for the bump and no bump tests.

Units KJ	Bump				No Bump			
	Hard tail		Suspension		Hard tail		Suspension	
Subject No.	mean		mean		mean		mean	
	9th min	10th min	9th min	10th min	9th min	10th min	9th min	10th min
1	42.73		30.48		30.41		32.46	
	42.06	43.41	30.71	30.26	30.69	30.12	32.32	32.61
2	51.86		39.98		31.09		32.18	
	52.43	51.30	40.05	39.92	31.07	31.10	32.92	31.44
3	42.84		28.00		24.42		31.96	
	42.17	43.52	27.33	28.67	24.20	24.64	31.46	32.46
4	39.25		25.93		23.81		26.78	
	39.80	38.70	25.32	26.55	24.34	23.28	26.68	26.89
5	43.67		32.68		31.06		31.22	
	43.20	44.15	32.00	33.36	30.68	31.45	31.86	30.59
6	43.75		27.85		27.87		30.73	
	43.10	44.40	28.93	27.78	27.50	28.25	30.65	30.81
7	54.90		31.73		31.63		33.32	
	55.97	53.83	32.51	30.94	31.82	31.44	33.18	33.45
8	47.50		34.42		33.28		33.72	
	47.08	47.91	34.17	34.67	33.38	33.18	39.47	37.98
aver-	45.81		31.39		29.20		32.17	
age	45.73	45.90	31.25	31.51	29.21	29.18	32.32	32.03

Table A.3: Table of individual results for energy expenditure values for the bump and no bump tests.

Subject No.	Bump						No Bump					
	Hard tail			Suspension			Hard tail			Suspension		
		mean			mean			mean			mean	
	3rd min	6th min	9.5th min	3rd min	6th min	9.5th min	3rd min	6th min	9.5th min	3rd min	6th min	9.5th min
1	11	10.667	10	9	9	9	9	9.667	10	10	10	10
2	14	14.667	16	13	12.667	12	10	10.667	11	9	9.333	10
3	11	10.333	10	10	9.667	9	8	8.667	9	11	11.667	13
4	15	15.667	17	10	9.667	9	10	10.333	10	10	11	11
5	12	12	12	13	13	13	9	9	9	9	9.667	10
6	11	11.333	12	9	9	9	9	10	11	9	10	10
7	12	13	15	8	10.667	12	11	11	11	11	11	11
8	12	12.667	13	12	12	12	7	7.667	8	8	8.667	9
average	12.25	12.542	13.125	10.5	10.708	10.625	9.125	9.625	9.875	9.625	10.167	10.5

Table A.4: Table of individual results for RPE values for the bump and no bump tests.

Subject No.	Bump								No Bump							
	Hard tail				Suspension				Hard tail				Suspension			
	3rd min	mean	6th min	9.5th min	3rd min	mean	6th min	9.5th min	3rd min	mean	6th min	9.5th min	3rd min	mean	6th min	9.5th min
1	2	1.667	1	2	4	4	4	4	4	4	4	4	4	4	4	4
2	2	2	2	2	2	2	2	2	4	4	4	4	4	4	4	4
3	1	0.667	0	1	3	3	3	3	4	4	4	4	4	3.667	4	3
4	1	1	1	1	4	4	4	4	4	4	4	4	4	4	4	4
5	1	1	1	1	2	2	2	2	4	4	4	4	4	4	4	4
6	2	1.667	2	1	4	4	4	4	5	4.333	4	4	4	3.667	4	3
7	2	1.333	1	1	5	3.667	3	3	5	5	5	5	5	5	5	5
8	2	1.333	1	1	3	3	3	3	5	5	5	5	4	4	4	4
average	1.625	1.333	1.125	1.250	3.375	3.208	3.125	3.125	4.375	4.292	4.250	4.250	4.125	4.042	4.125	3.875

Table A.5: Table of individual results for comfort values for the bump and no bump tests.

A.2 Mechanical Results

Units g's	Bump				No Bump			
	Hard tail		Suspension		Hard tail		Suspension	
Subject No.	mean		mean		mean		mean	
	max	min	max	min	max	min	max	min
1	-2e-005		4.49e-006		5.52e-008		-6.38e-007	
1	1.628	-1.642	1.034	-0.877	0.077	-0.079	0.072	-0.072
2	-1.16e-005		-3.2e-006		3.19e-007		-1.32e-007	
2	1.243	-0.984	0.943	-0.853	0.080	-0.091	0.056	-0.057
3	2.84e-005		-4.73e-006		-6.42e-007		9.94e-008	
3	1.599	-1.129	0.995	-0.797	0.063	-0.076	0.053	-0.052
4	2.33e-005		1.13e-005		-5.18e-007		-1.03e-006	
4	1.323	-1.159	0.907	-0.841	0.112	-0.119	0.076	-0.077
5	2.98e-005		5.74e-006		-8.52e-007		1.17e-006	
5	1.723	-1.306	1.086	-0.710	0.069	-0.069	0.059	-0.056
6	1.3e-005		2.52e-005		-1.38e-006		6.84e-007	
6	1.824	-1.426	1.259	-1.120	0.085	-0.087	0.071	-0.072
7	-3.86e-006		4.38e-006		-2.87e-006		-2.52e-007	
7	1.646	-1.278	0.905	-0.763	0.077	-0.079	0.070	-0.068
8	-9.89e-006		-1.75e-006		-1.42e-006		9.56e-007	
8	1.287	-1.414	0.848	-0.794	0.081	-0.088	0.071	-0.070
Average	6.14e-006		5.18e-006		-9.14e-007		1.07e-007	
Average	1.534	-1.292	0.997	-0.844	0.081	-0.086	0.066	-0.065

Table A.6: Mean, maximum and minimum values of handlebar acceleration for each subject during the bump and no bump tests.

Units m/s	Bump				No Bump			
	Hard tail		Suspension		Hard tail		Suspension	
Subject No.	mean		mean		mean		mean	
	max	min	max	min	max	min	max	min
1	-4.14e-006		-2.22e-007		7.46e-007		6.38e-007	
	0.255	-0.199	0.069	-0.092	0.011	-0.010	0.009	-0.009
2	-1.68e-005		0.0809		-1.05e-007		4.72e-007	
	0.175	-0.132	0.081	-0.079	0.012	-0.011	0.008	-0.009
3	7.28e-006		2.65e-006		-2.85e-007		-5.62e-008	
	0.227	-0.157	0.072	-0.079	0.011	-0.011	0.008	-0.009
4	-8.6e-006		-3.72e-006		-1.49e-006		4.98e-007	
	0.215	-0.147	0.072	-0.081	0.015	-0.015	0.009	-0.009
5	1.95e-005		3.54e-006		-5.78e-007		2.23e-007	
	0.241	-0.180	0.070	-0.087	0.010	-0.011	0.010	-0.009
6	-5.46e-006		-1.33e-006		-5.76e-007		-4.08e-007	
	0.200	-0.174	0.088	-0.108	0.011	-0.011	0.008	-0.008
7	-4.57e-006		3.59e-006		-1.5e-006		3.38e-007	
	0.234	-0.180	0.070	-0.078	0.011	-0.009	0.008	-0.008
8	-3.26e-006		6.93e-006		-8.47e-008		-2.62e-007	
	0.250	-0.140	0.083	-0.078	0.011	-0.011	0.009	-0.009
Average	-2e-006		1.74e-006		-4.83e-007		1.8e-007	
	0.225	-0.164	0.076	-0.085	0.012	-0.011	0.009	-0.009

Table A.7: Mean, maximum and minimum values of handlebar velocity for each subject during the bump and no bump tests.

Units mm / Subject No.	Bump Hard tail mean max	min	Bump Suspension mean max	min	No Bump Hard tail mean max	min	No Bump Suspension mean max	min
1	0.00041		-0.00037		1.9e-006		3.5e-005	
1	7.31	-4.71	1.95	-2.16	0.41	-0.41	0.31	-0.32
2	-0.00019		3.2e-005		-2.9e-005		-4.6e-006	
2	6.15	-5.28	2.28	-2.32	0.51	-0.49	0.28	-0.29
3	-0.00094		0.00043		-7.4e-006		1.3e-005	
3	7.60	-6.13	1.89	-2.04	0.48	-0.44	0.32	-0.32
4	-0.00045		-0.00054		1.9e-005		7.7e-005	
4	6.01	-4.77	2.20	-2.73	0.63	-0.62	0.30	-0.30
5	-0.00029		0.00022		-1.7e-005		-8e-005	
5	7.93	-5.01	1.79	-1.86	0.45	-0.44	0.38	-0.41
6	-0.0011		-0.00048		-4.5e-006		-7.5e-005	
6	4.81	-4.91	2.27	-2.75	0.45	-0.45	0.30	-0.30
7	0.00027		-0.00016		5.8e-005		2.3e-006	
7	7.37	-5.67	1.85	-2.15	0.40	-0.40	0.26	-0.26
8	0.0005		0.0004		-3.5e-005		-2.6e-005	
8	6.30	-5.63	2.48	-3.22	0.42	-0.41	0.30	-0.30
Average	-0.00022		-5.9e-005		-1.6e-006		-7.2e-006	
Average	6.69	-5.26	2.09	-2.40	0.47	-0.46	0.31	-0.31

Table A.8: Mean, maximum and minimum values of handlebar displacement for each subject during the bump and no bump tests.

Units g's	Bump				No Bump			
	Hard tail		Suspension		Hard tail		Suspension	
Subject	mean		mean		mean		mean	
Subject No.	max (I) max (L)	min	max (I) max (L)	min	max	min	max	min
1	-3.32e-005		-1.41e-005		7.6e-006		1.12e-005	
	2.7253	-3.1516	1.1654	-2.5082	0.3026	-0.3112	0.2720	-0.2993
	6.4113		4.8888					
2	-4.11e-005		-6.77e-005		4.04e-007		-5.02e-006	
	2.5772	-2.7624	1.1154	-2.5792	0.2926	-0.3141	0.2579	-0.2693
	5.8513		4.7406					
3	8.75e-007		3.48e-005		1.02e-005		3.43e-006	
	2.4913	-2.8408	1.0325	-2.2573	0.2807	-0.3023	0.3018	-0.3325
	6.6399		4.6146					
4	8.08e-005		-1.38e-005		7.72e-006		-1.99e-006	
	2.5618	-2.8492	1.1759	-3.1908	0.3064	-0.3315	0.2952	-0.3275
	5.4128		5.6041					
5	2.41e-006		3.91e-005		-9.31e-006		4e-006	
	2.4428	-2.8502	1.2141	-2.4408	0.2910	-0.3041	0.2622	-0.2860
	6.8250		5.2457					
6	1.26e-006		-3.66e-005		-3.3e-006		4.57e-006	
	2.8534	-3.1146	1.2831	-2.7051	0.2801	-0.2993	0.2881	-0.2850
	7.5862		5.4878					
7	-4.67e-005		-1.38e-005		3.79e-006		2.79e-006	
	2.5588	-2.7899	1.0590	-2.3746	0.2642	-0.2816	0.2759	-0.3098
	6.8908		4.5234					
8	2.53e-005		1.24e-005		-2.76e-006		-4.12e-007	
	2.7100	-2.8448	1.2415	-3.3476	0.3246	-0.3409	0.3336	-0.3561
	6.2283		5.6122					
Average	-1.28e-006		-7.45e-006		1.8e-006		2.32e-006	
	2.6151	-2.9004	1.1609	-2.6754	0.2928	-0.3106	0.2858	-0.3082
	6.4807		5.0896					

Table A.9: Mean, maximum and minimum values of saddle acceleration for each subject during the bump and no bump tests. Key: (I) is the maximum acceleration resulting from bump impact (for bump test only). (L) is the maximum acceleration resulting from ground impact (landing) after leaving the bump (for bump test only).

Units m/s	Bump				No Bump			
	Hard tail		Suspension		Hard tail		Suspension	
Subject No.	mean		mean		mean		mean	
	max	min	max	min	max	min	max	min
1	-2.539e-005		6.077e-006		1.77e-006		1.206e-006	
	0.5702	-0.6646	0.3009	-0.3557	0.0401	-0.0436	0.0392	-0.0413
2	-1.81e-005		8.815e-006		1.848e-006		9.938e-008	
	0.5368	-0.6613	0.3122	-0.3038	0.0421	-0.0452	0.0434	-0.0416
3	3.265e-005		1.692e-006		-1.003e-006		-2.322e-006	
	0.5550	-0.7042	0.3060	-0.3197	0.0523	-0.0545	0.0596	-0.0637
4	9.382e-006		-1.587e-005		9.637e-007		-3.241e-007	
	0.5022	-0.6147	0.3555	-0.3505	0.0430	-0.0455	0.0397	-0.0424
5	3.76e-005		1.629e-005		6.298e-007		-5.69e-006	
	0.5677	-0.7032	0.3247	-0.3655	0.0586	-0.0606	0.0547	-0.0611
6	3.637e-007		-1.241e-006		-3.313e-007		1.076e-006	
	0.5269	-0.7673	0.3144	-0.3729	0.0373	-0.0400	0.0382	-0.0380
7	-1.112e-005		-2.524e-006		-4.751e-007		1.279e-006	
	0.4913	-0.7628	0.3123	-0.3110	0.0360	-0.0376	0.0382	-0.0419
8	-7.469e-006		2.136e-007		-1.372e-007		6.138e-007	
	0.5392	-0.6645	0.3489	-0.3753	0.0441	-0.0462	0.0451	-0.0482
Average	2.24e-006		1.681e-006		4.082e-007		-5.077e-007	
	0.5362	-0.6928	0.3219	-0.3443	0.0442	-0.0467	0.0447	-0.0473

Table A.10: Mean, maximum and minimum values of saddle velocity for each subject during the bump and no bump tests.

Units mm	Bump				No Bump			
	Hard tail		Suspension		Hard tail		Suspension	
Subject	mean		mean		mean		mean	
No.	max	min	max	min	max	min	max	min
1	0.0001956		0.001234		-6.372e-005		-0.0002359	
1	17.1665	-7.1353	7.1416	-5.5212	1.4024	-1.3888	1.4755	-1.3878
2	-0.001043		0.001794		1.834e-005		0.000182	
2	17.0179	-8.0918	6.9147	-4.9119	1.6157	-1.4952	1.6279	-1.5612
3	-0.0009096		0.0005074		-8.441e-005		6.642e-005	
3	18.6680	-7.7595	6.5140	-4.8418	2.1497	-1.8114	2.5019	-2.3137
4	-0.0008154		0.0004414		-5.151e-005		-0.0001209	
4	15.1791	-6.4126	7.5873	-6.5344	1.6358	-1.5234	1.5270	-1.4279
5	0.0002522		-0.001041		-2.312e-006		-0.0001225	
5	18.9447	-8.0385	6.9023	-5.0822	2.5698	-2.2651	2.6274	-2.3975
6	6.365e-005		0.001862		0.0001222		-0.0001696	
6	15.0291	-8.0453	7.5241	-6.4054	1.3167	-1.3283	1.3952	-1.3407
7	0.0006233		0.0004599		-6.938e-005		4.975e-006	
7	16.1166	-7.6036	7.0851	-5.5802	1.2479	-1.2596	1.5251	-1.4718
8	-0.0009714		-0.0001165		9.095e-005		-8.627e-005	
8	16.8822	-7.6208	6.8387	-5.6002	1.4829	-1.4448	1.6544	-1.5813
Average	-0.0003256		0.0006426		-4.975e-006		-6.023e-005	
Average	16.8755	-7.5884	7.0635	-5.5597	1.6776	-1.5646	1.7918	-1.6852

Table A.11: Mean, maximum and minimum values of saddle displacement for each subject during the bump and no bump tests.

Units m/s	Bump		No Bump	
	Hard tail	Suspension	Hard tail	Suspension
Subject No.	mean	mean	mean	mean
1	1.147	1.096	1.1	1.267
2	1.049	1.066	1.06	1.22
3	1.093	1.002	1.058	1.026
4	1.317	1.283	1.497	1.273
5	1.023	1.191	0.9138	1.177
6	1.093	1.095	1.101	1.291
7	0.9298	1.033	1.123	1.101
8	1.073	0.9422	1.141	1.111
Average	1.091	1.089	1.124	1.183

Table A.12: Mean values of tangential crank velocity at pedal for each subject during the bump and no bump tests.

Units	Bump				No Bump			
Newtons	Hard tail		Suspension		Hard tail		Suspension	
Subject	mean		mean		mean		mean	
No.	max	min	max	min	max	min	max	min
1	119.8		69.8		85.9		55.5	
	242.5	-1.0	139.2	1.8	145.4	25.0	78.3	28.1
2	123.9		53.9		85.3		53.3	
	248.6	1.2	87.1	-11.5	118.4	29.1	63.3	28.6
3	128.9		59.8		72.3		81.4	
	278.7	-6.2	131.4	-4.4	117.5	26.3	121.3	37.7
4	89.6		53.6		58.2		69.0	
	203.2	-0.2	129.3	2.4	98.9	24.6	110.8	23.1
5	129.9		56.4		92.1		48.3	
	240.3	9.0	96.3	3.6	151.6	26.0	67.4	23.3
6	126.5		72.0		79.1		52.9	
	275.0	-2.2	147.2	1.2	130.3	9.9	76.0	20.8
7	138.7		51.5		89.9		72.1	
	265.0	0.4	123.7	-16.6	133.6	25.7	100.0	20.2
8	136.5		105.0		78.8		79.2	
	277.2	-3.4	196.4	0.0	114.8	22.5	120.2	28.8
Aver-	124.2		65.2		80.2		64.0	
age	253.8	-0.3	131.3	-2.9	126.3	23.6	92.2	26.3

Table A.13: Mean, maximum and minimum values of tangential crank force at pedal for each subject during the bump and no bump tests.

Units Watts	Bump				No Bump			
	Hard tail		Suspension		Hard tail		Suspension	
Subject No.	mean		mean		mean		mean	
	max	min	max	min	max	min	max	min
1	137.5		76.4		94.5		70.3	
	278.3	-1.2	152.5	2.0	160.0	27.5	99.2	35.7
2	130.0		57.5		90.4		65.1	
	260.8	1.2	92.9	-12.3	125.5	30.8	77.2	34.9
3	140.9		59.9		76.5		83.5	
	304.6	-6.8	131.7	-4.4	124.3	27.8	124.5	38.6
4	117.9		68.8		87.2		87.8	
	267.5	-0.2	166.0	3.1	148.1	36.9	141.0	29.4
5	132.9		67.2		84.1		56.8	
	245.9	9.2	114.8	4.3	138.5	23.8	79.3	27.4
6	138.3		78.8		87.0		68.3	
	300.4	-2.4	161.2421	1.3	143.4	10.9	98.1	26.9
7	129.0		53.2		100.9		79.4	
	246.4	0.3	127.8	-17.2	150.0	28.9	110.0	22.3
8	146.4		98.9		89.9		88.0	
	297.4	-3.6	185.0	0.0	131.0	25.7	133.5	32.0
Average	134.1		70.1		88.8		74.9	
	275.2	-0.4	141.5	-2.9	140.1	26.5	107.9	30.9

Table A.14: Mean, maximum and minimum values of power transmitted through the crank arms for each subject during the bump and no bump tests.

Units m/s	Bump		No Bump	
	Hard tail	Suspension	Hard tail	Suspension
Subject No.	mean	mean	mean	mean
1	3.468	3.476	3.562	3.542
2	3.248	3.364	3.419	3.403
3	3.159	3.263	3.301	3.308
4	3.455	3.514	3.556	3.561
5	3.18	3.246	3.304	3.287
6	3.412	3.473	3.556	3.605
7	3.242	3.264	3.506	3.569
8	3.391	3.916	3.579	3.585
Average	3.319	3.44	3.473	3.483

Table A.15: Mean values of tangential surface velocity of the roller for each subject during the bump and no bump tests.

Units Newtons / Subject No.	Bump — Hard tail		Bump — Suspension		No Bump — Hard tail		No Bump — Suspension	
	mean force (tot)		mean force (tot)		mean force (tot)		mean force (tot)	
	mean force (pdl)		mean force (pdl)		mean force (pdl)		mean force (pdl)	
	mean force (oth)		mean force (oth)		mean force (oth)		mean force (oth)	
	max	min	max	min	max	min	max	min
1	18.8		28.3		26.3		30.1	
	39.6		22.0		26.5		19.8	
	-20.9		6.3		0.8		10.3	
	245.6	-454.8	218.9	-221.1	82.3	-30.7	94.0	-39.5
2	43.8		17.0		26.9		26.1	
	40.0		17.1		26.4		19.1	
	3.9		-0.1		0.5		7.0	
	337.3	-496.7	229.9	-293.1	94.2	-46.2	103.7	-50.0
3	38.5		17.3		26.1		36.4	
	44.6		18.4		23.2		25.2	
	-6.1		1.2		4.0		11.2	
	264.9	-451.7	250.4	-280.2	97.5	-43.3	107.9	-38.5
4	39.5		21.2		32.2		34.9	
	34.1		19.6		24.5		24.7	
	5.4		1.6		9.6		10.2	
	280.0	-464.4	244.8	-281.8	132.9	-42.2	115.9	-38.5
5	42.1		16.4		23.2		17.8	
	41.8		20.7		25.5		17.3	
	0.3		-4.3		-2.2		0.5	
	270.6	-443.1	212.3	-276.7	76.8	-33.2	95.9	-64.0
6	29.6		29.6		25.2		23.0	
	40.5		22.7		24.5		19.0	
	-10.9		6.9		1.1		4.1	
	345.5	-521.6	289.1	-279.8	108.1	-53.0	111.2	-49.6
7	36.1		6.9		24.3		25.1	
	39.8		16.3		28.8		22.2	
	-3.7		-9.4		-4.5		2.9	
	294.0	-432.1	268.8	-281.5	107.7	-66.5	103.7	-58.7
8	26.2		30.1		31.7		32.6	
	43.2		25.3		25.1		24.6	
	-17.0		5.2		6.5		8.1	
	297.9	-491.9	262.0	-258.8	99.8	-40.6	104.9	-46.7
Average	34.3		20.8		27.0		28.2	
	40.5		20.2		25.6		21.5	
	-6.1		0.9		2.0		6.8	
	292.0	-469.5	247.0	-271.6	99.9	-44.5	104.6	-48.2

Table A.16: Mean, maximum and minimum values of force measured at the front bracket for each subject during the bump and no bump tests.

Units	Bump				No Bump			
Watts	Hard tail		Suspension		Hard tail		Suspension	
Subject	mean		mean		mean		mean	
No.	max	min	max	min	max	min	max	min
1	65.2		98.2		93.6		106.8	
	843.5	-1578.4	717.3	-745.8	293.9	-109.7	333.4	-140.2
2	142.4		57.1		92.1		88.8	
	1067.2	-1591.6	762.6	-980.5	320.8	-157.3	352.7	-170.0
3	121.6		55.7		86.0		120.0	
	819.6	-1432.9	807.0	-912.0	320.3	-142.6	353.7	-127.7
4	137.5		74.7		114.6		124.4	
	957.5	-1607.0	848.6	-986.5	473.2	-150.2	413.4	-137.2
5	133.6		53.2		76.6		58.6	
	838.6	-1407.6	679.5	-893.8	251.3	-108.7	311.1	-208.4
6	102.4		102.9		89.7		82.9	
	1172.0	-1785.0	982.6	-962.3	383.1	-188.2	400.0	-178.5
7	118.3		21.5		84.8		89.7	
	930.3	-1383.7	864.0	-910.5	377.3	-234.1	364.7	-207.2
8	89.0		118.4		113.4		117.0	
	1003.5	-1677.9	1023.3	-1008.7	356.9	-144.9	376.1	-167.6
Average	113.8		72.7		93.8		98.5	
	954.0	-1558.0	835.6	-925.0	347.1	-154.5	363.1	-167.1

Table A.17: Mean, maximum and minimum values of the estimated power transmitted to the roller for each subject during the bump and no bump tests.

Appendix B

Calculations and Adapted Power Model

B.1 Calculations

B.1.1 General Calculations

Time calculations

All calculations are calculated from a roller surface velocity ν_{bump} of $3.33\text{m} \cdot \text{s}^{-1}$. The horizontal distance between the axle of the rear wheel, at the point of contact between the bump and the rear tyre, and the front of the bumps is $X_{impact\ dist.}$ (see Figure B.1).

$$t_{of\ impact} = \frac{X_{impact\ dist.}}{3.33} = 0.03 \text{ sec}$$

$$t_{at\ top\ of\ bump} = \frac{W_{bump}}{\nu_{bump}} = 0.021 \text{ sec}$$

$$R_{wheel} : = 0.33 \text{ m}$$

$$R_{roller} = 0.31 \text{ m}$$

$$R_{top \ of \ bump} = 0.34 \text{ m}$$

$$X_{impack \ dist.} = \sqrt{R_{bump}^2 - \frac{R_{bump}^2 - R_{wheel}^2 + 0.64^2}{1.28}}$$

$$= 0.1 \text{ m}$$

$$\alpha = 0.028 \text{ rad}$$
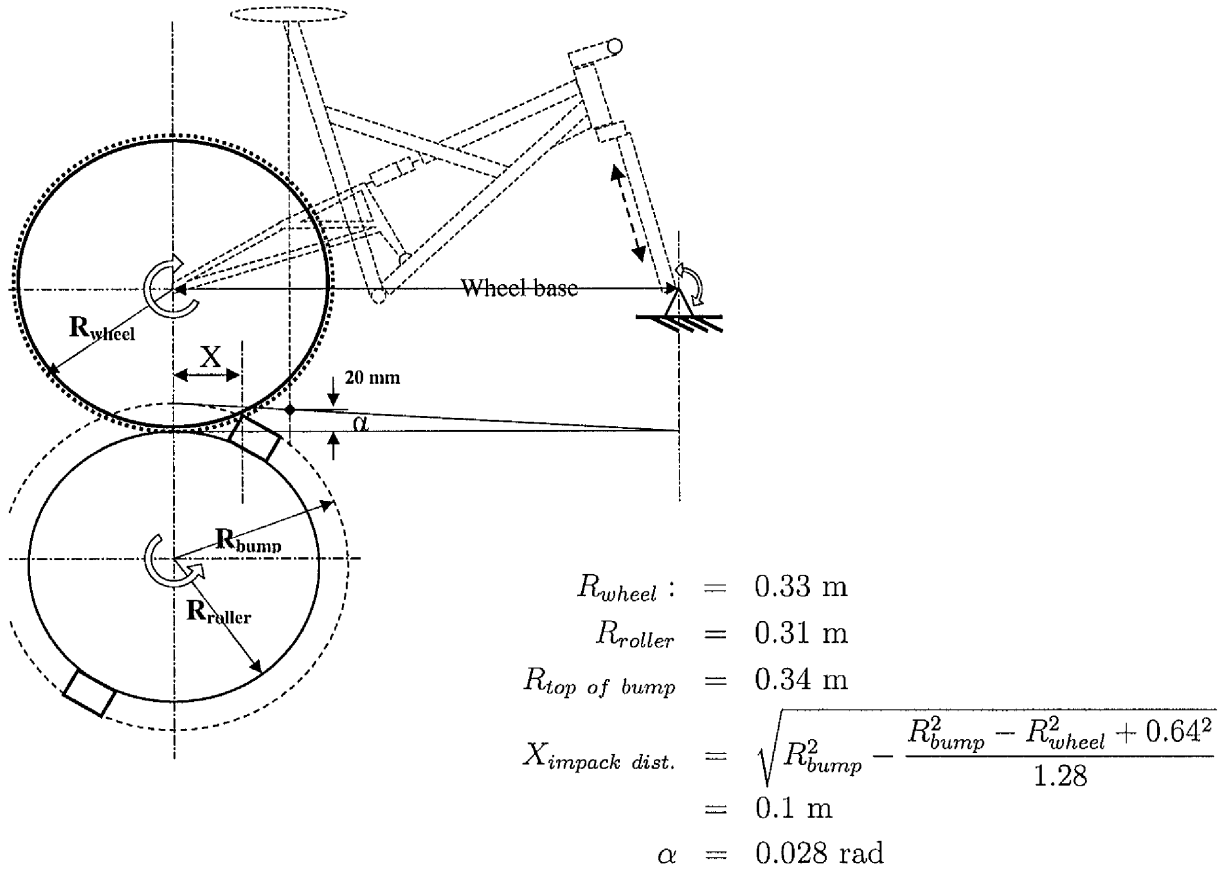
Figure B.1: Schematic of bicycle, rear wheel and roller.

$$t_{cont. \ with \ bump} = \frac{2 \cdot X_{impackdist.} + W_{bump}}{\nu_{bump}} = 0.081 \text{ sec}$$

$$t_{between \ impact} = \frac{C_{roller} - 2 \cdot W_{bump} - 4 \cdot X_{impact \ dist.}}{\nu_{bump}} = 0.21 \text{ sec}$$

B.1.2 Inertia Calculations

To simulate rear wheel bump impact on the rig equal to bump impact while cycling on a flat surface, the inertia of the roller had to be equivalent to the inertia of the cyclist and bicycle.

NOTE: Roller and bicycle are not scaled equally
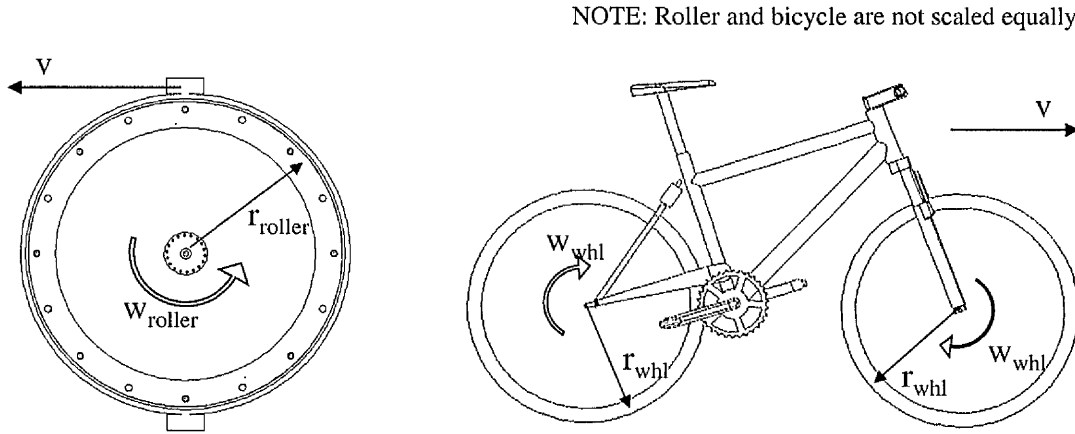
Figure B.2: Schematic of the bicycle and roller for the equivalent inertia calculations.

Energy conservation was used to determine the required inertia of the roller (see Equations B.1 to B.4).

$$
\begin{aligned}
Ek_{roller} &= \frac{1}{2} \cdot I_{roller} \cdot \omega^2, \\
&= \frac{1}{2} \cdot I_{roller} \cdot \frac{\nu^2}{r_{roller}^2},
\end{aligned}
\tag{B.1}
$$

and

$$
\begin{aligned}
Ek_{bicycle/cyclist} &= \frac{1}{2} \cdot M_{bicycle/cyclist} \cdot \nu^2 + \frac{1}{2} \cdot I_{rear\ whl} \cdot \omega_{whl}^2 + \frac{1}{2} \cdot I_{frt\ whl} \cdot \omega_{whl}^2 \\
&= \frac{1}{2} \cdot M_{bicycle/cyclist} \cdot \nu^2 + \frac{1}{2} \cdot \frac{\nu^2}{r_{whl}^2} \cdot \left(I_{rear\ whl} + I_{frt\ whl} \right)
\end{aligned}
\tag{B.2}
$$

To calculate the equivalent inertia $Ek_{roller} = Ek_{bicycle/cyclist}$.

$$\frac{1}{2} \cdot I_{roller} \cdot \frac{\nu^2}{r_{roller}^2} \; = \; \frac{1}{2} \cdot M_{bicycle/cyclist} \cdot \nu^2 + \frac{1}{2} \cdot \frac{\nu^2}{r_{whl}^2} \cdot (I_{rear\ whl} + I_{frt\ whl}) \quad \text{(B.3)}$$

therefore

$$\begin{aligned} I_{roller} \; &= \; M_{bicycle/cyclist} \cdot r_{roller}^2 + (I_{rear\ whl} + I_{frt_w hl}) \frac{r_{roller}^2}{r_{whl}^2} \qquad \text{(B.4)} \\[2mm] &= \; (74 + 12) \cdot 0.305^2 + (0.131 + 0.13) \cdot \frac{0.305^2}{0.368^2} \\[2mm] &= \; 8.18 \quad \text{kg} \cdot \text{m}^2 \end{aligned}$$

The values for $I_{rear\ whl}$ and $I_{frt_w hl}$ were obtained from Wang & Hull (1996). The required inertia of the roller was confirmed using equivalent inertia equations from Gorman & Kennedy (1998) p. 6.

The inertia value of the roller was calculated manually (see Equations B.5 to B.12) and confirmed using the solid modelling package on which the roller was designed.

$$I_{pipe} = \quad \tfrac{1}{2} \cdot M \cdot (R^2 + r^2) \qquad = 5.41 \quad \text{kg} \cdot \text{m}^2 \qquad \text{(B.5)}$$

$$I_{clamp\ ring\ (a)} = \quad \tfrac{1}{2} \cdot M \cdot (R^2 + r^2) \cdot 2 \qquad = 1.05 \quad \text{kg} \cdot \text{m}^2 \qquad \text{(B.6)}$$

$$I_{clamp\ ring\ (b)} = \quad \tfrac{1}{2} \cdot M \cdot (R^2 + r^2) \cdot 2 \qquad = 0.92 \quad \text{kg} \cdot \text{m}^2 \qquad \text{(B.7)}$$

$$I_{clamp\ rods} = \quad \left(\tfrac{1}{2} \cdot M \cdot r^2 + M \cdot l^2\right) \cdot 8 \quad = 0.23 \quad \text{kg} \cdot \text{m}^2 \qquad \text{(B.8)}$$

$$I_{wheels} = \quad I_{wheel} \cdot 2 \qquad = 0.10 \quad \text{kg} \cdot \text{m}^2 \qquad \text{(B.9)}$$

$$I_{bumps} = \quad \left(\tfrac{M}{12} \cdot (d^2 + c^2) + m \cdot l^2\right) \cdot 2 \quad = 0.41 \quad \text{kg} \cdot \text{m}^2 \qquad \text{(B.10)}$$

$$I_{carpet} = \quad \tfrac{1}{2} \cdot M \cdot (R^2 + r^2) \qquad = 0.19 \quad \text{kg} \cdot \text{m}^2 \qquad \text{(B.11)}$$

$$I_{roller} = \quad \sum_{n=1}^{n} I_{components} \qquad \text{where } n = \text{number of components} \quad \text{(B.12)}$$

$$= \quad 8.21 \quad \text{kg} \cdot \text{m}^2$$

B.1.3 Body Movement Calculations

The values of the variables used in equations B.13 to B.19 are reasonable estimates and therefore the calculated acceleration and distances can be used as guidelines.

From Figure 6.23 it was estimated that the pedalling frequency $(f_{pedals}) \simeq 2$ Hz and the maximum inertial force is roughly 50 N during the no bump test. The mass of the torso of the cyclist is $(M_{torso}) \simeq 35$ kg.

$$F_{inertia} = M_{torso} \cdot a_{torso} \quad \text{(N)} \qquad \text{(B.13)}$$

$$\text{therefore} \quad a_{torso} = 1.43 \quad (m \cdot s^{-2}) \qquad \text{(B.14)}$$

$$\text{and} \quad x = A \cdot \sin(\omega \cdot t) \qquad \text{(B.15)}$$

$$\text{differentiated gives} \quad \nu = -\omega \cdot A \cdot \cos(\omega \cdot t) \qquad \text{(B.16)}$$

$$\text{differentiated gives} \quad a = -\omega^2 \cdot A \cdot \sin(\omega \cdot t)$$

$$\text{substituting for } A \cdot \sin(\omega \cdot t) \quad \cdots \quad = -\omega^2 \cdot x \qquad \text{(B.17)}$$

$$\text{where} \quad \omega = 2 \cdot \pi \cdot f$$

$$= 12.6 \text{ rad} \cdot s^{-1} \qquad \text{(B.18)}$$

$$\text{from equ B.17 and B.18} \quad x = \frac{a_{torso}}{-\omega^2}$$

$$= 1 \text{ cm} \qquad \text{(B.19)}$$

The above equations indicate that the body needs to move forward and backward by 1 cm twice in one second to produce a force of 50 N at the front bracket. This is reasonable and provides an explanation for the extra force measured at the front bracket during the no bump tests.

B.2 Adapted Power Model

The power model for road cycling was developed by Martin et al. (1998) using fundamental engineering and physical principles to predict and analyse the power required to propel a bicycle and rider. The model was verified by experimentation.

B.2.1 The Model

The model includes aerodynamic drag, rolling resistance, wheel bearing friction, rate of change of potential and kinetic energy and friction in the drive chain.

The power to overcome aerodynamic resistance (P_{aero}) is described by equation B.20

$$P_{aero} = \frac{1}{2} \cdot \rho \cdot (C_d \cdot A + F_W) \cdot \nu_{air}^2 \cdot \nu_{grnd} \text{ (W)} \tag{B.20}$$

where F_W is the drag area of the spokes, ν_{air} is the air velocity and ν_{grnd} is the ground velocity .

The power to overcome rolling resistance $P_{rol\ res}$ is described by equation B.21

$$P_{rol\ res} = \nu_{grnd} \cdot cos[tan^{-1}(G_{rd})] \cdot C_{rol\ res} \cdot M_{tot} \cdot g \text{ (W)} \tag{B.21}$$

where G_{rd} is the road gradient, $C_{rol\ res}$ is the coefficient of rolling resistance and M_{tot} is the total mass.

The power to overcome wheel bearing frictional losses $P_{frc\ brg}$ is described by equation B.22

$$P_{frc\ brg} = \nu_{grnd} \cdot (91 + 8.7 \cdot \nu_{grnd}) \cdot 10^{-3} \text{ (W)} \tag{B.22}$$

The power to overcome changes in potential energy P_{Ep} is described by equation B.23

$$P_{Ep} = \nu_{grnd} \cdot M_{tot} \cdot g \cdot sin[tan^{-1}(G_{rd})] \text{ (W)} \qquad \text{(B.23)}$$

The power to overcome changes in kinetic energy P_{Ek} is described by equation B.24

$$P_{Ek} = \frac{1}{2} \cdot (M_{tot} + \frac{I}{r^2}) \cdot \frac{(\nu^2_{grnd\ f} - \nu^2_{grnd\ i})}{t_i - t_f} \text{ (W)} \qquad \text{(B.24)}$$

where $\nu_{grnd\ i}$ is the initial ground velocity, $\nu_{grnd\ f}$ is the final ground velocity and t_i and t_f is the initial and final times.

B.2.2 The Model Adaptation for Off-Road Predictions

The percentage power outputs were determined at zero road gradient with no wind and a small change in the beginning and end speed.

Variables were changed to adapt the model to off-road cycling conditions. The coefficient of rolling resistance was increased from 0.0032, which is the averaged rolling resistance of high pressure clincher road bicycle tyre, to 0.013 which is the rolling resistance of a 26 inch knobbly mountain bicycle tyre (Berry et al. 2000) and coefficient of aerodynamic drag $(C_d \cdot A)$ was increased from 0.299 m^2 to 0.4 m^2. There are four riding positions used during road and track cycling, the upright position where the hands are placed on the upper part of the handlebars, the drop position where they are on the bottom of the handlebars, the aero position where the elbows are placed on the pads of the aero-handlebars commonly used during time-trials and the Obree's position used during track cycling where the hands are placed in support under the

chest and the forearms tucked on the arms. Grappe et al. (1997) determined that the Obree's position gives the best coefficient of drag, 0.216 m^2, the aero position and the drop position, 0.262 m^2 and 0.276 m^2 respectively and the upright position, 0.299 m^2. To the author's knowledge the coefficient of drag for the riding position of a mountain bicycle has not been measured. The handlebars of a mountain bicycle are wider than those of a road bicycle and the riding position and style produces a larger frontal area so it was reasonable to increase the coefficient of drag to 0.4 m^2.

B.2.3 Adjusted Model Results
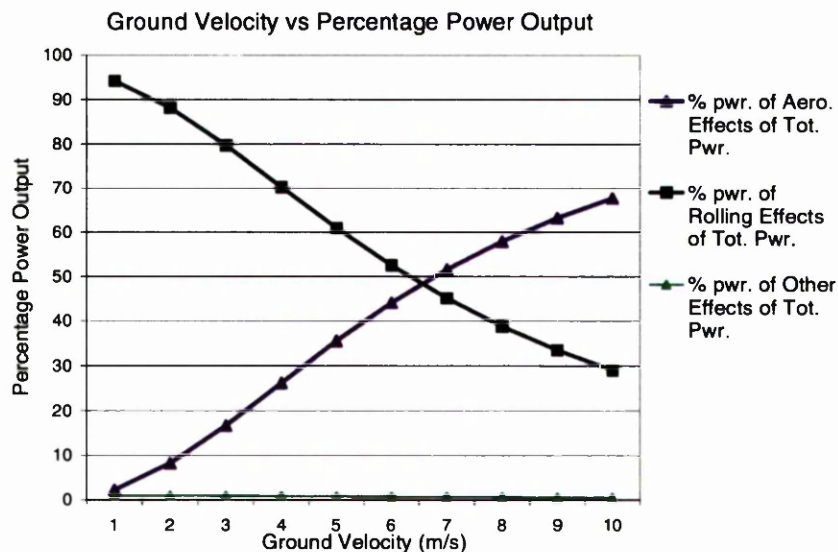
Figure B.3: Plotted results from the Adjusted Power Model.

Aerodynamic resistance is 90% of the total resistance on a road cyclist at race speed (Grappe et al. 1997). The average speed of professional road races is close to $40\ km \cdot h^{-1}$ ($11.11\ m \cdot s^{-1}$) and that of professional off-road cyclists is about $20\ km \cdot h^{-1}$ ($5.55\ m \cdot s^{-1}$). This reduced speed combined with the effect of the increase in rolling

resistance means that the power to overcome aerodynamic resistance is no longer the major form of resistance as it is in road cycling (Berry et al. 2000).

The model shows that to increase the speed of the cross country cyclist an improvement in rolling resistance and bicycle/cyclist efficiency rather than improvement in aerodynamics is required. The riding position and style of cross country cyclists is designed for control of the bicycle and does not allow for many changes in rider position. This makes improvement in aerodynamics very difficult.

Appendix C

Processed Data Analysis

This appendix contains results of processed data which were used to verify the use of data manipulation code and to discuss other data anomalies.

C.1   Filtered Data

Figure C.1 demonstrates the effect of applying the low pass filter to the acceleration, velocity and displacement signals. From the power spectral density (PSD) plots it can be seen that all frequencies above 1.5 Hz have not been affected by the filter but the problem of drift has been removed.

C.2   Velocity Data Correction

Subsequent to the analysis of the pedal velocity data, results indicated inconsistencies which occurred just after the left pedal passed the base of its stroke. Re-evaluation of the pedal velocity measuring equipment indicated the source of these inconsistencies
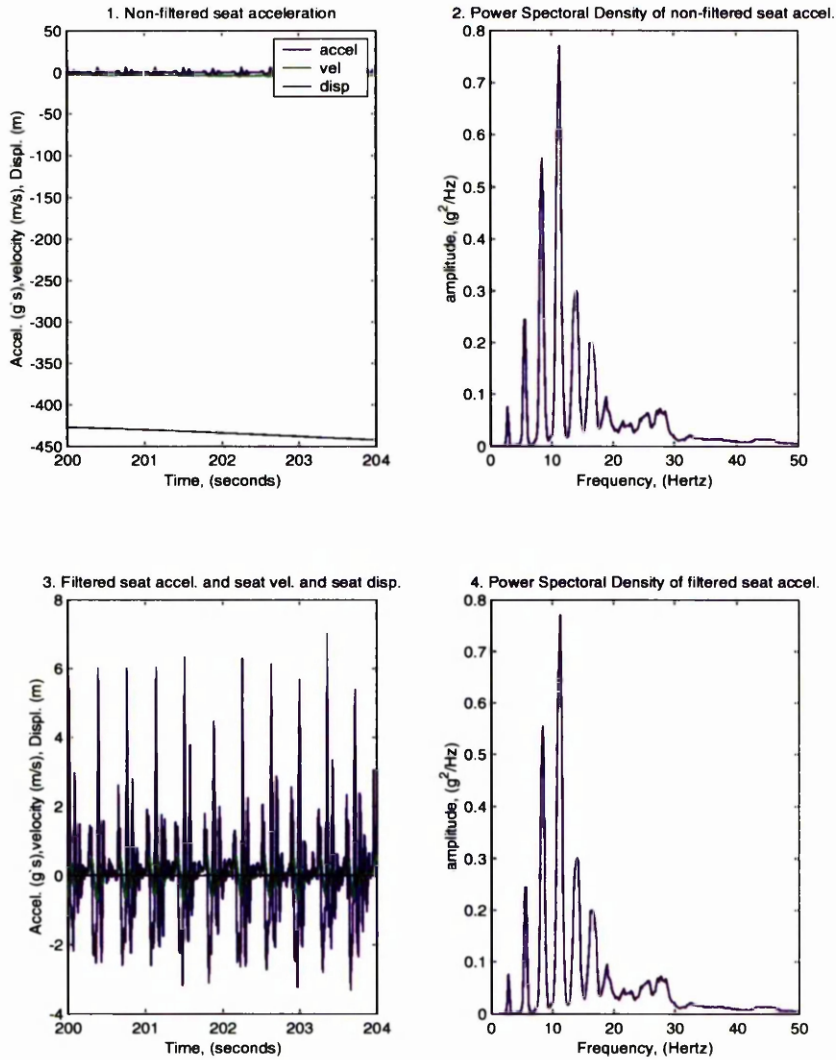
Figure C.1: Saddle acceleration and PSD of saddle acceleration plots for filtered and unfiltered data.

to be damage to the optical disc, which presumably occurred during testing. Due to the large number of subjects involved in the tests it was considered impractical to

repeat this work. However, meaningless data has been replaced with zeros and the mean value for the pedal velocity was then calculated from this modified data set. The calculated mean values were adjusted to correct for the addition of the zero values. See appendix D for code used to correct data.
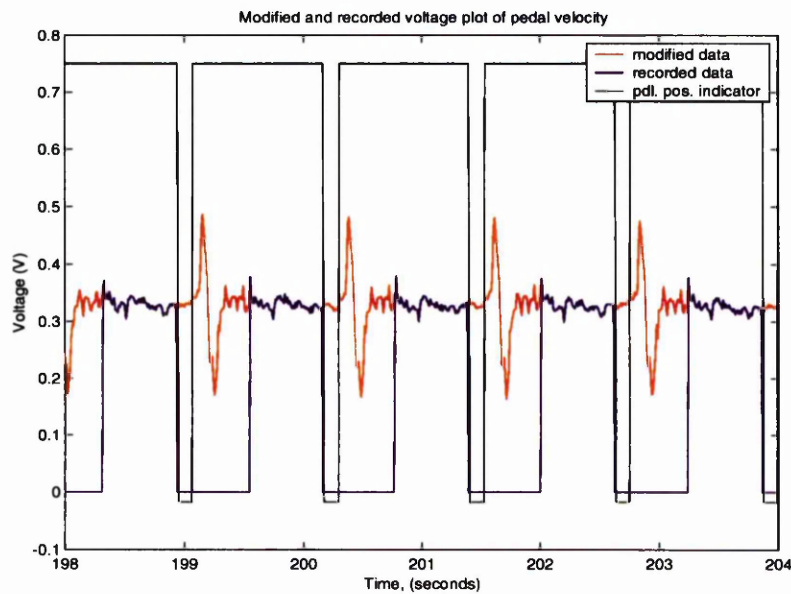
Figure C.2: Recorded and modified pedal velocity output voltage and pedal position indicator plot.

C.3   Slip Ring Disconnection

During some of the tests the slip rings momentarily disconnected from the brushes resulting in a sharp spike toward zero in the pedal force data. A possible reason for disconnection is the brushes sticking in their housing.

Appendix D

Data Analysis Programs

D.1   Physiological Data Analysis Code

```
%DATA ANALYSIS CODE FOR CYCLING PROJECT (Physiological readings)
%
%*********************************************************************
%clear variables in the memory
%*********************************************************************
clear
clc
%
%*********************************************************************
%Input physiological variables
%*********************************************************************

Subject=input('Enter the subjects name/code?','s')
AtmPres=input('What was the Atmospheric Pressure at the time of the test?')
Wght=input('What was the subjects weight at the time of the test?')

hr9=input('What was the subjects heart rate in the 9th minute?')
hr10=input('What was the subjects heart rate in the 10th minute?')

rpe3=input('what was the Rating of Perceived Exertion in the 3rd min.?')
rpe6=input('what was the Rating of Perceived Exertion in the 6th min.?')
rpe9=input('what was the Rating of Perceived Exertion in the 9th min.?')

cmft3=input('what was the Perceived Comfort in the 3rd min.?')
cmft6=input('what was the Perceived Comfort in the 6th min.?')
cmft9=input('what was the Perceived Comfort in the 9th min.?')
```

```
%First Bag inputs

Ivol1=input('What is the initial volume of bag 1?')
Fvol1=input('What is the final volume of bag 1?')
CO2E1=input('What was the percentage volume of CO2 bag 1?')
O2E1=input('What was the percentage volume of O2 bag 1?')
Temp1=input('What was the temperature of the expired air in bag 1?')
Duration1=input('What was the duration of the gas intake for bag 1?')

%Second Bag inputs

Ivol2=input('What is the initial volume of bag 2?')
Fvol2=input('What is the final volume of bag 2?')
CO2E2=input('What was the percentage volume of CO2 bag 2?')
O2E2=input('What was the percentage volume of O2 bag 2?')
Temp2=input('What was the temperature of the expired air in bag 2?')
Duration2=input('What was the duration of the gas intake for bag 2?')


%***********************************************************************
%Atmospheric constants
%***********************************************************************

N2I = 79.04;                    %  %N2 in the atmosphere
O2I = 20.93;                    %  %O2 in the atmosphere
CO2I = 0.03;                    %  %CO2 in the atmosphere

Exptemp = 10:1:30;
sliceA = [9.2 9.84 10.5 11.23 11.98 12.78 13.63 14.52 15.47 16.47]; %temp range 10 - 19 d
sliceB = [17.5 18.7 19.8 21.1 22.4 23.8 25.2 26.7 28.4 30.0 31.8];  %temp range 20 - 30 d
Vappress = [sliceA sliceB];


%***********************************************************************
%Physiological equations
%***********************************************************************

RQrange = 0.71:0.01:1;
sliceC = [4.69 4.702 4.714 4.727 4.739 4.751 4.764 4.776 4.788 4.801];  %kcal/volO2
sliceD = [4.813 4.825 4.838 4.850 4.862 4.875 4.887 4.899 4.911 4.924]; %kcal/volO2
sliceE = [4.936 4.948 4.961 4.973 4.985 4.998 5.010 5.022 5.035 5.047]; %kcal/volO2
Concon = [sliceC sliceD sliceE];                 %conversion constant to kcal/L O2

%FIRST BAG EQUATIONS

PresH2O1 = interp1(Exptemp,Vappress,Temp1,'spline');

N2Eb1 = (100-O2E1-CO2E1);
VEatps1 = (Fvol1-Ivol1+0.5)/Duration1;
```

```
VEstpd1 = VEatps1*((273.15/(273.15+Temp1))*((AtmPres-PresH2O1)/760));
VO21 = VEstpd1*(((N2Eb1/N2I)*O2I/100)-O2E1/100);          %l/min
VO21ml = (1000*VO21)/Wght;                                %ml/kg/min
VCO21 = VEstpd1*((CO2E1/100)-(CO2I/100)) ;                %l/min
RQ1 = VCO21/VO21 ;
rqkcale1 = interp1(RQrange,Concon,RQ1,'spline');
EE1 = VO21*rqkcale1*4186.8 ;                              %joules/min


%SECOND BAG EQUATIONS


PresH2O2 = interp1(Exptemp,Vappress,Temp2,'spline');


N2Eb2 = (100-O2E2-CO2E2);
VEatps2 = (Fvol2-Ivol2+0.5)/Duration2;
VEstpd2 = VEatps2*((273.15/(273.15+Temp2))*((AtmPres-PresH2O2)/760));
VO22 = VEstpd2*(((N2Eb2/N2I)*O2I/100)-O2E2/100);          %l/min
VO22ml = (1000*VO22)/Wght;                                %ml/kg/min
VCO22 = VEstpd2*((CO2E2/100)-(CO2I/100));                 %l/min
RQ2 = VCO22/VO22 ;
rqkcale2 = interp1(RQrange,Concon,RQ2,'spline');
EE2 = VO22*rqkcale2*4186.8 ;                              %joules/min


%HEART RATE, PERCIVED EXERTION AND COMFORT AVERAGES/DIFFERENCES


HRave=(hr9+hr10)/2;
EEave=(EE1+EE2)/2;


if VO21ml<VO22ml
    VO2pdiff=((VO22ml-VO21ml)/VO21ml)*100;
else
    VO2pdiff=((VO21ml-VO22ml)/VO22ml)*100;
end


%************************************************************************
%Variable to be saved to file
%************************************************************************


filename = [ Subject,'.txt' ];
pdatafile = fopen(filename,'w');
fprintf(pdatafile,'Subject code > - - - - - - - - - - - - - - - - %s \r\n\n',Subject);
fprintf(pdatafile,'Weight of the cyclist (kg) > - - - - - - - - - - %7.3f \r\n',Wght);
fprintf(pdatafile,'Atmospheric pressure at the time of test (mmHg)> %7.3f \r\n\n',AtmPres
%Volume of O2 used per kg per min
fprintf(pdatafile,'VO2 bag 1 (ml/kg/min) > - - - - - - - - - - - - %7.3f \r\n',VO21ml);
fprintf(pdatafile,'VO2 bag 2 (ml/kg/min) > - - - - - - - - - - - - %7.3f \r\n',VO22ml);
fprintf(pdatafile,'VO2 percentage difference >- - - - - - - - - - - %7.3f \r\n\n',VO2pdif
%Respirator Quosent
fprintf(pdatafile,'RQ bag 1 > - - - - - - - - - - - - - - - - - - - %7.3f \r\n',RQ1);
fprintf(pdatafile,'RQ bag 2 > - - - - - - - - - - - - - - - - - - - %7.3f \r\n\n',RQ2);
%Inspired energy
```

```
fprintf(pdatafile,'Energy expended in the 9th minute (J/min)> - - - %d \r\n',EE1);
fprintf(pdatafile,'Energy expended in the 10th minute (J/min)>- - - %d \r\n',EE2);
fprintf(pdatafile,'Average energy expended 9th and 10th min.(J/min)>%d \r\n\n',EEave);
%Heart rate
fprintf(pdatafile,'Heart rate in the 9th minute > - - - - - - - - - %d \r\n',hr9);
fprintf(pdatafile,'Heart rate in the 10th minute >  - - - - - - - - %d \r\n',hr10);
fprintf(pdatafile,'Average heart rate > - - - - - - - - - - - - - - %5.2f \r\n\n',HRave);
%Rating of percieved exertion and percived comfort
fprintf(pdatafile,'Rating of Perceived Exertion for the 3rd minute > %d \r\n',rpe3);
fprintf(pdatafile,'Rating of Perceived Exertion for the 6th minute > %d \r\n',rpe6);
fprintf(pdatafile,'Rating of Perceived Exertion for the 9th minute > %d \r\n\n',rpe9);
fprintf(pdatafile,'Perceived Comfort in the 3rd min. > - - - - - - - %d \r\n',cmft3);
fprintf(pdatafile,'Perceived Comfort in the 6th min. > - - - - - - - %d \r\n',cmft6);
fprintf(pdatafile,'Perceived Comfort in the 9th min. > - - - - - - - %d \r\n\n',cmft9);

fclose(pdatafile)
%
%
```

D.2   Mechanical Data analysis code

```
%
    %DATA ANALYSIS CODE FOR CYCLING PROJECT
    %****************************************************************
    %clear variables in the memory
    %****************************************************************

clear
clc
dir

    %****************************************************************
    %Load data from text file
    %****************************************************************

name=input('Which data file would you like to process? ','s') ;
datafile = [ name,'.txt' ]

data = load (datafile);

ch1 = data(:,1);               % Handle bar accelerometer
ch2 = -(data(:,2));            % Seat Accelerometer
ch3 = data(:,3);              % Front Strain Gauge
ch4 = data(:,4);              % Cranks strain Gauge
ch5 = data(:,5);              % Crank speed
ch6 = data(:,6);              % Roller speed
ch7 = data(:,7);              % Bump indicator
ch8 = (data(:,8)/2)+1.5;       % Left pedal indicator
```

```
M=size(data,1)                    %Number of data rows
n = [1:M]';                       %column vector from 1 to M

fs=100                            %sampling frequency in Hz
T = n/fs;                         %Time in seconds

    %*******************************************************************
    %limits
    %*******************************************************************

l = 6000;        %lower limit, beginning of test
nl = 54000;      %beginning of 9th min
tl = 60000;      %beginning of 10th min
u = 66000;       %upper limit, end of test


    %*******************************************************************
    %Signal filtering (butterworth filter)
    %*******************************************************************

[b,a] = butter(10,0.15);               % Hz low pass filter
spdfilgrnd = filtfilt(b,a,ch6);
spdfilcrnk = filtfilt(b,a,ch5);

[e,f] = butter(10,3/100,'high');       % Hz high pass filter
ch1fil = filtfilt(e,f,ch1);            % filtered handlebar acceleration
ch2fil = filtfilt(e,f,ch2);            % filtered seat acceleration

    %*******************************************************************
    %Beginning and end averages and linear differences (Offset and drift removal)
    %*******************************************************************

ch3zero = mean(ch3(1:300));            %average of first 300 points
ch4zero = mean(ch4(1:300));            %average of first 300 points
ch3zeroend = mean(ch3((M-300):M));     %average of last 300 points
ch4zeroend = mean(ch4((M-300):M));     %average of last 300 points

ych3 = ((ch3zeroend-ch3zero)/M)*n + ch3zero;  %y-values diff. of ch3 at point n
ych4 = ((ch4zeroend-ch4zero)/M)*n + ch4zero;  %y-values diff. of ch4 at point n

    %*******************************************************************
    %Variable calculation unfiltered
    %*******************************************************************

grndvel = 5.5455*ch6 + 0.011;               %tan velocity of roller
Crnkforce = (10.877*(ch4-ych4)-0.1232)*9.806;  %tan force applied at the pedals
Tanforce = (0.0776-60.798*(ch3-ych3))*9.806;   %tan force on roller (measured)
Tanpower = Tanforce*(mean(grndvel(1:u)));
```

```
%*************************************************************
%velocity correction
%*************************************************************

cnt = 1;
for z = 1:M-1
    if ch8(z) > 0.5 & ch8(z+1) < 0.5;
        ns(cnt) = z;
        cnt = cnt + 1;
    end
end

for z = 1:ns(1);
    ch5mod = ch5;
end

for x =1:cnt-2;
    dp = (ns(x+1)-ns(x));           %difference between marker points
    a = mod(dp,2);
    if a > 0
        mp = ns(x)+(dp-1)/2;        %mid point if diff is odd
    else
        mp =ns(x)+dp/2;             %mid point if diff is even
    end
    for z = ns(x):mp-1;
        ch5mod(z)= 0;               %speed data corrected
    end
    for z=mp:ns(x+1);
        ch5mod(z)=ch5(z);           %speed data actual
    end
end

pr = 0;
for y = 6000:66000;
    if  ch5mod(y) == 0;
        pr = pr+1;
    end
end

crnkvel = 3.1923*ch5mod + 0.006;    %tangential velocity of pedal
Crnkpower = Crnkforce*(mean(crnkvel(1:u))*(60000/(60000-pr)));


    %*************************************************************
    %Mean values
    %*************************************************************
ch1mean = mean(ch1);
ch2mean = mean(ch2);
ch1filmean = mean(ch1fil);
ch2filmean = mean(ch2fil);
```

```
grndvelmean = mean(grndvel(1:u));
crnkvelmean = mean(crnkvel(1:u))*(60000/(60000-pr));
Crnkforcemean = mean(Crnkforce(1:u));
Tanforcemean = mean(Tanforce(1:u));
Crnkpowermean = mean(Crnkpower(1:u));
Tanpowermean = mean(Tanpower(1:u));

    %************************************************************
    %Frequency isolation
    %************************************************************

[Pch1,Fch1] = pwelch(ch1,512,fs);
[Pch1f,Fch1f] = pwelch(ch1fil,512,fs);

[Pch2,Fch2] = pwelch(ch2,512,fs);
[Pch2f,Fch2f] = pwelch(ch2fil,512,fs);

[Pgv,Fgv] = pwelch((grndvel-grndvelmean),512,fs);
[Pcv,Fcv] = pwelch((crnkvel-crnkvelmean),512,fs);
[Ptf,Ftf] = pwelch(Tanforce,512,fs);
[Pcf,Fcf] = pwelch((Crnkforce-Crnkforcemean),512,fs);

    %************************************************************
    %Rieman sum of values
    %************************************************************

vs = (cumsum((ch2-ch2mean)*9.806)*(1/fs));
vhb = (cumsum((ch1-ch1mean)*9.806)*(1/fs));

ds = cumsum(vs)*(1/fs);
dhb = cumsum(vhb)*(1/fs);

    %************************************************************
    %Rieman sum of filtered values
    %************************************************************

vsf = cumsum((ch2fil-ch2filmean)*9.806)*(1/fs);
vhbf = cumsum((ch1fil-ch1filmean)*9.806)*(1/fs);
vsfil = filtfilt(e,f,vsf);
vhbfil = filtfilt(e,f,vhbf);

vsfilave = mean(vsfil);      %mean velocity values
vhbfilave=mean(vhbfil);

dsf = cumsum((vsfil-vsfilave))*(1/fs);
dhbf = cumsum(vhbfil)*(1/fs);
dsfil = filtfilt(e,f,dsf);
dhbfil = filtfilt(e,f,dhbf);
```

```
%********************************************************************
%Rieman sum of power values to compute energy
%********************************************************************

dmppwr(n) = 0.375*84.5*grndvelmean;
EngyCrnk = cumsum(Crnkpower(1:u))*(1/fs);
EngyTan = cumsum(Tanpower(1:u))*(1/fs);
Engydmp = cumsum(dmppwr(1:u))*(1/fs);


   %********************************************************************
   %Front bracket force separation into components
   %********************************************************************

gearatio = crnkvelmean/grndvelmean;   %gear ratio used during test
Tanfrcpdl = Crnkforce*gearatio;        %front bracket force from the pedals
Tanfrcbmp = Tanforce-Tanfrcpdl;        %front bracket force from other effects
Tanfrcpdlmean = mean(Tanfrcpdl(1:u)); %mean front bracket force from pedals
Tanfrcbmpmean = mean(Tanfrcbmp(1:u)); %mean front bracket force from other effects
%
```

D.3   Maximum, Minimum and Mean Value Calculation Code

```
%DATA ANALYSIS CODE FOR CYCLING PROJECT
%MEANS and MEAN MAXIMUMS AND MINIMUMS
%MUST BE RUN AFTER eng*.m
%ONLY FOR BUMP TESTS!!!
%********************************************************************
m0 = 6000;       %lower limit, beginning of test
m10 = 66000;         %upper limit, end of test

%MEAN VALUES
ahbmean = mean(ch1fil(m0:m10));
asmean = mean(ch2fil(m0:m10));
vhbmean = mean(vhbfil(m0:m10));
vsmean = mean(vsfil(m0:m10));
dhbmean = mean(dhbfil(m0:m10));
dsmean = mean(dsfil(m0:m10));
vpmean = mean(crnkvel(m0:m10));
vrmean = mean(grndvel(m0:m10));
fpmean = mean(Crnkforce(m0:m10));
ffbmean = mean(Tanforce(m0:m10));
pffbmean = mean(Tanfrcpdl(m0:m10)); %mean horiz frc on frt brk from pedal eff
bffbmean = mean(Tanfrcbmp(m0:m10)); %mean horiz frc on frt brk from other eff
ppmean = mean(Crnkpower(m0:m10));
pfbmean = mean(Tanpower(m0:m10));
```

```
%MAXIMUM AND MINIMUM VALUES
for z = 1:M;
   if ch7(z) > 1
       impsmax(z) = max(ch2fil(z-10:z));      %max impact accel of seat
       landsmax(z) = max(ch2fil(z:z+10));     %max landing accel of seat
       impsmin(z) = min(ch2fil(z-10:z+10));   %min landing accel of seat
       vsmax(z) = max(vsfil(z-10:z+10));      %max seat velocity
       vsmin(z) = min(vsfil(z-10:z+10));      %min seat velocity
       dsmax(z) = max(dsfil(z-10:z+10));      %max seat displacement
       dsmin(z) = min(dsfil(z:z+30));         %min seat displacement
       imphbmax(z) = max(ch1fil(z:z+15));     %max impact accel of handlebars
       imphbmin(z) = min(ch1fil(z:z+15));     %min impact accel of handlebars
       vhbmax(z) = max(vhbfil(z-10:z+10));    %max handlebar velocity
       vhbmin(z) = min(vhbfil(z-10:z+10));    %min handlebar velocity
       dhbmax(z) = max(dhbfil(z-10:z+12));    %max handlebar displacement
       dhbmin(z) = min(dhbfil(z:z+38));       %min handlebar displacement
       pdlmin(z) = min(Crnkforce(z:z+70));    %min force at the pedals
       fbfmax(z) = max(Tanforce(z:z+20));     %max force at front bracket
       fbfmin(z) = min(Tanforce(z-8:z+8));    %min force at front bracket
       ppmin(z) = min(Crnkpower(z:z+70));     %min power at the pedals
       pfbmax(z) = max(Tanpower(z:z+20));     %max power at front bracket
       pfbmin(z) = min(Tanpower(z-8:z+8));    %min power at front bracket
   end
end

for z = 1:M;
   if ch8(z) < 0.5
       pdlmax1(z) = max(Crnkforce(z-45:z));   %max pedal force of left leg
       pdlmax2(z) = max(Crnkforce(z:z+45));   %max pedal force of right leg
       ppmax1(z) = max(Crnkpower(z-45:z));    %max pedal power of left leg
       ppmax2(z) = max(Crnkpower(z:z+45));    %max pedal power of right leg
   end
end

%ACCELERATION VALUES
[A,B]=size(impsmax);
cntix = 0;
sumix = 0;
for z = 1:B;
   if impsmax(z) > 0;
       sumix = impsmax(z) + sumix;
       cntix = cntix + 1;
   end
end
mnix = sumix/cntix                    %seat max ave impact accel

[A,C]=size(impsmin);
cntin = 0;
sumin = 0;
for z = 1:C;
```

```
   if impsmin(z) < 0;
       sumin = impsmin(z) + sumin;
       cntin = cntin + 1;
   end
end
mnin = sumin/cntin                  %seat min ave impact accel

[A,D]=size(landsmax);
cntl = 0;
suml = 0;
for z = 1:D;
   if landsmax(z) > 0;
       suml = landsmax(z) + suml;
       cntl = cntl + 1;
   end
end
mnlx = suml/cntl                    %seat max ave landing accel

[A,E]=size(imphbmax);
cnthbi = 0;
sumhbi = 0;
for z = 1:E;
   if imphbmax(z) > 0;
       sumhbi = imphbmax(z) + sumhbi;
       cnthbi = cnthbi + 1;
   end
end
mnhbi = sumhbi/cnthbi               %handlebar max ave accel

[A,F]=size(imphbmin);
cnthbl = 0;
sumhbl = 0;
for z = 1:F;
   if imphbmin(z) < 0;
       sumhbl = imphbmin(z) + sumhbl;
       cnthbl = cnthbl + 1;
   end
end
mnhbl = sumhbl/cnthbl               %handlebar min ave accel

%VELOCITY
[A,G]=size(vsmax);
cntvsx = 0;
sumvsx = 0;
for z = 1:G;
   if vsmax(z) > 0;
       sumvsx = vsmax(z) + sumvsx;
       cntvsx = cntvsx + 1;
   end
end
```

```
mnvsx = sumvsx/cntvsx              %seat max average vel

[A,H]=size(vsmin)    ;
cntvsn = 0;
sumvsn = 0;
for z = 1:H;
    if vsmin(z) < 0;
        sumvsn = vsmin(z) + sumvsn;
        cntvsn = cntvsn + 1;
    end
end
mnvsn = sumvsn/cntvsn              %seat min average vel

[A,I]=size(vhbmax)   ;
cntvhbx = 0;
sumvhbx = 0;
for z = 1:I;
    if vhbmax(z) > 0;
        sumvhbx = vhbmax(z) + sumvhbx;
        cntvhbx = cntvhbx + 1;
    end
end
mnvhbx = sumvhbx/cntvhbx           %hanblebar max average vel

[A,J]=size(vhbmin);
cntvhbn = 0;
sumvhbn = 0;
for z = 1:J;
    if vhbmin(z) < 0;
        sumvhbn = vhbmin(z) + sumvhbn;
        cntvhbn = cntvhbn + 1;
    end
end
mnvhbn = sumvhbn/cntvhbn           %hanblebar min average vel

%DISPLACEMENT
[A,K]=size(dsmax);
cntdsx = 0;
sumdsx = 0;
for z = 1:K;
    if dsmax(z) > 0;
        sumdsx = dsmax(z) + sumdsx;
        cntdsx = cntdsx + 1;
    end
end
mndsx = sumdsx/cntdsx             %seat max average displ

[A,L]=size(dsmin)    ;
cntdsn = 0;
sumdsn = 0;
```

```
for z = 1:L;
    if dsmin(z) < 0;
        sumdsn = dsmin(z) + sumdsn;
        cntdsn = cntdsn + 1;
    end
end
mndsn = sumdsn/cntdsn              %seat min average displ

[A,N]=size(dhbmax);
cntdhbx = 0;
sumdhbx = 0;
for z = 1:N;
    if dhbmax(z) > 0;
        sumdhbx = dhbmax(z) + sumdhbx;
        cntdhbx = cntdhbx + 1;
    end
end
mndhbx = sumdhbx/cntdhbx           %hanblebar max average displ

[A,P]=size(dhbmin);
cntdhbn = 0;
sumdhbn = 0;
for z = 1:P;
    if dhbmin(z) < 0;
        sumdhbn = dhbmin(z) + sumdhbn;
        cntdhbn = cntdhbn + 1;
    end
end
mndhbn = sumdhbn/cntdhbn           %hanblebar min average displ

%FRONT BRACKET FORCE and POWER
[A,Q]=size(fbfmin);
cntfbfn = 0;
sumfbfn = 0;
for z = 1:Q;
    if fbfmin(z) < 0;
        sumfbfn = fbfmin(z) + sumfbfn;
        cntfbfn = cntfbfn + 1;
    end
end
mnfbfn = sumfbfn/cntfbfn           %frt brk min average frc

[A,R]=size(fbfmax);
cntfbfx = 0;
sumfbfx = 0;
for z = 1:R;
    if fbfmax(z) > 0;
        sumfbfx = fbfmax(z) + sumfbfx;
        cntfbfx = cntfbfx + 1;
    end
```

```
end
mnfbfx = sumfbfx/cntfbfx          %frt brk max average frc

[A,S]=size(pfbmin);
cntpfbn = 0;
sumpfbn = 0;
for z = 1:S;
   if pfbmin(z) < 0;
      sumpfbn = pfbmin(z) + sumpfbn;
      cntpfbn = cntpfbn + 1;
   end
end
mnpfbn = sumpfbn/cntpfbn          %frt brk min average pwr

[A,U]=size(pfbmax);
cntpfbx = 0;
sumpfbx = 0;
for z = 1:U;
   if pfbmax(z) > 0;
      sumpfbx = pfbmax(z) + sumpfbx;
      cntpfbx = cntpfbx + 1;
   end
end
mnpfbx = sumpfbx/cntpfbx          %frt brk max average pwr


%PEDAL FORCE AND POWER
[A,V]=size(pdlmax1);
cntpdl1 = 0;
sumpdl1 = 0;
cntpdl2 = 0;
sumpdl2 = 0;
for z = 1:V;
   if pdlmax1(z) > 0;
      sumpdl1 = pdlmax1(z) + sumpdl1;
      cntpdl1 = cntpdl1 + 1;
   end
   if pdlmax2(z) > 0;
      sumpdl2 = pdlmax2(z) + sumpdl1;
      cntpdl2 = cntpdl2 + 1;
   end
end
mnpdlfx = (sumpdl1+sumpdl2)/(cntpdl1+cntpdl2)   %pdl max ave frc

[A,W]=size(pdlmin);
cntpdln = 0;
sumpdln = 0;
for z = 1:W;
   if pdlmin(z) < 0;
```

```
        sumpdln = pdlmin(z) + sumpdln;
        cntpdln = cntpdln + 1;
    end
end
mnpdlfn = sumpdln/cntpdln              %pdl min average frc

[A,X]=size(ppmax1);
cntpp1 = 0;
sumpp1 = 0;
cntpp2 = 0;
sumpp2 = 0;
for z = 1:X;
    if ppmax1(z) > 0;
        sumpp1 = ppmax1(z) + sumpp1;
        cntpp1 = cntpp1 + 1;
    end
    if ppmax2(z) > 0;
        sumpp2 = ppmax2(z) + sumpp1;
        cntpp2 = cntpp2 + 1;
    end
end
mnppx = (sumpp1+sumpp2)/(cntpp1+cntpp2) %pdl max average pwr

[A,Y]=size(ppmin);
cntppn = 0;
sumppn = 0;
for z = 1:Y;
    if ppmin(z) < 0;
        sumppn = ppmin(z) + sumppn;
        cntppn = cntppn + 1;
    end
end
mnppn = sumppn/cntppn                   %pdl min average pwr

filename = [ name,'ave.txt' ];
pdatafile = fopen(filename,'w');

fprintf(pdatafile,'%s \r\n\n\n',name);

fprintf(pdatafile,'%4e \n',ahbmean);
fprintf(pdatafile,'%4e \n',mnhbi);
fprintf(pdatafile,'%4e \n',mnhbl);

fprintf(pdatafile,'%4e \n',vhbmean);
fprintf(pdatafile,'%4e \n',mnvhbx);
fprintf(pdatafile,'%4e \n',mnvhbn);

fprintf(pdatafile,'%4e \n',dhbmean);
fprintf(pdatafile,'%4e \n',mndhbx);
fprintf(pdatafile,'%4e \n',mndhbn);
```

```
fprintf(pdatafile,'%4e \n',asmean);
fprintf(pdatafile,'%4e \n',mnix);
fprintf(pdatafile,'%4e \n',mnlx);
fprintf(pdatafile,'%4e \n',mnin);

fprintf(pdatafile,'%4e \n',vsmean);
fprintf(pdatafile,'%4e \n',mnvsx);
fprintf(pdatafile,'%4e \n',mnvsn);

fprintf(pdatafile,'%4e \n',dsmean);
fprintf(pdatafile,'%4e \n',mndsx);
fprintf(pdatafile,'%4e \n',mndsn);

fprintf(pdatafile,'%4e \n',vpmean);
%fprintf(pdatafile,'%4e \n',cvmmax);
%fprintf(pdatafile,'%4e \n',cvmmin);

fprintf(pdatafile,'%4e \n',fpmean);
fprintf(pdatafile,'%4e \n',mnpdlfx);
fprintf(pdatafile,'%4e \n',mnpdlfn);

fprintf(pdatafile,'%4e \n',ppmean);
fprintf(pdatafile,'%4e \n',mnppx);
fprintf(pdatafile,'%4e \n',mnppn);

fprintf(pdatafile,'%4e \n',vrmean);
%fprintf(pdatafile,'%4e \n',gvmmax);
%fprintf(pdatafile,'%4e \n',gvmmin);

fprintf(pdatafile,'%4e \n',ffbmean);
fprintf(pdatafile,'%4e \n',pffbmean);
fprintf(pdatafile,'%4e \n',bffbmean);
fprintf(pdatafile,'%4e \n',mnfbfx);
fprintf(pdatafile,'%4e \n',mnfbfn);

fprintf(pdatafile,'%4e \n',pfbmean);
fprintf(pdatafile,'%4e \n',mnpfbx);
fprintf(pdatafile,'%4e \n',mnpfbn);

fclose(pdatafile) ;
%
```

Appendix E

Cycling Rig Drawings and Photographs

Figure E.1: Photograph of subject cycling on rig during a no bump test.

Figure E.2: Photograph of pedal force measurement instrumentation.

ITEM NO.	QTY.	PART NO.	DESCRIPTION
1	1	FARG 014	FRAME
2	1	FAIW 036	ROLLER
4	1	Platform Assembly	
5	1	FALU 001 with fork support	

DO NOT SCALE
UNITS: Millimeters

DRAWING No:

COMPONENT:

DATE:

MATERIAL:

REVISION:

DRAWN BY:
J K Titlestad

CONTACT NO.:

APPROVED:

PROJECT:

SHT.No.   OF

THIS DRAWING MUST BE RETURNED TO THE DESIGNER ON COMPLETION OF THE COMPONENT OR ON REQUEST. THIS DRAWING MAY NOT BE REPRODUCED OR BE DISTRIBUTED WITHOUT THE WRITTEN CONSENT OF THE DESIGNER

Figure E.3: Full assembly of rig.

ITEM NO.	QTY.	PART NO.	DESCRIPTION
1	1	SALU 002	FIXED BASE
	1	PTLU 003	
	2	PTLU 004	
	1	PTLU 005	
2	1	PTLU 006	AXLE
3	1	SALU 007	HINGED
	1	PTLU 008	
	2	PTLU 009	
	1	PTLU 010	
	1	PTLU 011	
4	6	PTLU 012	BUSHING
5	1	PTLU 013	FORK AXLE

COMPONENT: FULL FRONT LOAD ASSEMBLY

DRAWING No: **FALU 001**	MATERIAL:	
DATE: 10-03-2000	DRAWN BY: J K Titlestad	CONTACT NO.:
REVISION:	PROJECT:	SHT.No. OF
APPROVED:		

DO NOT SCALE
UNITS: Millimeters

THIS DRAWING MUST BE RETURNED TO THE DESIGNER ON COMPLETION OF THE COMPONENT OR ON REQUEST. THIS DRAWING MAY NOT BE REPRODUCED OR BE DISTRIBUTED WITHOUT THE WRITTEN CONSENT OF THE DESIGNER.

Figure E.4: Front bracket sub-assembly.

QUANTITY:

ITEM NO.	QTY.	PART NO.	DESCRIPTION
1	1	SAIW 037	ROLLER PIPE
	1	PTIW 038	
	2	PTIW 039	
2	2	SAIW 042	BICYCLE RIM
	1	PTIW 044	
	1	PTIW 043	
3	2	PTIW 040	CLAMPING DISC
4	8	PTIW 045	CLAMPING ROD

DRAWING No: **FAIW 036**	COMPONENT: IMPACT WHEEL ASSEMBLY	
DATE: 12-03-2000	MATERIAL:	
REVISION:	DRAWN BY: J K Titlestad	CONTACT NO.:
APPROVED:	PROJECT:	SHT.No. OF

DO NOT SCALE
UNITS: Millimeters

THIS DRAWING MUST BE RETURNED TO THE DESIGNER ON COMPLETION OF THE COMPONENT OR ON REQUEST. THIS DRAWING MAY NOT BE REPRODUCED OR BE DISTRIBUTED WITHOUT THE WRITTEN CONSENT OF THE DESIGNER.

Figure E.5: Roller sub-assembly.

ITEM NO.	QTY.	PART NO.	DESCRIPTION
1	1	SARG 015	CROSS MEMBER
	1	PTRG 016	
	2	PTRG 017	
2	2	SARG F 018	FRT BRK SUPPORT
	2	PTRG 016	
	1	PTRG 019	
	2	PTRG 020	
	1	PTRG 017	
	2	PTRG 021	
3	1	PTRG 035	MOUNTING PLATE
4	1	SARG R 022	ROLLER SUPPORT
	1	PTRG 023	
	1	PTRG 024	
	1	PTRG 025	
	1	PTRG 027	
	1	PTRG 028	
	1	PTRG 026	
5	1	SARG L 029	ROLLER SUPPORT
	1	PTRG 030	
	1	PTRG 031	
	1	PTRG 034	
	1	PTRG 033	
	1	PTRG 027	
	1	PTRG 032	

DO NOT SCALE
UNITS: Millimeters

COMPONENT: FULL RIG FRAME ASSEMBLY

DRAWING No: FARG 014

MATERIAL:

DATE: 12-03-2000

DRAWN BY: J K Titlestad

CONTACT NO.:

REVISION:

PROJECT:

SHT.No. OF

APPROVED:

THIS DRAWING MUST BE RETURNED TO THE DESIGNER ON COMPLETION OF THE COMPONENT OR ON REQUEST. THIS DRAWING MAY NOT BE REPRODUCED OR BE DISTRIBUTED WITHOUT THE WRITTEN CONSENT OF THE DESIGNER.

Figure E.6: Frame sub-assembly.

Appendix F

Bicycle Geometries

Bicycle Geometries		
	Marin Rocky Ridge	Marin Mount Vision
Size	18.5 inches	17.5 inches
Head Angle	71 degrees	71 degrees
Seat Angle	74 degrees	74 degrees
Top Tube	23 inches	$22\frac{3}{8}$ inches
Chainstay	$16\frac{3}{4}$ inches	$16\frac{1}{2}$ inches
BB height	$11\frac{5}{8}$ inches	13 inches
Wheel Base	$42\frac{1}{2}$ inches	42 inches
Head Tube	150 mm	120 mm
Standover	32.2 inches	31.4 inches
Seat Post	27 mm	30 mm
Stem Length	120 mm	120 mm

Table F.1: Table of bicycle frame geometries for the Marin Rocky Ridge and the Marin Mount Vision. The values were obtained from the Marin Bicycles Web Page (http://www.marinbikes.com). Traditionally bicycle sizes are described in imperial units, and the units used in this table are those used by Marin Bicycles.

Appendix G

RPE and Comfort Scales

1	**Very Uncomfortable**
2	**Fairly Uncomfortable**
3	**Fairly comfortable**
4	**Comfortable**
5	**Very Comfortable**

Figure G.2: Comfort scale

6 7 8	**Very very light**
9 10	**Very light**
11 12	**Fairly light**
13 14	**Somewhat hard**
15 16	**Hard**
17 18	**Very hard**
19 20	**Very very hard**

Figure G.1: RPE scale

Appendix H

Electronic Circuitry Drawings
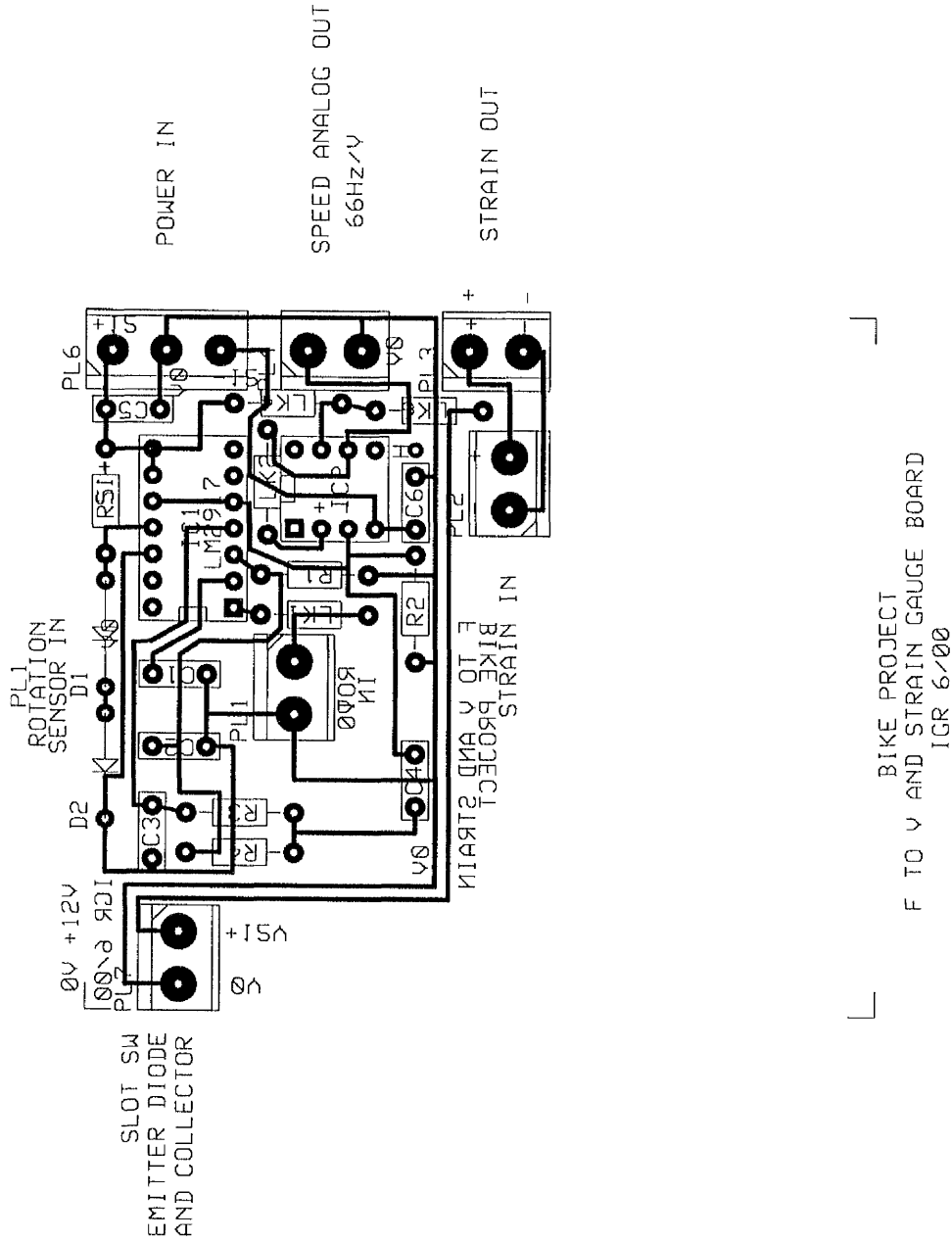
Figure H.1: Bottom bracket circuitry with the frequency to voltage conversion circuitry for speed measurement.
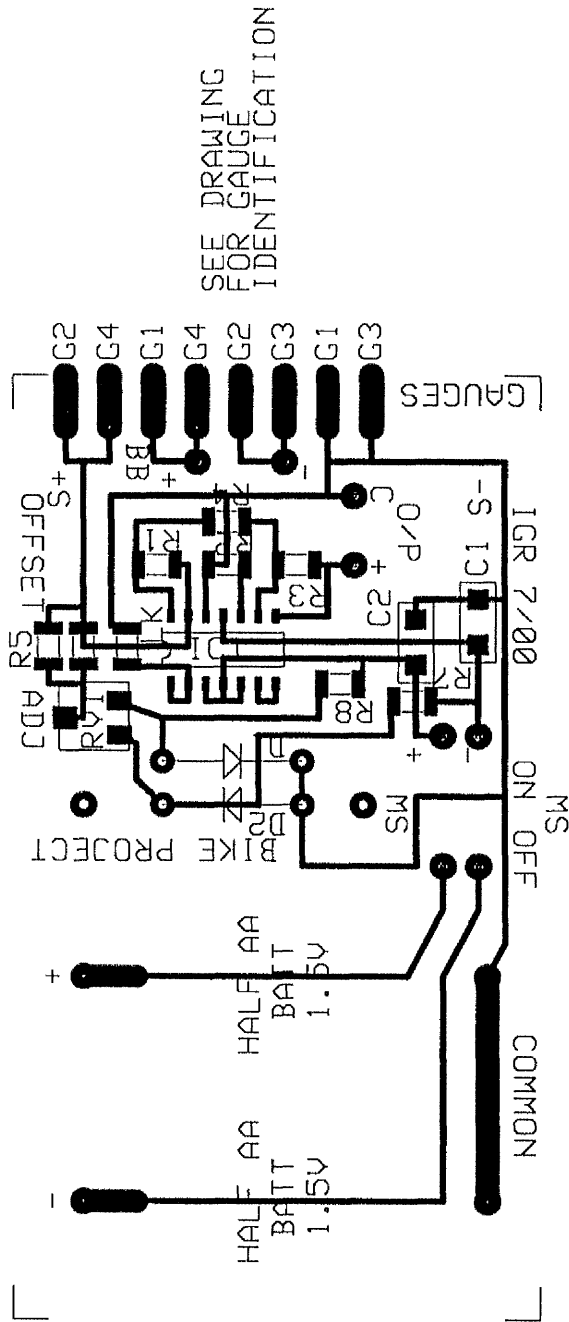
Figure H.2: 2000 times strain gauge amplifier and 9 volt battery circuitry.
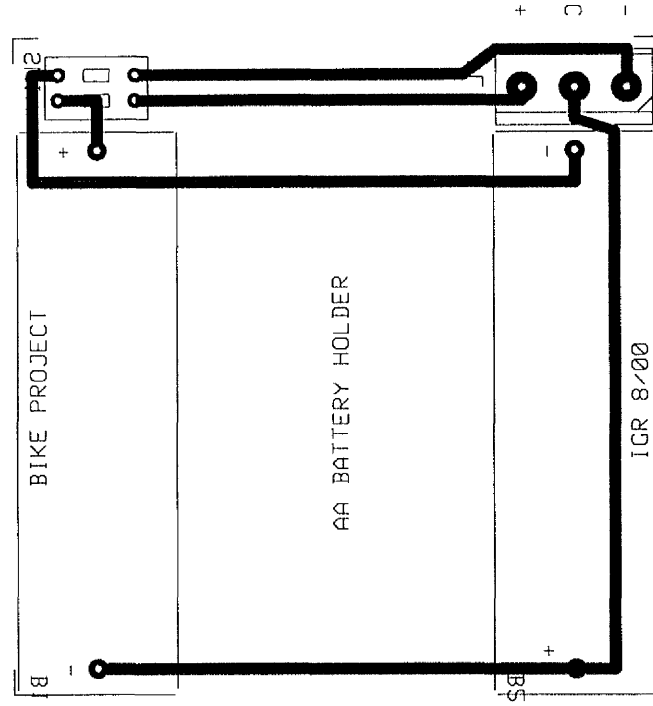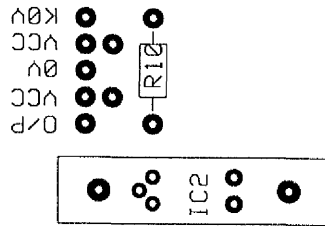
Figure H.3: Battery board for 1.5 volt strain gauge bridge power supply and optical sensor board.